NASA Contractor Report 3684

Analysis of Nonplanar Wing-Tip-Mounted Lifting Surfaces on Low-Speed Airplanes

C. P. van Dam

GRANT NSG-1633
JUNE 1983

25th Anniversary
1958-1983

NASA

NASA Contractor Report 3684

Analysis of Nonplanar Wing-Tip-Mounted Lifting Surfaces on Low-Speed Airplanes

C. P. van Dam
University of Kansas Center for Research, Inc.
Lawrence, Kansas

Prepared for
Langley Research Center
under Grant NSG-1633

National Aeronautics
and Space Administration

**Scientific and Technical
Information Branch**

1983

upwind wing tip and aileron, which is induced by the stalled winglet, causes aileron stick force reversal. Winglets produce only small changes in Dutch roll and roll mode characteristics. Conversely, a significant increment can be observed in the level of Dutch roll excitation following an aileron control step input.

A discussion is presented of the considerations involved in the design of winglets for low-speed general aviation airplanes.

TABLE OF CONTENTS

TABLE OF CONTENTS (continued)

LIST OF TABLES

LIST OF FIGURES

LIST OF FIGURES (continued)

LIST OF FIGURES (continued)

LIST OF SYMBOLS

AR	aspect ratio, b^2/S
b	wing span, ft (m)
C_D	drag coefficient
C_L	lift coefficient
C_{L_α}	lift curve slope, $\partial C_L/\partial\alpha$, rad^{-1}
C_ℓ	rolling moment coefficient
C_{ℓ_o}	rolling moment coefficient for trimmed condition
C_{ℓ_o}'	rolling moment coefficient for zero sideslip, aileron, and rudder angle
C_{ℓ_p}	variation of rolling moment coefficient with roll rate, $\partial C_\ell/\partial(pb/2V)$, rad^{-1}
C_{ℓ_r}	variation of rolling moment coefficient with yaw rate, $\partial C_\ell/\partial(rb/2V)$, rad^{-1}
C_{ℓ_β}	variation of rolling moment coefficient with sideslip angle, $\partial C_\ell/\partial\beta$, rad^{-1} or deg^{-1}
$C_{\ell_{\delta_a}}$	variation of rolling moment coefficient with aileron angle, $\partial C_\ell/\partial\delta_a$, rad^{-1}
$C_{\ell_{\delta_r}}$	variation of rolling moment coefficient with rudder angle, $\partial C_\ell/\partial\delta_r$, rad^{-1}
C_m	pitching moment coefficient
C_{m_o}	pitching moment coefficient for zero lift coefficient
C_n	yawing moment coefficient
C_{n_o}	yawing moment for trimmed condition
C_{n_o}'	yawing moment coefficient for zero sideslip, aileron, and rudder angle
C_{n_p}	variation of yawing moment coefficient with roll rate, $\partial C_n/\partial(pb/2V)$, rad^{-1}

C_{n_r}	variation of yawing moment coefficient with yaw rate, $\partial C_n/\partial(rb/2V)$, rad^{-1}
C_{n_β}	variation of yawing moment coefficient with sideslip angle, $\partial C_n/\partial\beta$, rad^{-1} or deg^{-1}
$C_{n_{\delta_a}}$	variation of yawing moment coefficient with aileron angle, $\partial C_n/\partial\delta_a$, rad^{-1}
$C_{n_{\delta_r}}$	variation of yawing moment coefficient with rudder angle, $\partial C_n/\partial\delta_r$, rad^{-1}
C_p	pressure coefficient, $(p_{port} - p)/\bar{q}$
C_y	side force coefficient
C_{y_o}	side force coefficient for trimmed condition
C_{y_o}'	side force coefficient for zero sideslip, aileron, and rudder angle
C_{y_p}	variation of side force coefficient with roll rate, $\partial C_y/\partial(pb/2V)$, rad^{-1}
C_{y_r}	variation of side force coefficient with yaw rate, $\partial C_y/\partial(rb/2V)$, rad^{-1}
C_{y_β}	variation of side force coefficient with sideslip angle, $\partial C_y/\partial\beta$, rad^{-1} or deg^{-1}
$C_{y_{\delta_a}}$	variation of side force coefficient with aileron angle, $\partial C_y/\partial\delta_a$, rad^{-1}
$C_{y_{\delta_r}}$	variation of side force coefficient with rudder angle, $\partial C_y/\partial\delta_r$, rad^{-1}
c_n	sectional normal force coefficient
c_r	root chord, ft (m)
c_t	tip chord, ft (m)
F_{δ_a}	aileron stick force, right aileron stick force is positive, lb(N)

F_{δ_e}	elevator stick force, elevator stick force toward pilot is positive, lb(N)
F_{δ_r}	rudder pedal force, right rudder force is positive, lb(N)
I_x	moment of inertia about X body axis, slug-ft^2 (kg-m^2)
I_{xz}	product of inertia, slug-ft^2 (kg-m^2)
I_y	moment of inertia about Y body axis, slug-ft^2 (kg-m^2)
I_z	moment of inertia about Z body axis, slug-ft^2 (kg-m^2)
$i_{w\ell t}$	winglet incidence angle, deg
j	$\sqrt{-1}$
$K_{\phi_{\delta_a}}$	gain constant in ϕ/δ_a transfer function, rad/rad
L_p	dimensional variation of rolling moment with roll rate, $\bar{q}Sb^2C_{\ell_p}/(2I_xV)$, sec^{-1}
L_r	dimensional variation of rolling moment with yaw rate, $\bar{q}Sb^2C_{\ell_r}/(2I_xV)$, sec^{-1}
L_β	dimensional variation of rolling moment with sideslip angle, $\bar{q}SbC_{\ell_\beta}/I_x$, sec^{-2}
L_{δ_a}	dimensional variation of rolling moment with aileron angle, $\bar{q}SbC_{\ell_{\delta_a}}/I_x$, sec^{-2}
ℓ	winglet length, ft (m)
M	Mach number
M_r	wing-root bending moment, ft-lb (N-m)
m	airplane mass, slugs (kg)
N_β	dimensional variation of yawing moment with sideslip angle, $\bar{q}SbC_{n_\beta}/I_z$, sec^{-2}
N_{δ_a}	dimensional variation of yawing moment with aileron angle, $\bar{q}SbC_{n_{\delta_a}}/I_z$, sec^{-2}

P	roll rate, rad/sec or deg/sec
P_{ss}	steady state roll rate, deg/sec
p	perturbed roll rate, rad/sec
p	static pressure, lb/in^2 (N/m^2)
p'	measured static pressure, not corrected for position error, lb/in^2 (N/m^2)
p_{port}	local static pressure, lb/in^2 (N/m^2)
$\bar{q}$	dynamic pressure, $1/2\rho V^2$, lb/in^2 (N/m^2)
q_c'	measured dynamic pressure, not corrected for position error, lb/in^2 (N/m^2)
r	perturbed yaw rate, rad/sec
S	wing or winglet area, ft^2 (m^2)
s	Laplace variable, $\sigma + j\omega$
t	time, sec
T_R	roll mode time constant, sec
T_S	spiral mode time constant, sec
V	true airspeed, knots
V_c	calibrated airspeed, knots
V_c'	measured calibrated airspeed, not corrected for position error, knots
Y_β	dimensional variation of side force coefficient with sideslip angle, $\bar{q}SC_{y_\beta}/m$, ft/sec^2 (m/sec^2)
y	distance along winglet span from wing-winglet junction, ft (m)

α	angle of attack, rad or deg
β	sideslip angle, rad or deg
Γ	dihedral angle, deg
γ	winglet cant angle, $(90 - \Gamma_{w\ell t})$, deg
δ_a	aileron deflection angle, $(\delta_{a_r} + \delta_{a_\ell})/2$, left aileron deflected down and right aileron deflected up is positive, rad or deg
δ_e	elevator deflection angle, elevator deflected down is positive, rad or deg
δ_r	rudder deflection angle, rudder deflected to the left is positive, rad or deg
ΔC_p	difference in pressure coefficient between lower and upper surface, $C_{p_\ell} - C_{p_u}$
ε	twist angle, washout is negative, deg
ζ_D	Dutch roll damping ratio
ζ_ϕ	damping ratio of numerator of ϕ/δ_a transfer function
$\eta_{w\ell t}$	nondimensional winglet span station, $y/\ell_{w\ell t}$
Λ	sweep angle, deg
λ	taper ratio, c_t/c_r
σ	real part of Laplace operator, sec^{-1}
ϕ	bank angle, rad or deg
$(\phi/\beta)_D$	ratio of roll-to-sideslip at Dutch roll natural frequency
ω	imaginary part of Laplace operator, rad/sec
ω_{n_D}	Dutch roll undamped natural frequency, rad/sec
ω_{n_ϕ}	undamped natural frequency of numerator of ϕ/δ_a transfer function, rad/sec

Subscripts

ℓ	lower surface; left wing
r	right wing
u	upper surface
$w\ell t$	winglet

LIST OF ACRONYMS

ACD	Analysis and Computation Division (at LaRC)
AFCS	Automatic Flight Control System
AFFDL	Air Force Flight Dynamics Laboratory
AIAA	American Institute of Aeronautics and Astronautics
ARI	Aileron-Rudder Interconnect
CAM	Civil Aeronautics Manual
C.G.	Center of Gravity
CRINC	(KU) Center for Research, Inc.
D.E.	Doctor of Engineering
FAA	Federal Aviation Administration
FM	Frequency Modulated
FRL	Flight Research Laboratory (at KU)
GA(W)	General Aviation (Whitcomb) airfoil
ICAS	International Council of the Aeronautical Sciences
KCAS	Knots Calibrated Airspeed
KIAS	Knots Indicated Airspeed
KU	University of Kansas
LaRC	(NASA) Langley Research Center
LSAD	Low Speed Aerodynamics Division (at LaRC)
MAC	Mean Aerodynamic Chord
NACA	National Advisory Committee on Aeronautics
NARUVL	North American Rockwell Unified Vortex Lattice Method
NASA	National Aeronautics and Space Administration
NLF	Natural Laminar Flow
NPLS	Non-Planar Lifting Surface method

LIST OF ACRONYMS (continued)

QVLM	Quasi-Vortex-Lattice Method
SAE	Society of Automotive Engineers, Inc.
USNTPS	U. S. Naval Test Pilot School
WFC	(NASA) Wallops Flight Center

CHAPTER 1

INTRODUCTION

For many years it has been recognized that modifying the shape of the wing tip of an airplane may result in significant drag reduction at lifting conditions. Because of soaring fuel prices and fuel shortages in the past decade, the interest in nonplanar drag reduction devices has been revitalized. The increase in research has resulted in a number of concepts such as winglets, wing-tip sails, and vortex diffuser vanes (References 1, 2, and 3). These devices have been flight and/or wind-tunnel tested on airplanes ranging from high-speed, heavy transport jets to low-speed, light general aviation airplanes and sailplanes (References 4 through 11). The majority of these wing-tip development efforts have been oriented toward achieving airplane performance benefits, although alternative justifications have been made. Examples of alternative justifications are the use of winglets on canard configurations to provide direction stability (Reference 12), and the use of wing-tip devices on agricultural airplanes to modify the interaction between airplane wake and the materials dispensed in the wake (References 13, 14, and 53).

Nonplanar wing-tip devices must generate significant normal forces to maximize their effectiveness. Especially in the case of light general aviation and agricultural types of airplanes, these forces may cause a number of problems. First, aerodynamic loads resulting from the attachment of a highly efficient lifting airfoil to a lightly loaded wing create a structural problem at the wing tip.

Reference 15 presents a discussion on this loading mismatch. Second, structural weight required for load transmission in both wing tip and wing-tip device promotes the possibility of mass balance and aeroelastic effects detrimental to the behavior of the airplane. The airplane of Reference 16 provides a clear example of this problem. Third, nonplanar wing-tip modifications can drastically increase lateral stability (also called dihedral effect) of an airplane. This increase can seriously affect the damping of airplane lateral response characteristics (References 17 through 20).

The purpose of this report is to identify and explain the effects of nonplanar wing-tip-mounted lifting surfaces on the stability and control of light general aviation and agricultural airplanes. In addition, the effects of these surfaces on airplane performance and aerodynamic loading are also discussed. The discussions are based on flight-measured data, theoretical predictions, and considerations and data listed in the literature.

The flight test results are obtained with an agricultural research airplane at NASA Langley Research Center. These results include airplane lateral-directional characteristics in steady sideslips, lateral-directional mode and dynamic response characteristics, and stability and control parameters. Also, for a number of flight conditions, winglet pressure distributions and span loads are presented.

The theoretical results are obtained with various lifting surface methods. These results are correlated with flight-measured data when applicable. In addition to these correlations, a theoretical parameter study is conducted on a general aviation type wing configuration to

determine the effects of various winglet parameters on lateral-directional stability derivatives.

Use of trade names or names of manufacturers in this report does not constitute an official endorsement of such products or manufacturers, either expressed or implied, by the National Aeronautics and Space Administration.

CHAPTER 2

WINGLET PARAMETER STUDY

In this study, the nonplanar lifting surface method of Reference 21 has been used to compute the aerodynamic characteristics of a wing. The method is a quasi-vortex-lattice method (QVLM) and can be classified as a lifting surface method, since it does not have an aspect ratio restriction. A substantial number of lifting surface methods are available, which predict the longitudinal aerodynamic characteristics of planar and nonplanar wing configurations (e.g., References 22, 23, and 24). However, most existing methods for calculating lateral-directional stability derivatives are based on lifting-line type theories with or without empirical corrections (e.g., References 25 and 26). Although these methods provide a reasonable prediction of lateral-directional stability derivatives for conventional configurations, they are not applicable to complex planforms, such as a wing with winglets. For these nonconventional configurations, application of a lifting surface method is required.

Several theoretical parametric studies have been performed on the effects of winglets on the longitudinal aerodynamic characteristics and aerodynamic loading of a wing (References 27 and 28). This study, however, will concentrate on the lateral-directional aerodynamic characteristics. The first section of this chapter presents comparisons between experimental data and predicted results to assess the capabilities of the QVLM method. The second section discusses the effects of various winglet parameters on the lateral-directional stability deriv-

atives of a typical general aviation wing. In addition, several wing parameters are varied while the winglet geometry is kept approximately constant.

2.1 Computer Code Validation

The validation of the quasi-vortex-lattice method (QVLM) has been studied extensively in References 21 and 24 by comparison of its calculations with theoretical and experimental results. In this section, a small number of additional comparisons of QVLM results with wind-tunnel data are presented.

A comparison with wind-tunnel data for a wing with and without wing-tip-mounted end plates has been performed using the data of Reference 29. The configuration tested consisted of a wing and a number of end plates of various areas and shapes. The wing was unswept and untapered and had an aspect ratio of 4 and a NACA 64_1A412 airfoil section. In Figure 2.1a, clean wing experimental data are compared with QVLM results. The experimentally obtained zero-lift drag coefficient is used in the prediction of the drag coefficient. The predicted results show good agreement with the wind-tunnel data up through an angle of attack at which flow separation begins. Comparisons of wind-tunnel data and QVLM results for the wing with end plates (end plate J in Reference 29) are presented in Figure 2.1b. Again, the correlations show good agreement.

A comparison of sideslip derivatives for an isolated vertical-horizontal tail combination has been made using the wind-tunnel data

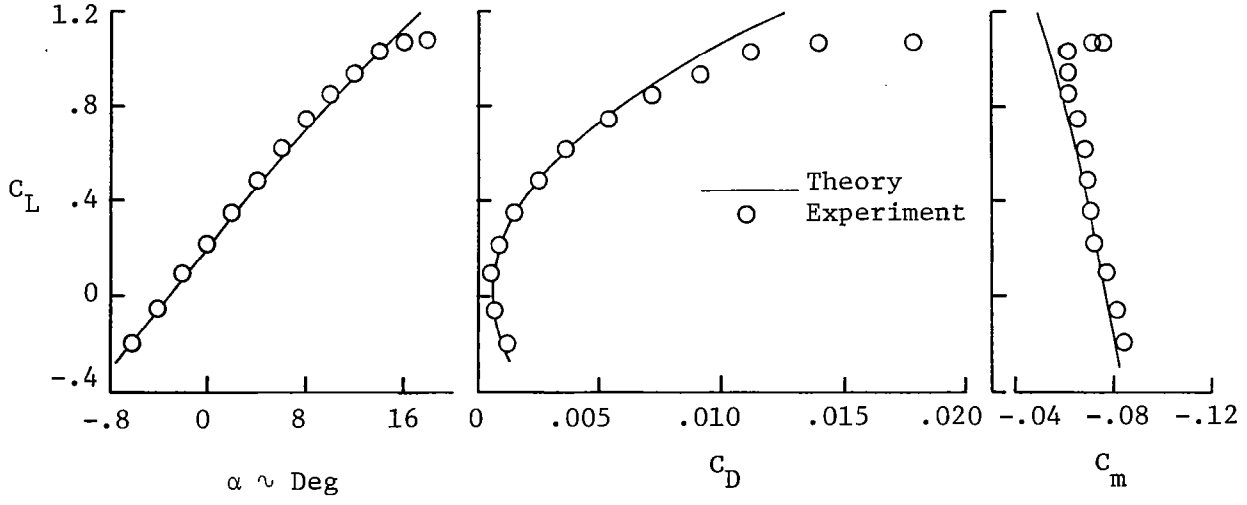

(a) Clean Wing (No End Plates)

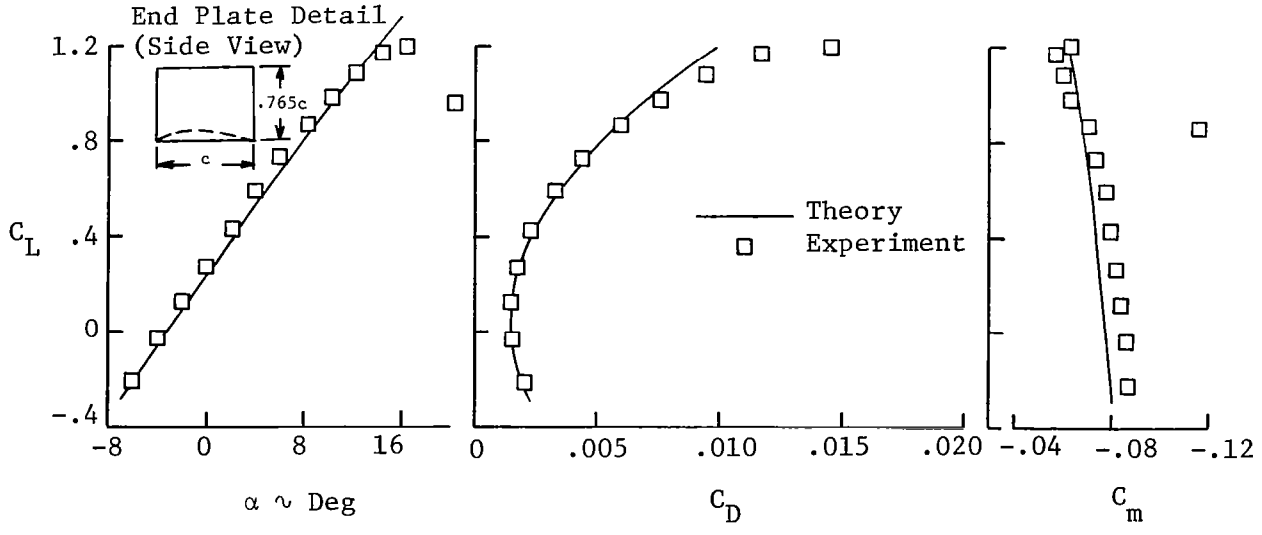

(b) Wing with End Plates

Figure 2.1: Longitudinal Aerodynamic Characteristics of an Aspect-Ratio-4 Rectangular Wing with and without End Plates

of Reference 30. The horizontal tail had an aspect ratio of 4.0 and a taper ratio of 0.6 and was unswept at the quarter-chord position. The vertical tail had an aspect ratio of 2.02 and a taper ratio of 0.60 and was also unswept at 25 percent of the chord. The sideslip derivatives are presented in Figure 2.2. Good agreement is shown between measured data and QVLM results. The discrepancy in the side force due to sideslip derivative can probably be attributed to the fact that the theory does not include skin friction drag effects.

In Reference 31, wind-tunnel measured lateral-directional stability derivatives are presented for an isolated wing. The wing had an aspect ratio of 3.6, a taper ratio of 0.455, and a leading-edge sweep angle of 41.6°. In Figure 2.3, a comparison of wind-tunnel data and predicted results is presented. The longitudinal aerodynamic characteristics are predicted with good accuracy, while the predicted lateral-directional stability derivatives show fair agreement with the experimental data up through an angle of attack at which flow separation starts.

The QVLM method of Reference 21 is used for the following parametric study. Comparisons of its solutions with experimental data have shown that the longitudinal aerodynamic characteristics of planar and nonplanar wing configurations are predicted very well. Use of the method to calculate lateral-directional stability derivatives has shown fair to good agreement with experimental data. Since the primary objective of the following study is to investigate the incremental effect of wing tip modifications on airplane stability characteristics, the correlation between QVLM results and experimental data appears adequate for cruise, climb, and approach angles of attack.

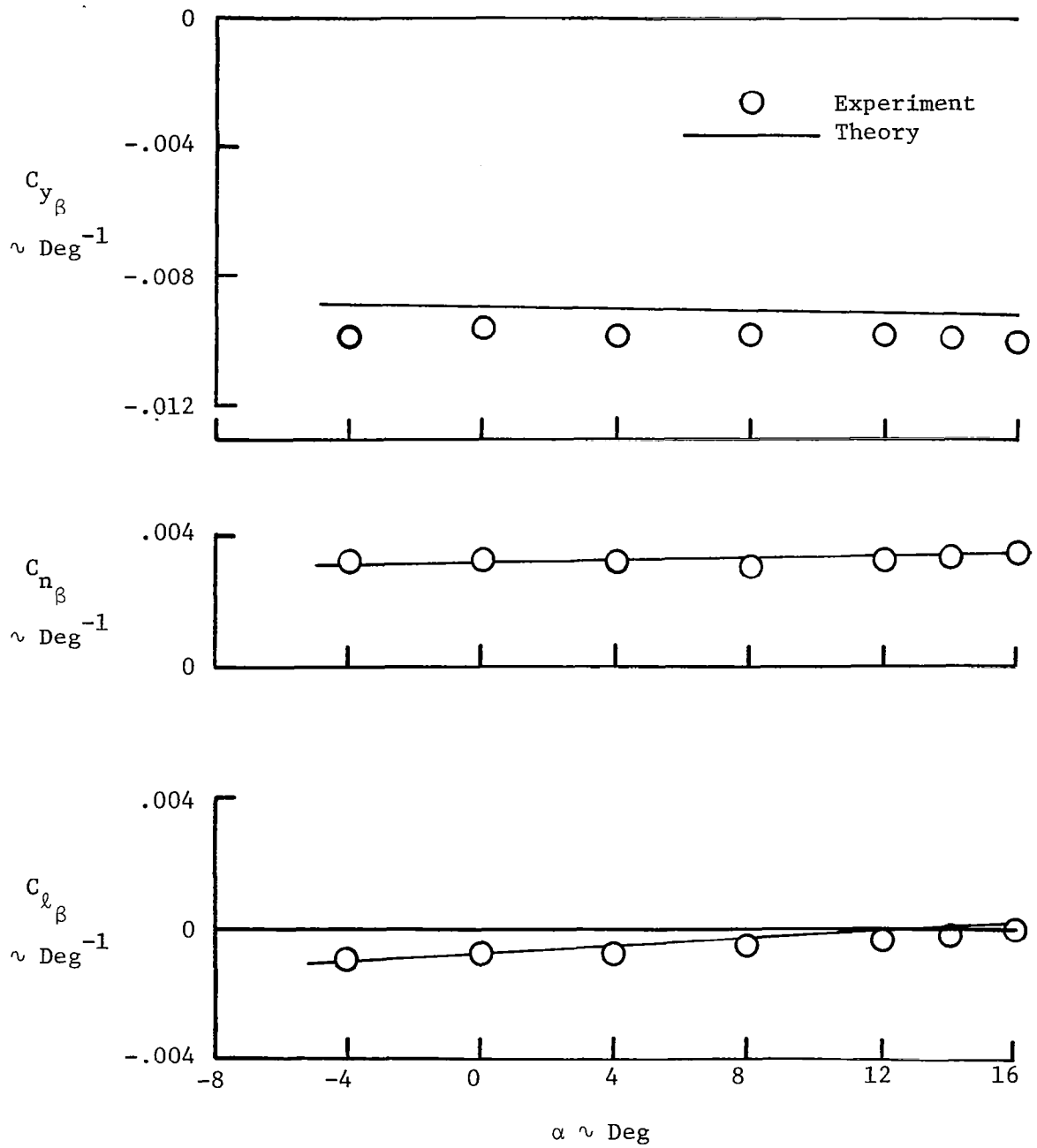

Figure 2.2: Sideslip Stability Derivatives for an Isolated Vertical and Horizontal Tail Combination

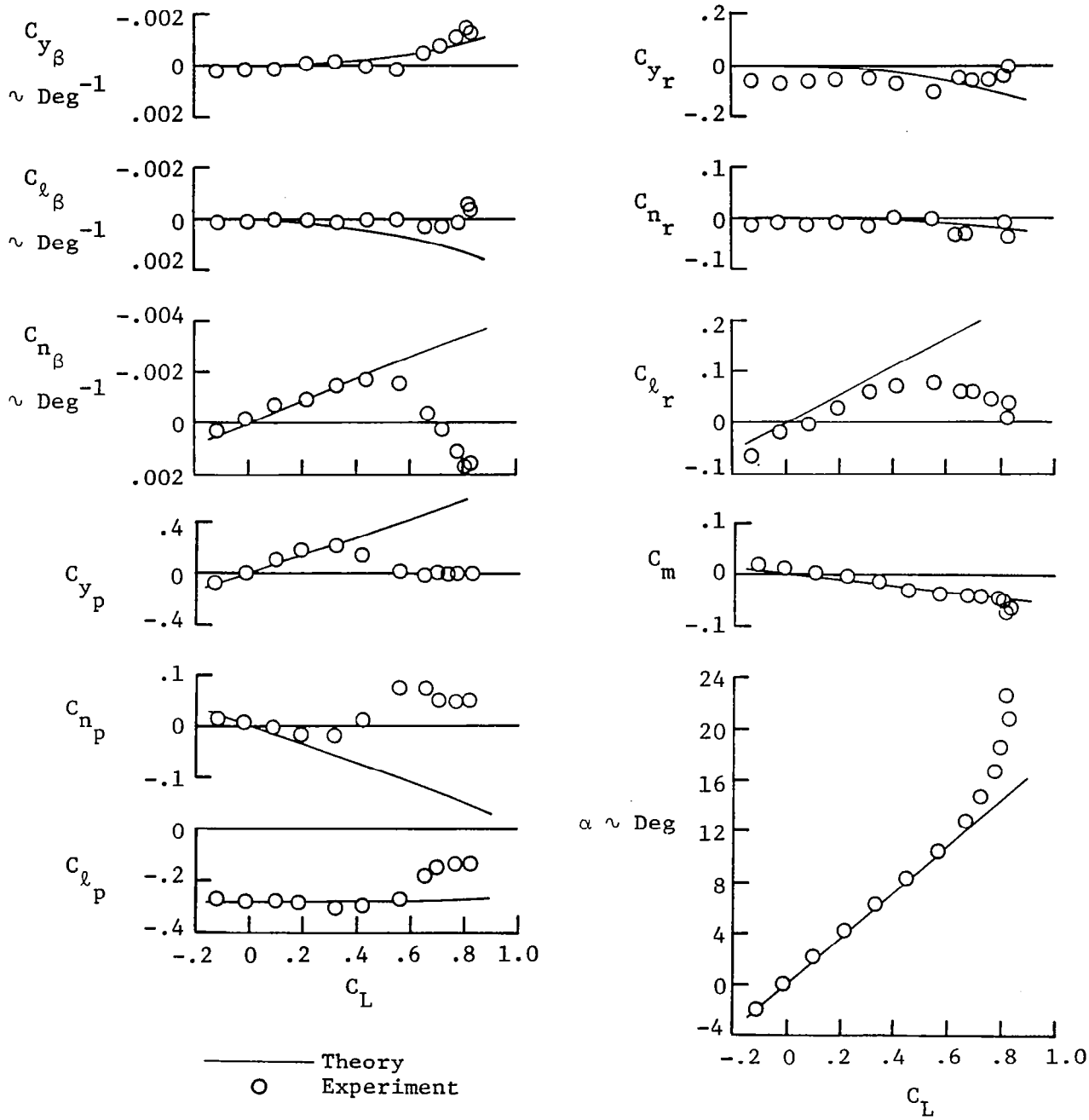

Figure 2.3: Longitudinal and Lateral-Directional Aerodynamic Characteristics of an Aspect-Ratio-3.60 Swept Wing

2.2 Parameter Variations

In this study, the unmodified (baseline) wing is represented by 60 singularities, 6 chordwise and 10 spanwise. The winglet is represented by an additional 36 singularities, 6 chordwise and 6 spanwise. Both wing and winglet are uncambered. The flow is assumed to be incompressible (zero Mach number). All forces and moments are nondimensionalized by using the geometry and area of the baseline wing.

This study consists of two parts. In part one the following winglet parameters are varied to determine the manner in which they affect the wing aerodynamic characteristics: (1) incidence angle, (2) chordwise location, (3) sweep angle, (4) taper and area, (5) taper and length, and (6) cant angle. In part two of the study, the following wing parameters are varied: (1) sweep angle, (2) twist angle, (3) dihedral angle, (4) taper ratio, and (5) span.

The plots which are presented for each parameter include lift coefficient, sideslip stability derivatives (C_{y_β}, C_{ℓ_β}, C_{n_β}), roll-rate derivatives (C_{y_p}, C_{ℓ_p}, C_{n_p}), and yaw-rate derivatives (C_{y_r}, C_{ℓ_r}, C_{n_r}). These coefficients are all plotted as function of angle of attack, and the stability derivatives are referred to the stability axes.

The planform of the baseline wing is sketched in Figure 2.4. The wing has an aspect ratio of 7, a taper ratio of 0.5, a quarter-chord sweep angle of 0°, no twist, and no dihedral. The C.G. is located at 25 percent of the MAC.

The planform of the baseline winglet is also shown in Figure 2.4. Its root section occupies 65 percent of the wing tip chord, and it is

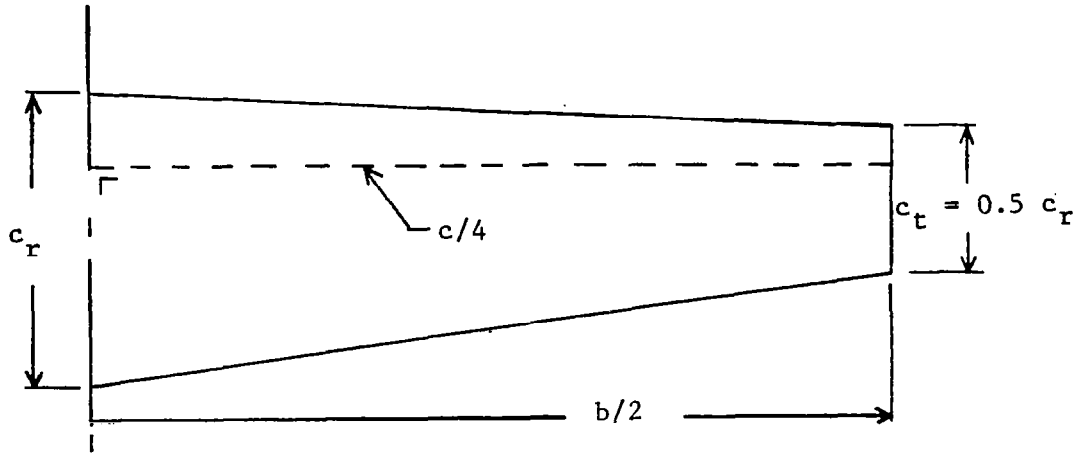

(a) Plan View of Basic Wing

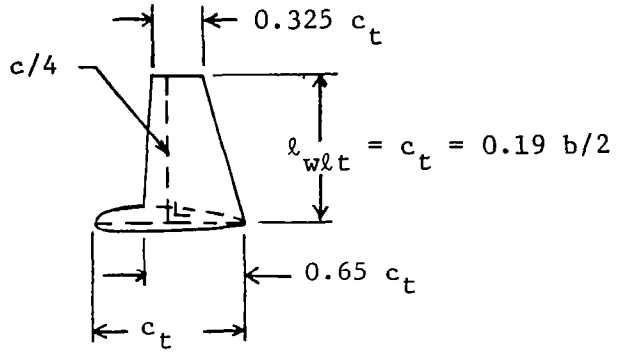

(b) Plan View of Basic Winglet

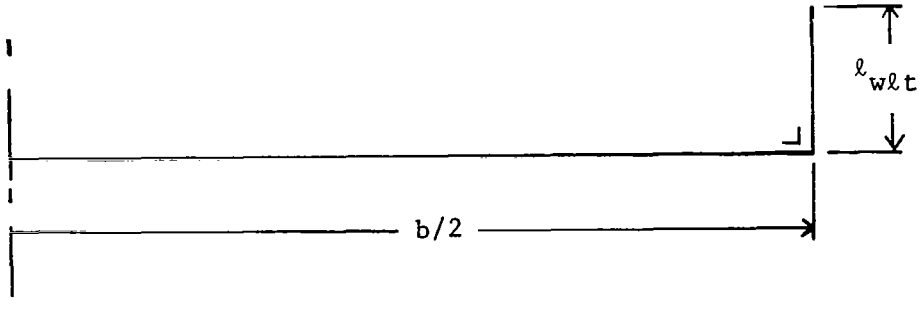

(c) Rear View of Wing and Winglet

Figure 2.4: Basic Wing and Winglet of Parametric Study

positioned on the wing such that its trailing edge intersects the wing trailing edge. The winglet has a taper ratio of 0.5, a quarter-chord sweep angle of 0°, and a length equal to the wing-tip chord. Winglet length is defined as the distance from the wing tip to the winglet-tip along a line perpendicular to the wing-tip chord line.

The first five winglet parameter variations are performed with a winglet cant angle of 0° (winglet dihedral angle is 90°).

2.2.1 Winglet Parameters

2.2.1.1 Incidence Angle

The effect of winglet incidence angle on the aerodynamic characteristics is studied with the baseline wing-winglet combination. Winglet incidence angle is varied from -5° to +5° in increments of 5°, as is shown in Figure 2.5. Lift coefficient and lateral-directional stability derivatives are plotted as function of angle of attack in Figure 2.6.

To begin with, a physical explanation will be presented for the various effects of the baseline winglet on the stability derivatives. These effects can be observed in Figure 2.6b. As a result of a positive sideslip angle, β, the normal force generated by the right winglet will exceed the force of the left winglet. Therefore, C_{y_β} becomes more negative compared to the C_{y_β} produced by the baseline wing alone. Due to this effect, the rolling moment derivative due to sideslip, C_{ℓ_β}, is also influenced in a stabilizing manner. At small angles of attack,

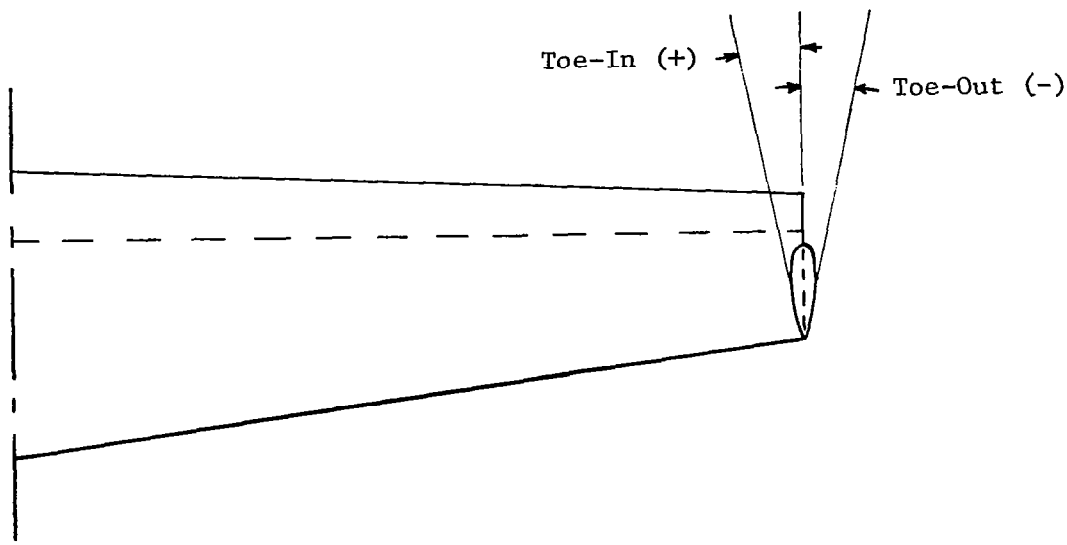

Figure 2.5: Winglet Incidence Angle Study

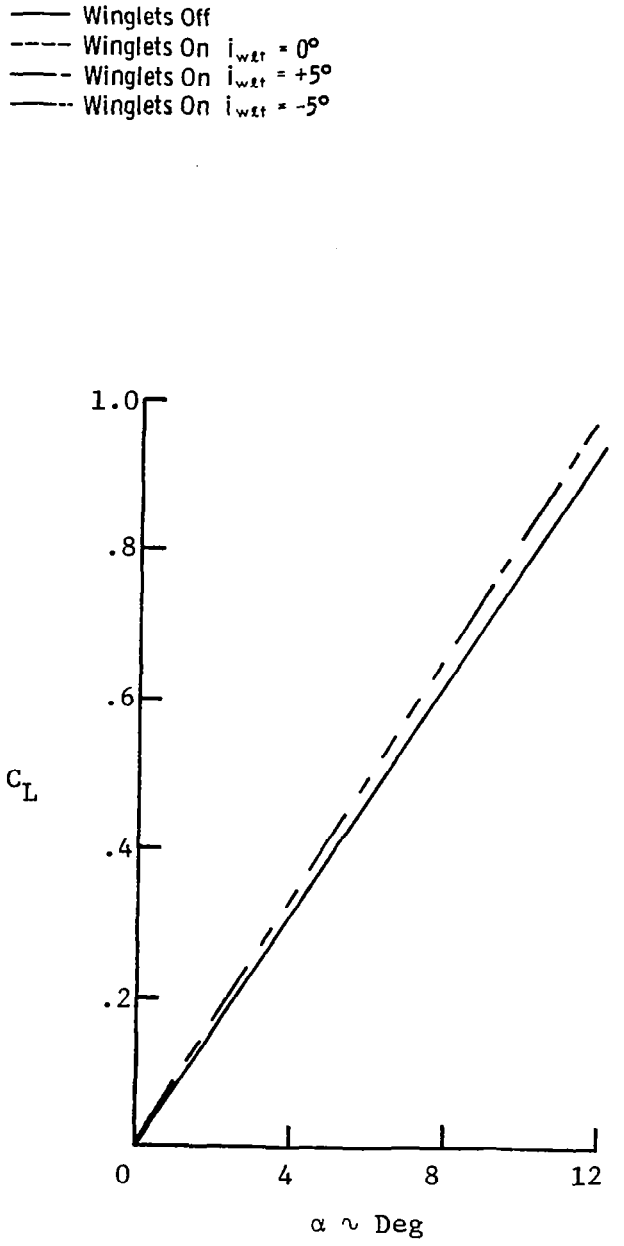

(a) Lift Curve

Figure 2.6: Effect of Winglet Incidence Angle

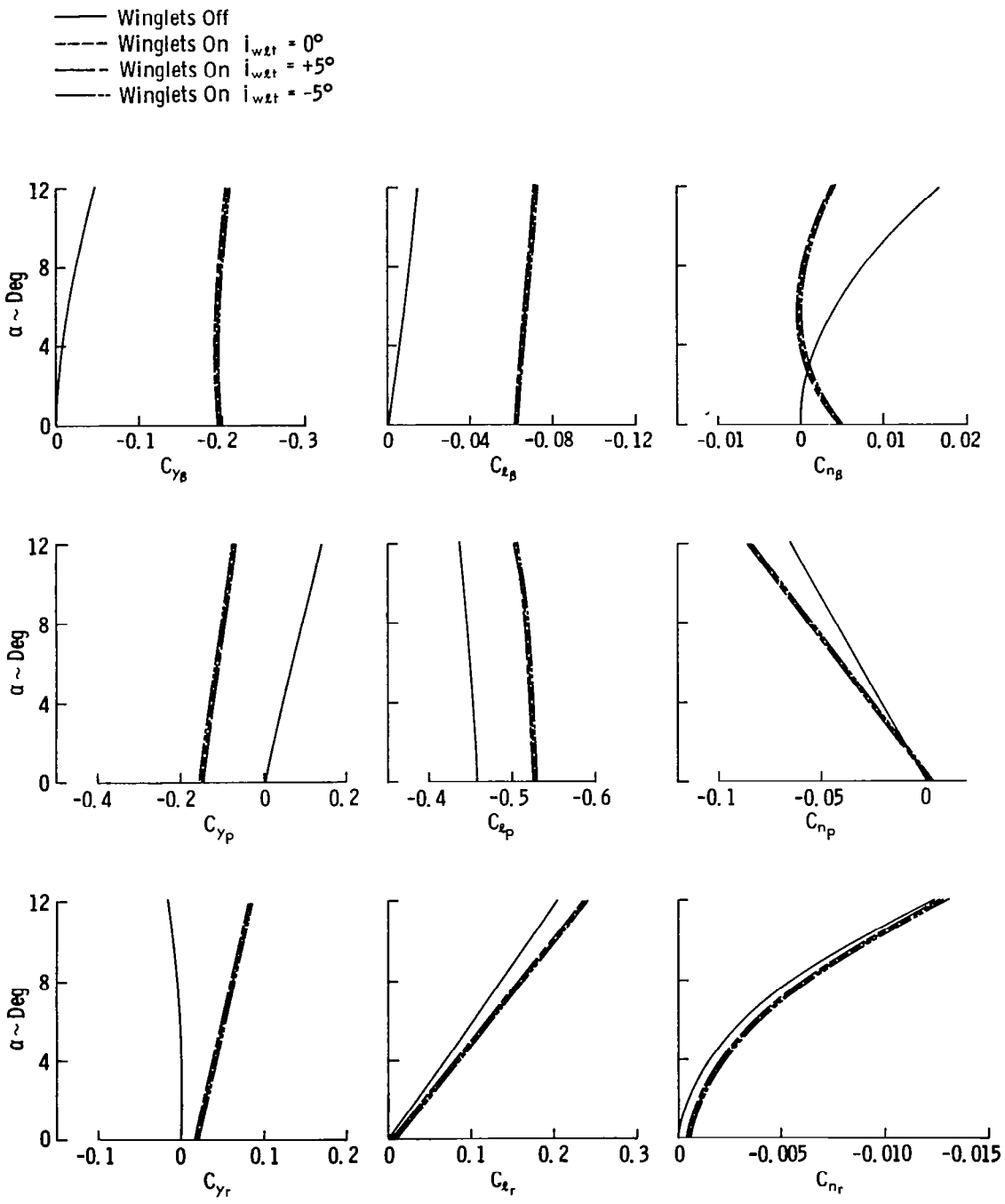

(b) Lateral-Directional Stability Derivatives

Figure 2.6: (Concluded)

the winglets slightly increase C_{n_β} because the winglet normal force vector points aft of the C.G. With increasing angle of attack, however, winglet loading increases; and, consequently, the normal force vector will rotate forward, which results in a destabilizing influence on C_{n_β}.

As a result of a positive roll rate, p, the right (left) wing experiences an increase (reduction) in angle of attack. Therefore, the aerodynamic loading of the right wing will be higher, which produces an increased loading for the right winglet compared to that of the left one. This results in a negative increment in C_{y_p} and C_{ℓ_p}, as is shown in Figure 2.6b. The winglet effect on C_{n_p} is small; this is due to the short moment arm of the force vector in relation to the C.G.

A physical explanation of the effect of yaw rate, r, on winglet normal force is that for positive r, the left winglet experiences a higher loading than the right winglet. This produces a positive increment in C_{y_r} and also C_{ℓ_r} and C_{n_r}.

In Reference 27 it is demonstrated that the effects of winglet incidence angle on wing lift-induced drag and wing-root bending moment can be significant. However, the results of Figure 2.6b show that the effects of winglet incidence angle on the lateral-directional stability derivatives of the baseline wing-winglet combination are negligible. This may not be true when the winglet cant angle is changed to an angle much larger or smaller than 0^o. Therefore, in the winglet cant angle study, the effect of incidence angle will be investigated once again.

The following four parameter variations will be performed for a constant incidence angle and cant angle of 0^o; winglet chordwise location, sweep angle, taper and area, and taper and length.

2.2.1.2 Chordwise Location

The effect of winglet chordwise location is investigated with the four winglet configurations shown in Figure 2.7. The parameter $(x/c)_{LE}$ indicates the location of the leading-edge of the winglet root chord with respect to the leading-edge of the wing-tip chord. The baseline winglet, $(x/c)_{LE} = 0.35$, is shifted forward to obtain the cases for $(x/c)_{LE} = -0.35$ and 0.0. The baseline winglet is moved aftward to obtain $(x/c)_{LE} = 0.70$. All four winglets have identical geometry and size.

The results of the analysis are shown in Figures 2.8a and 2.8b. The lift curves of the wing with the winglets in the various locations are shown in Figure 2.8a. As can be seen, the effect of the chordwise position on the lift curve slope is small.

The influence of chordwise position on the sideslip stability derivatives is substantial (Figure 2.8b). The results show that the strong stabilizing effect of the baseline winglet on C_{ℓ_β} can be reduced by moving the winglet aftward. This shift reduces the aerodynamic loading of the wing tip and the winglet due to diminished end plate effect. This causes a reduction in the level of stability of C_{y_β} and C_{ℓ_β}. This effect has also been noted in Reference 10. The aftward shift of the winglet has a stabilizing effect on C_{n_β}, as can be expected.

The shift in winglet chordwise position changes the level of wing tip suction. As a result, the side force derivatives C_{y_p} and C_{y_r} are affected. These derivatives, however, are generally not very important. The stability derivatives, C_{ℓ_p}, C_{n_p}, and C_{ℓ_r}, are hardly affected by

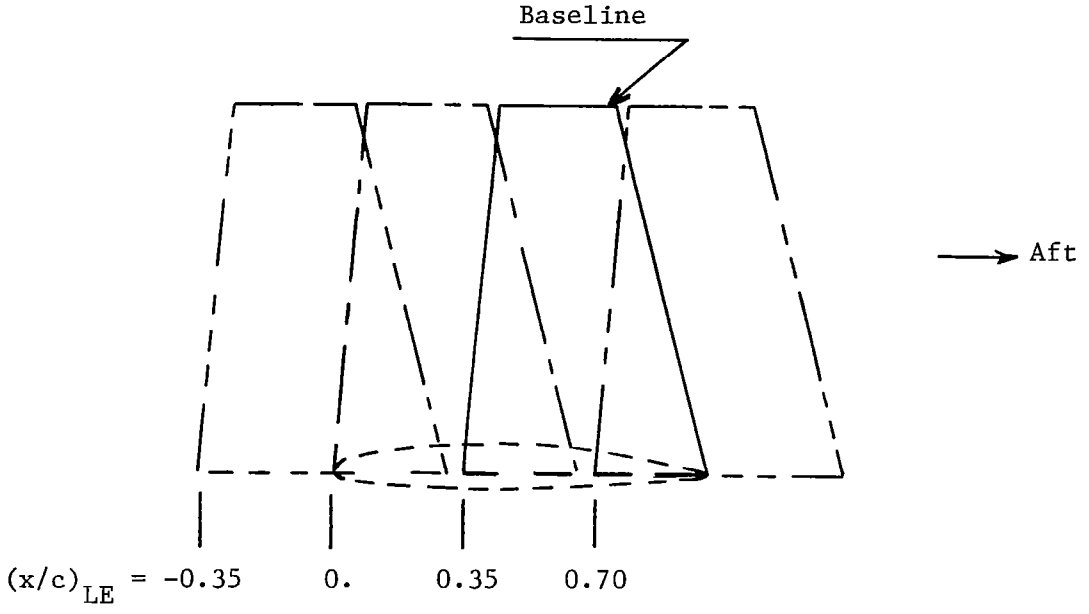

Figure 2.7: Winglet Chordwise Location Study

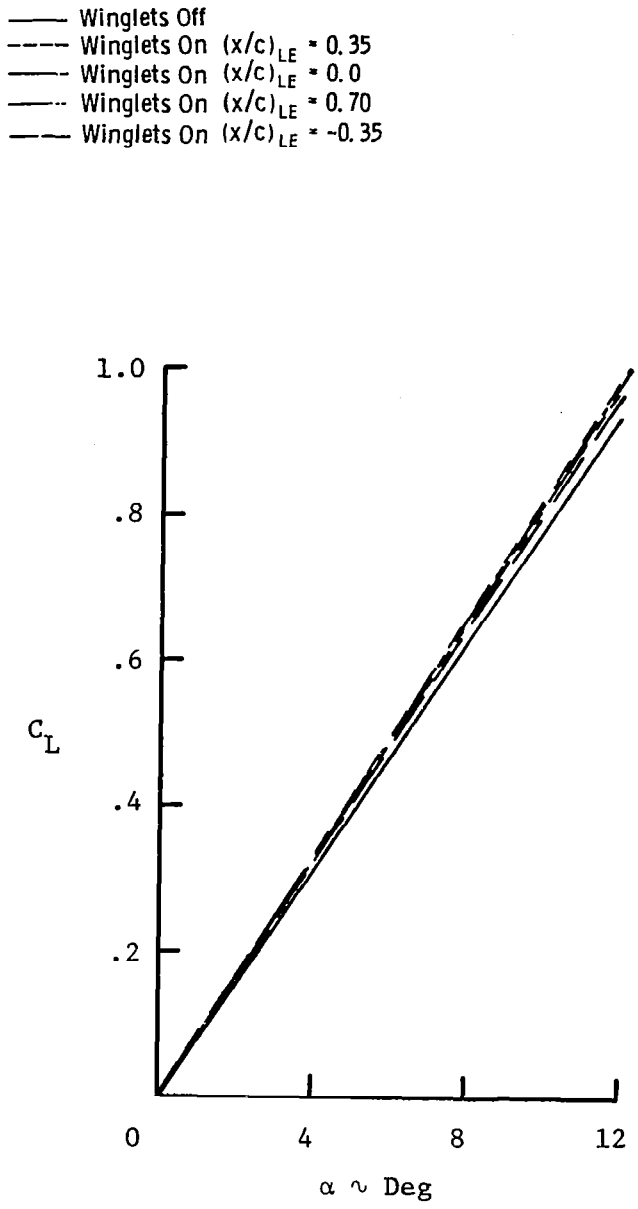

(a) Lift Curve

Figure 2.8: Effect of Winglet Chordwise Location

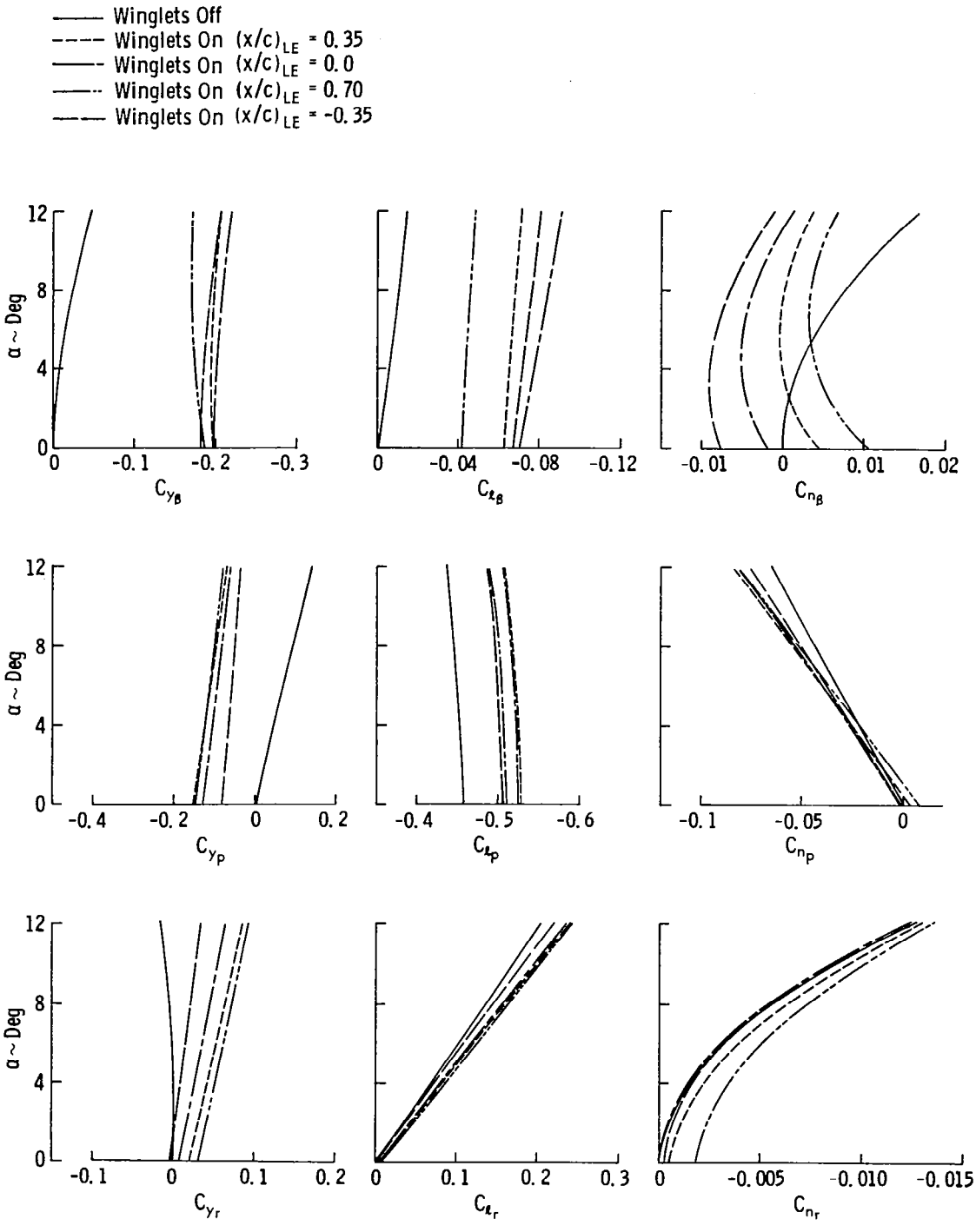

(b) Lateral-Directional Stability Derivatives

Figure 2.8: (Concluded)

the chordwise position of the winglet, while C_{n_r} is influenced in a manner similar to C_{n_β}.

A large increment in the stability of C_{ℓ_β} can result in problematic airplane lateral response characteristics. Aftward shift of the winglet reduces the increment in C_{ℓ_β} and provides a stabilizing contribution to C_{n_β} and C_{n_r} of the configuration. It is clear that from an airplane stability and control point of view, these changes are desirable. At the same time, aftward shift enhances the induced drag reduction produced by the winglet. However, moving the winglet further away from the elastic axis causes a concern for the structural dynamic and aeroelastic stability of the wing-winglet configuration.

2.2.1.3 Sweep Angle

Four different sweep angles are used to study the effect of winglet sweep on the aerodynamic characteristics. The quarter-chord sweep angles are -30°, 0° (baseline), 30°, and 60°. The winglet configurations are sketched in Figure 2.9. The winglets have the same chordwise location, length, area, and taper ratio.

The effects of winglet sweep are shown in Figures 2.10a and 2.10b. The influence of winglet sweep on the lift curve slope is negligible except at the extreme sweep angle of 60°. As the winglet is swept backward, the winglet and wing tip are unloaded, which results in a slight loss in lift for a given angle of attack.

Winglet sweep angle has a strong effect on the sideslip stability derivatives. An increase in sweep angle lowers the lift curve slope of the winglet. As a result, C_{y_β} and C_{ℓ_β} are reduced with increasing

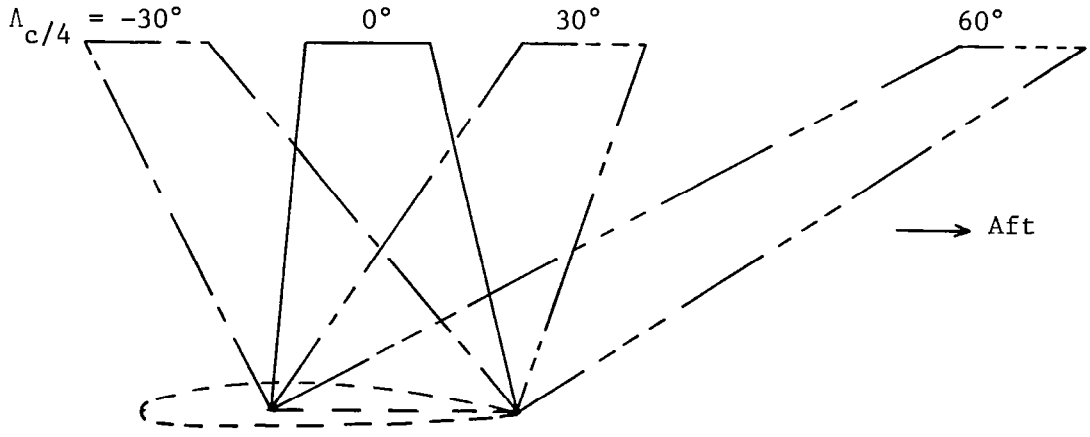

Figure 2.9: Winglet Sweep Angle Study

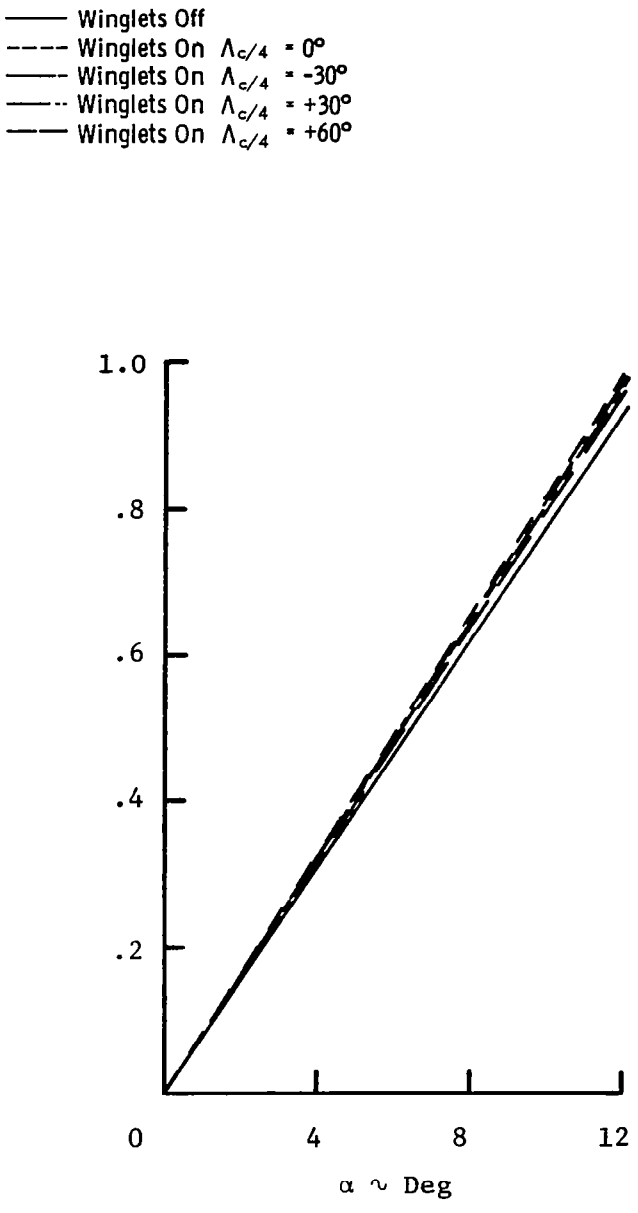

(a) Lift Curve

Figure 2.10: Effect of Winglet Sweep

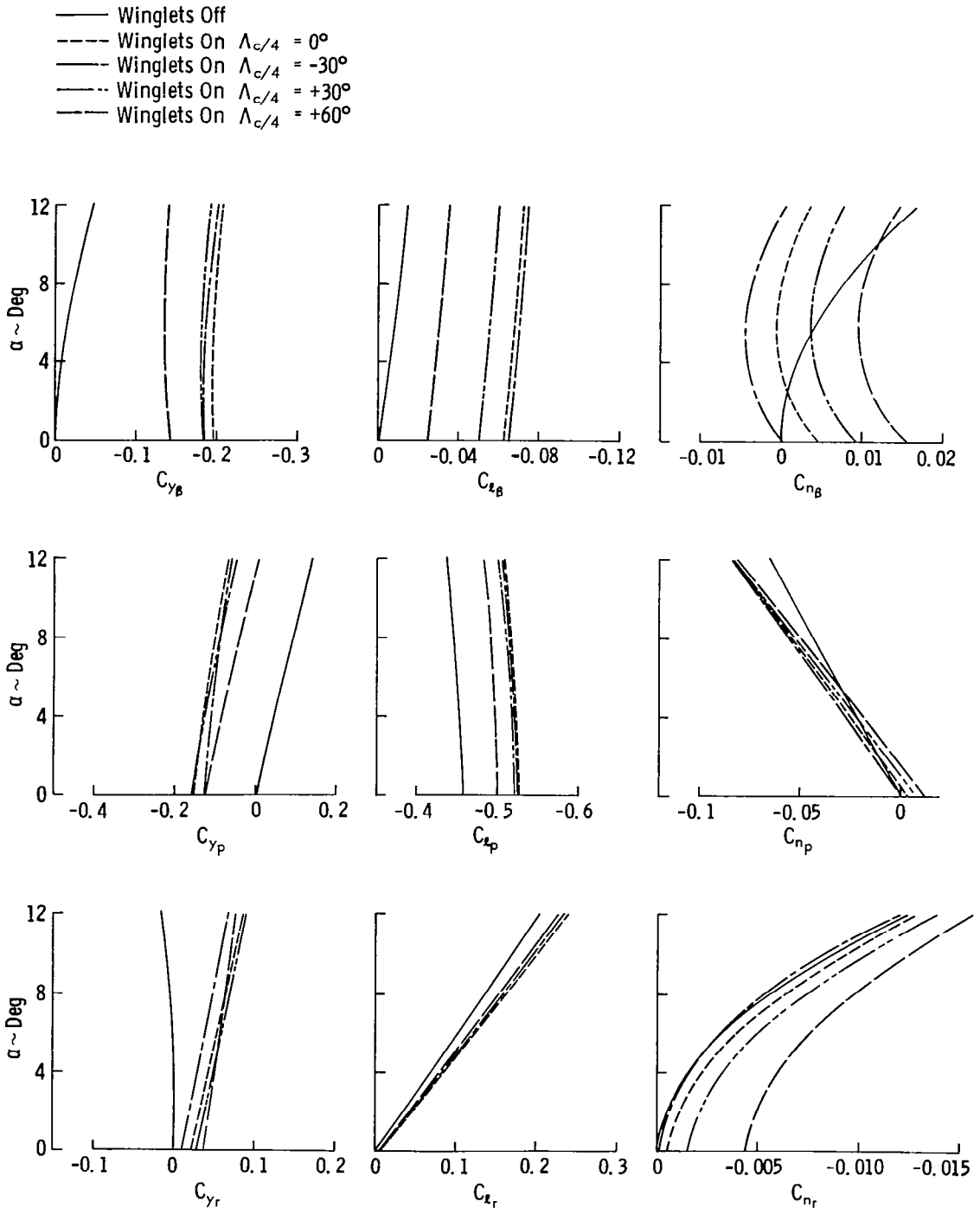

(b) Lateral-Directional Stability Derivatives

Figure 2.10: (Concluded)

backward sweep angle. Directional stability, however, increases when the winglet is swept backward due to the aftward shift of the winglet aerodynamic center. This shift also has a stabilizing influence on yaw damping.

The other derivatives are hardly affected by the change in winglet sweep, except for C_{ℓ_p} when the sweep angle reaches 60°. At that angle the stability of this derivative is reduced due to decreased loading of the wing tip.

In summary, winglet quarter-chord sweep angle has a similar effect on the stability derivatives as winglet chordwise location. Backward sweep reduces the increase in C_{ℓ_β} and provides an increment in directional stability and yaw damping. The influence of this parameter on induced drag and wing-root bending moment is minimal.

The winglet parameters investigated thus far include incidence angle, chordwise location, and sweep. Winglet area, length, taper ratio, and cant angle have been kept constant. Winglet sweep angle and chordwise location have a very significant influence on the stability derivatives of the configuration. Therefore, these parameters will be kept constant in the following analyses.

2.2.1.4 Taper and Area

For a winglet with a constant length and root chord, a change in winglet taper will affect winglet area. Therefore, the combined effect of these two parameters is studied in this section. The three winglet configurations are sketched in Figure 2.11. The taper ratios are 1.0, 0.5 (baseline), and 0. The taper ratio is adjusted by modifying the

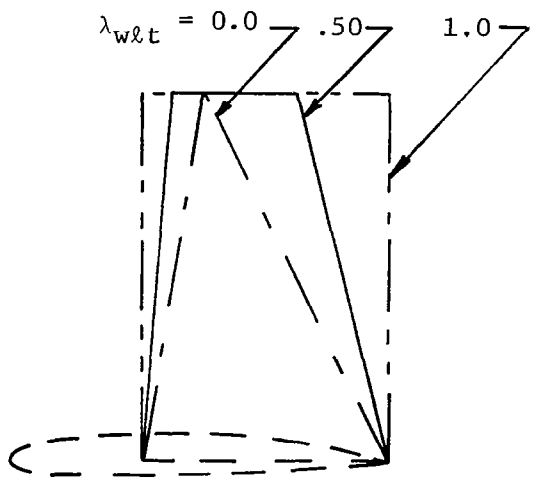

Figure 2.11: Winglet Taper and Area Study

——— Winglets Off
– – – – Winglets On $\lambda = 0.5$, $S/S_o = 1.0$
——— Winglets On $\lambda = 0.0$, $S/S_o = 0.667$
——— Winglets On $\lambda = 1.0$, $S/S_o = 1.333$

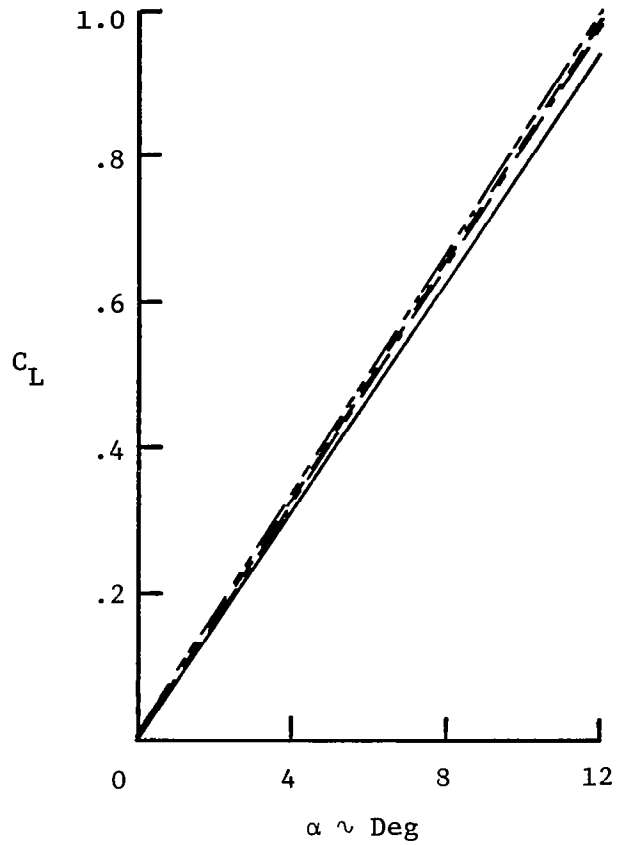

(a) Lift Curve

Figure 2.12: Effect of Winglet Taper and Area

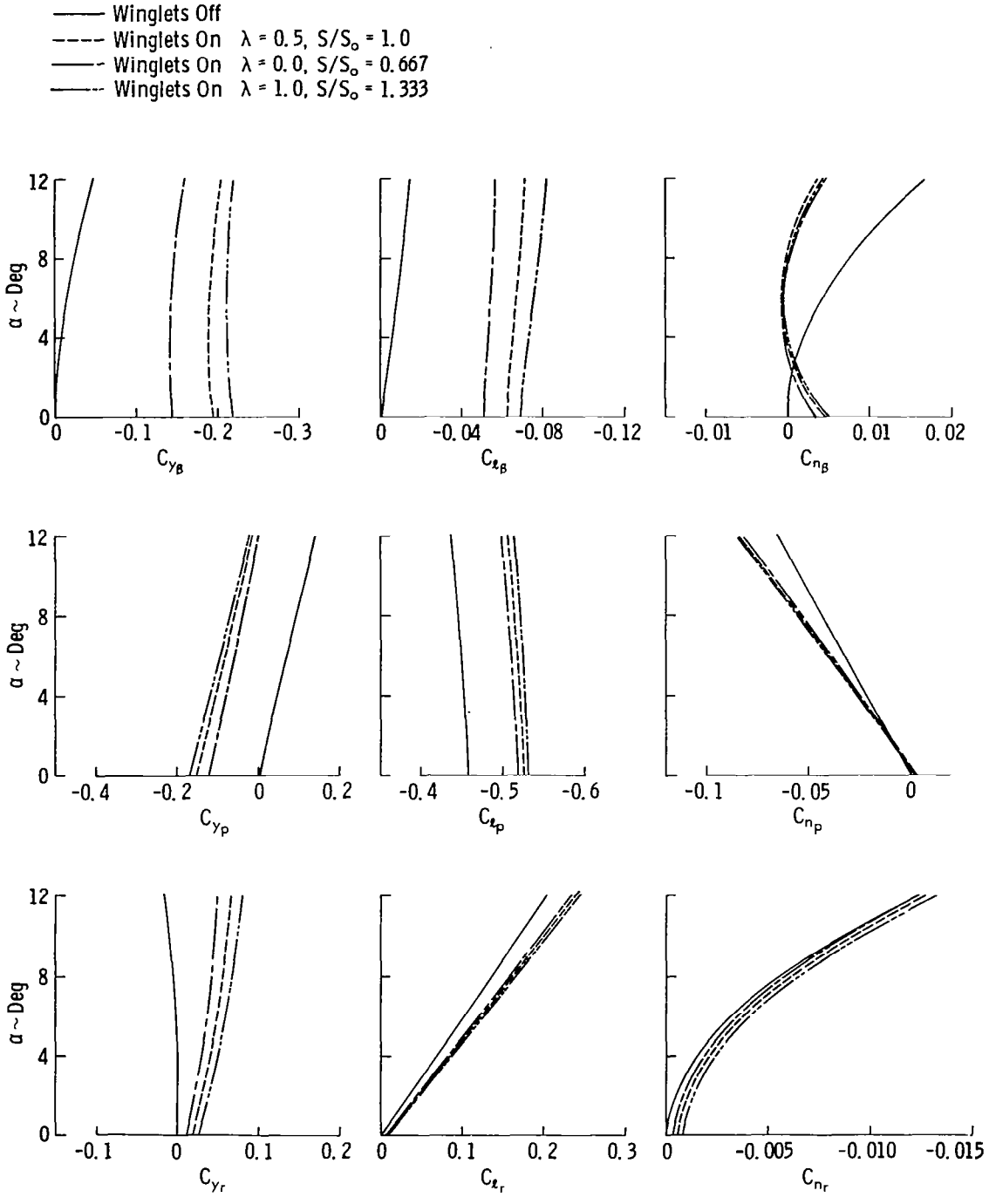

(b) Lateral-Directional Stability Derivatives

Figure 2.12: (Concluded)

length of the winglet tip chord. All three winglets have the same root chord, chordwise location, quarter-chord sweep angle, and length. As mentioned, the planform areas are not identical. Their relative areas, nondimensionalized by the baseline planform area, are 1.333, 1.0, and 0.667.

The only derivatives significantly affected by the changes in taper and area are C_{y_β} and C_{ℓ_β}, as shown in Figure 2.12b. In this study, increased taper reduces the planform area and therefore augments winglet aspect ratio. The reduction in area reduces C_{y_β}, while the increase in aspect ratio causes a slight increment in C_{y_β}. However, the total effect is a reduction in C_{y_β}. The reduction in C_{ℓ_β} is the result of this reduction in C_{y_β}.

According to References 27 and 28 the effects of taper ratio and planform area on induced drag and wing-root bending moment are very small.

2.2.1.5 Taper and Length

The three winglets selected for this study are sketched in Figure 2.13. Their lengths, normalized by the wing-tip chord, are 0.75, 1.0 (baseline), and 1.5. For this parameter study, chordwise location, quarter-chord sweep angle, and planform area are kept constant. Winglet taper ratio does change, however. The taper ratios are 1.0, 0.5, and 0.0, respectively. The corresponding winglet aspect ratios are 1.15, 2.05, and 4.61.

The results of this analysis are shown in Figures 2.14a and 2.14b. As can be seen, the only derivatives significantly influenced by a

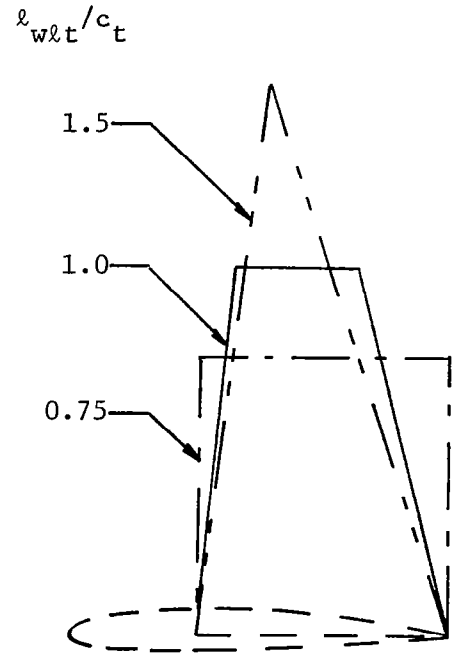

Figure 2.13: Winglet Taper and Length Study

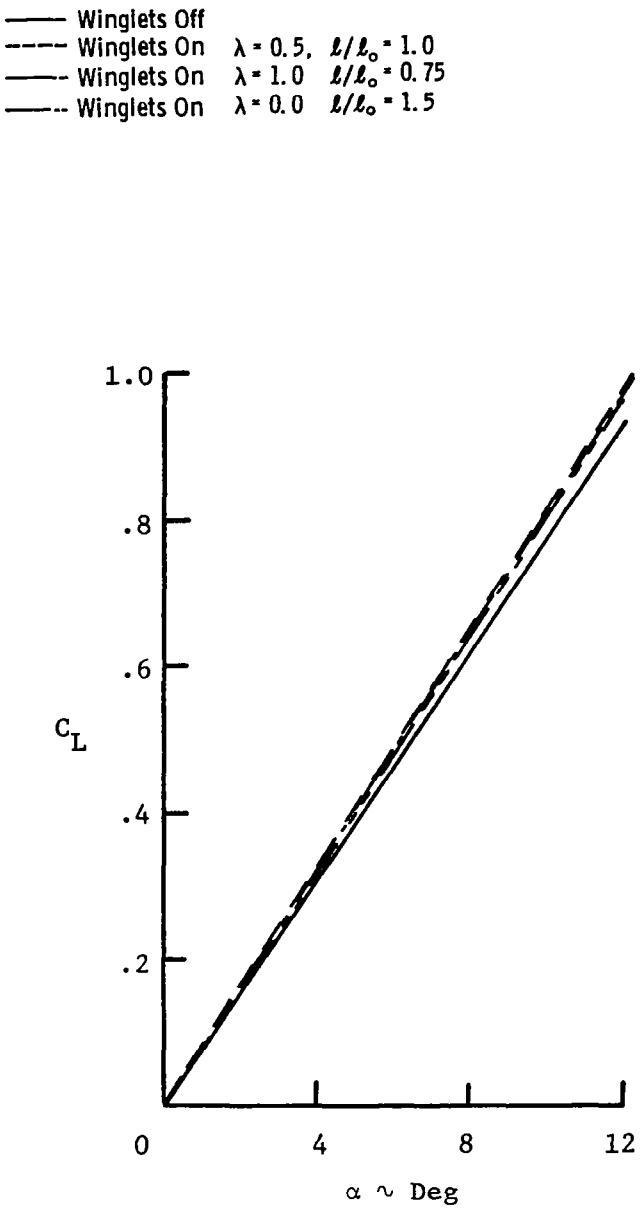

(a) Lift Curve

Figure 2.14: Effect of Winglet Taper and Length

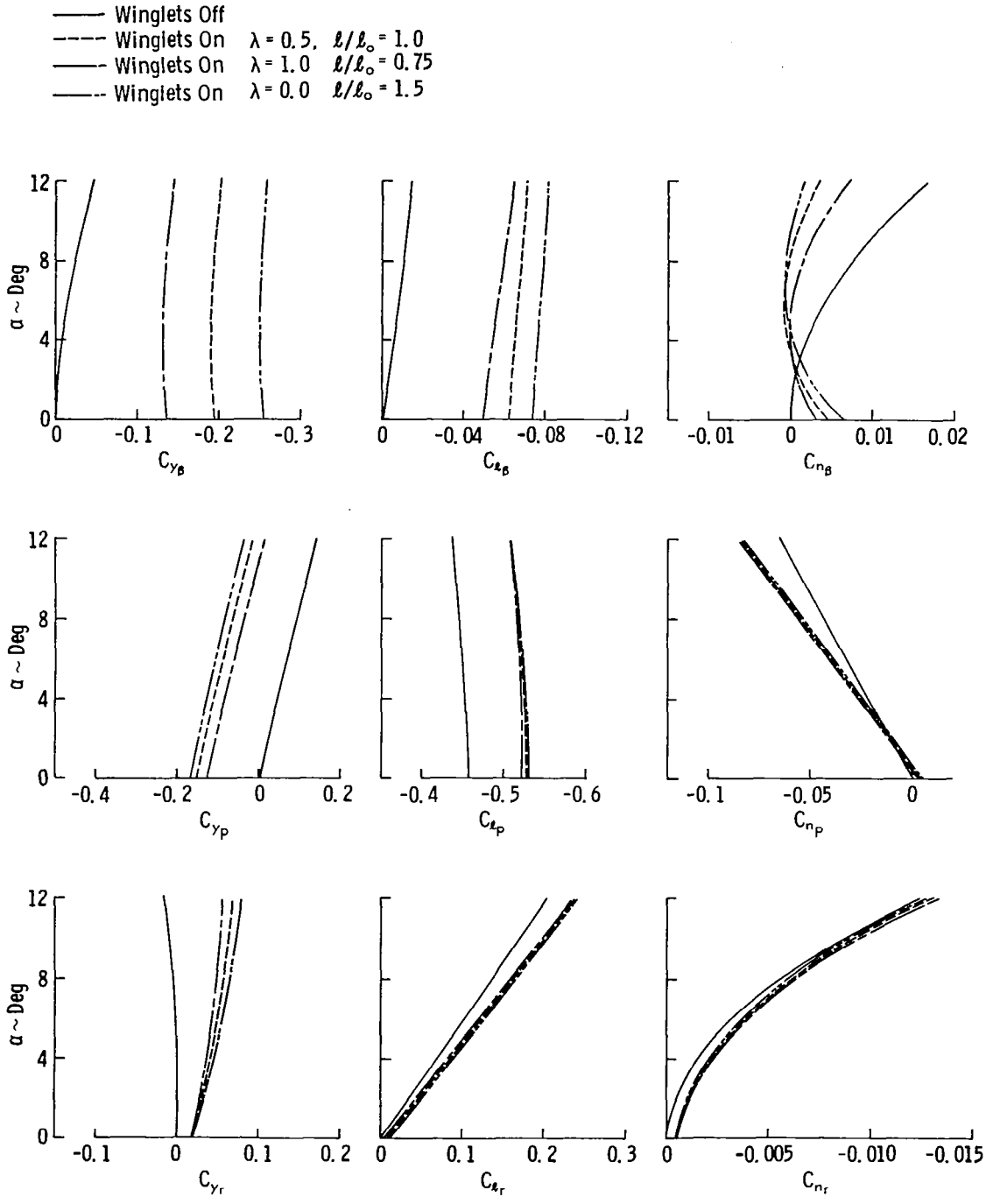

(b) Lateral-Directional Stability Derivatives

Figure 2.14: (Concluded)

change in winglet taper and length are C_{y_β} and C_{ℓ_β}. The combined effect of modifying taper and length is a change in winglet aspect ratio. The stability derivative C_{y_β} is approximately identical to the lift curve slope, C_{L_α}, of the winglet. Polhamus' equation shows the important effect of aspect ratio on lift curve slope, and this is also indicated by the change in C_{y_β} with winglet aspect ratio.

The change in winglet length, as illustrated in Figure 2.13, is not very realistic. Figure 2.15 demonstrates a winglet length reduction as it would appear in "reality." In this case winglet length, taper, and planform area are modified. The effects of this type of modification can be observed in Figure 2.16. The reduction in length has a very significant influence on C_{y_β} and C_{ℓ_β}. This is due to the combined effects of diminished area and aspect ratio.

Winglet length has an important effect on lift-induced drag and wing-root bending moment. The longer winglet pictured in Figure 2.15 produces an increase in induced efficiency. However, it also causes an increment in wing-root bending moment and a significant increase in dihedral effect, as shown in Figure 2.16.

2.2.1.6 Cant Angle

In this study, winglet cant angle is varied, while the geometry, area, and chordwise location of the winglet are identical to those of the baseline winglet. The cant angles are -20°, 0° (baseline), and +20° (Figure 2.17).

The lift curve is shown in Figure 2.18a. An increase in lift curve slope can be noted due to outward cant of the winglet. This can

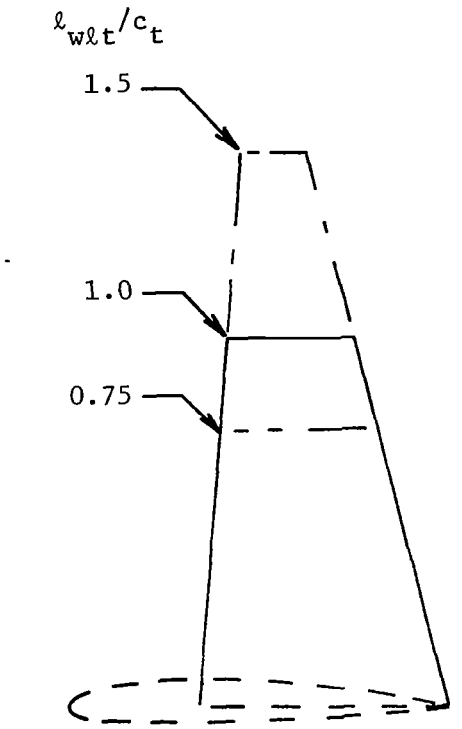

Figure 2.15: Winglet Length Study

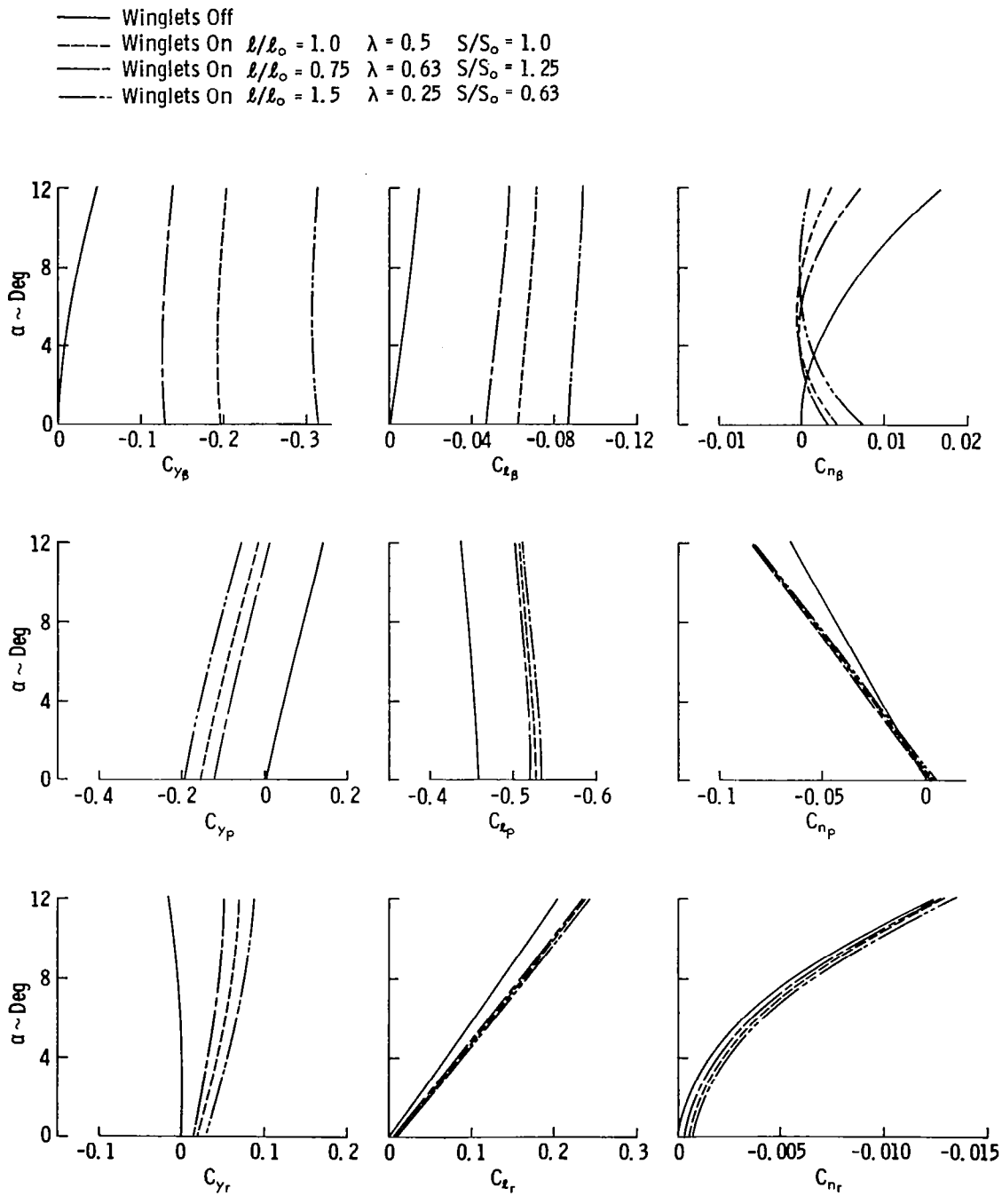

Figure 2.16: Effect of Winglet Length

be attributed to the contribution of the winglet normal force in the lift direction.

The influence of cant angle on the side force derivative, C_{y_β}, is small, as can be seen in Figure 2.18b. Both outward and inward cant produce a reduction in C_{y_β}. Cant angle, however, has a powerful effect on the lateral stability of the wing configuration. The increase in C_{ℓ_β} due to winglets reduces significantly when the winglets are canted inward. This effect is also reported in References 17, 18, and 20. Directional stability is hardly influenced by cant angle.

Another stability derivative strongly affected by cant angle is the roll damping derivative, C_{ℓ_p}. Outward cant enhances the loading of the winglet and therefore roll damping.

Winglet cant angle has a strong effect on induced drag. Induced drag will decrease with increasing cant, in part due to the increase in wing aspect ratio. At the same time, wing-root bending moment gets larger with increasing cant angle. However, it is possible to realize gains in induced efficiency at a very small penalty in root bending moment if the winglet is canted inward. As shown, an additional advantage of inward cant is a smaller increment in C_{ℓ_β} due to the addition of a winglet.

As mentioned previously, the influence of winglet incidence angle on lateral-directional stability derivatives should be reexamined for the outward canted winglet. For the baseline winglet with 20° cant, winglet incidence angle is changed from -5° to 5° in increments of 5°. In Figure 2.19, the derivatives are plotted as function of angle of attack. The results indicate that the influence of incidence angle

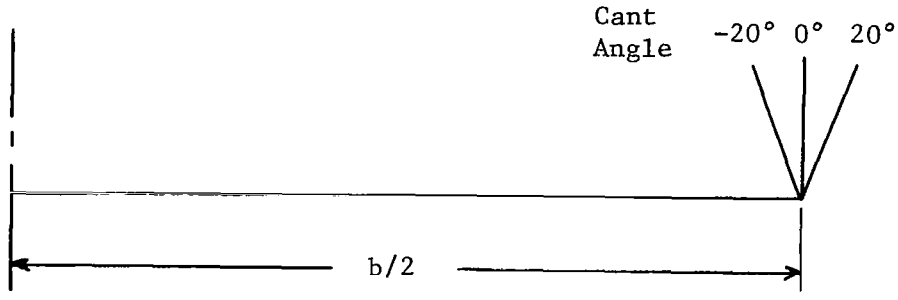

Figure 2.17: Winglet Cant Angle Study

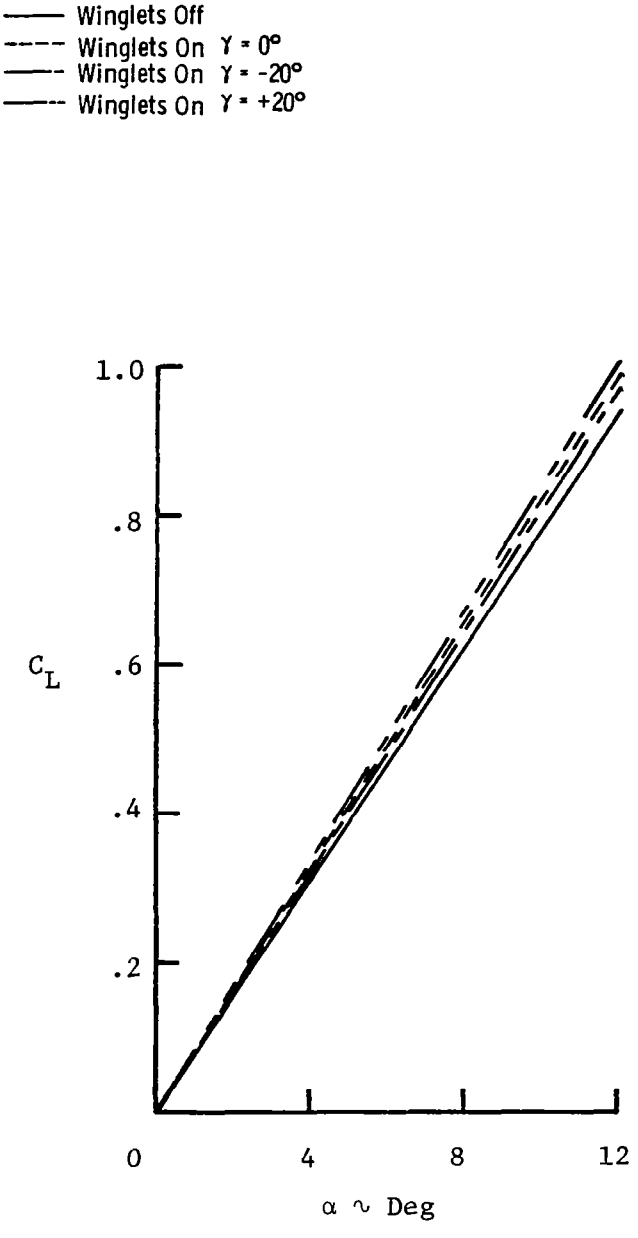

(a) Lift Curve

Figure 2.18: Effect of Winglet Cant Angle

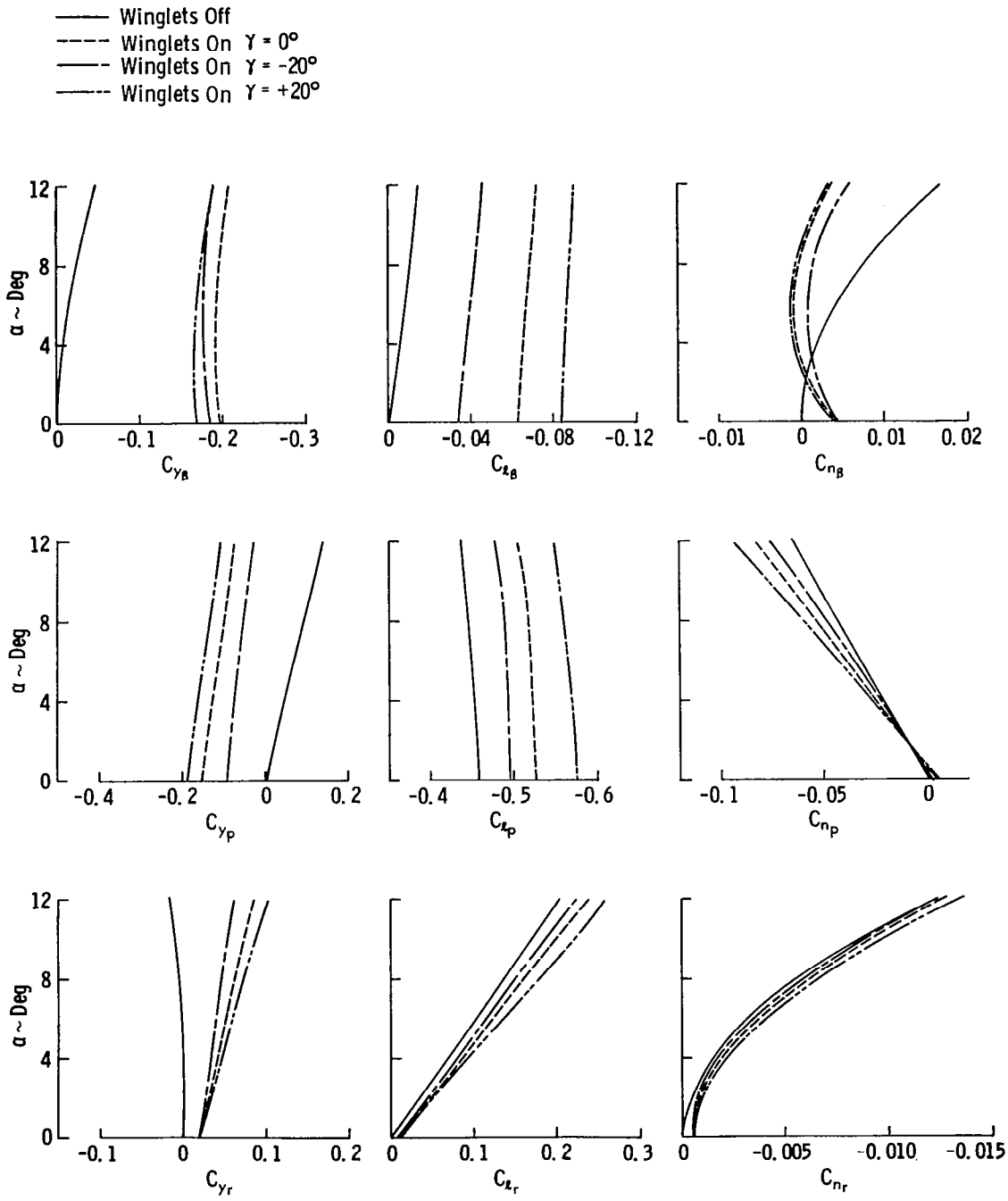

(b) Lateral-Directional Stability Derivatives

Figure 2.18: (Concluded)

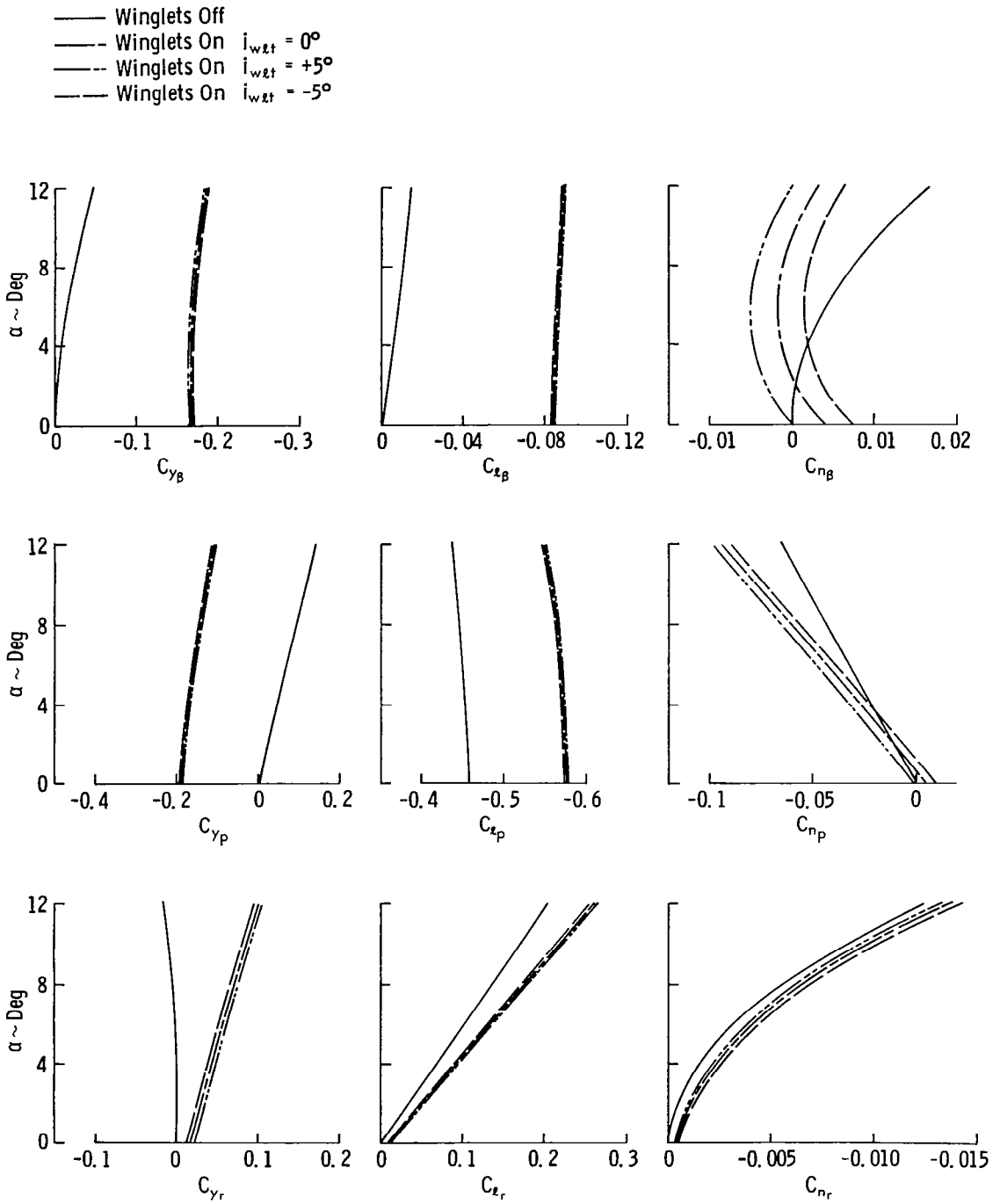

Figure 2.19: Effect of Winglet Incidence Angle (γ = 20°)

becomes more significant when the winglet is canted outward (or inward). Especially the yawing moment derivatives are affected, while the side force and rolling moment derivatives are virtually unchanged.

In summary, the effect of winglet incidence angle on the lateral-directional derivatives is very small for a winglet cant angle of 0°. When the winglet is canted inward or outward, the incidence angle starts to influence the yawing moment derivatives more noticeably. However, the overall effect appears to be small. Consequently, the incidence angle can be optimized to obtain, for example, maximum induced efficiency, minimum wing-root bending moment, or maximum wake modification, without significantly affecting airplane stability and control.

2.2.2 Wing Parameters

In the previous section, winglet parameters were varied to study their effects on the aerodynamic characteristics of a baseline wing. In this section, however, the winglet is kept identical to the baseline winglet as much as possible; and wing parameters are varied. The results of the parameter variation are plotted in a different manner compared to the previous section to identify the effects more clearly. In this section, Δ(derivative) is plotted as a function of angle of attack, where Δ(derivative) represents the change in a stability derivative for a particular wing due to addition of the winglet.

2.2.2.1 Sweep Angle

Three different wing configurations are used to analyze the effects of wing sweep angle on the aerodynamic characteristics of the winglet. The three wing configurations are shown in Figure 2.20; and the quarter-chord sweep angles are -20°, 0° (baseline), and 20°. Wing area, taper ratio, and span are unchanged. The winglet is identical to the baseline winglet for all three wing configurations (see Figure 2.4).

The results are shown in Figure 2.21. Backward and forward sweep results in a location change of the winglet aerodynamic center in relation to the C.G. Therefore, significant effects can be observed in the yawing moment derivatives C_{n_β}, C_{n_p}, and C_{n_r}. The results indicate that if the wing is swept back, it is possible to realize increases in directional stability and yaw damping. The effects of wing sweep on the winglet contribution to the other derivatives are relatively small.

Sweepback results in higher loading near the wing tip. As a result, a winglet is more effective on a swept wing than on an unswept wing.

2.2.2.2 Twist Angle

The effect of wing twist on the winglet contribution to the stability derivatives is analyzed with three wing configurations. The three wings have a twist angle of 0° (baseline), -2.5°, and -5°. In every other respect the three wings and winglets are identical to the baseline wing-winglet configuration shown in Figure 2.4.

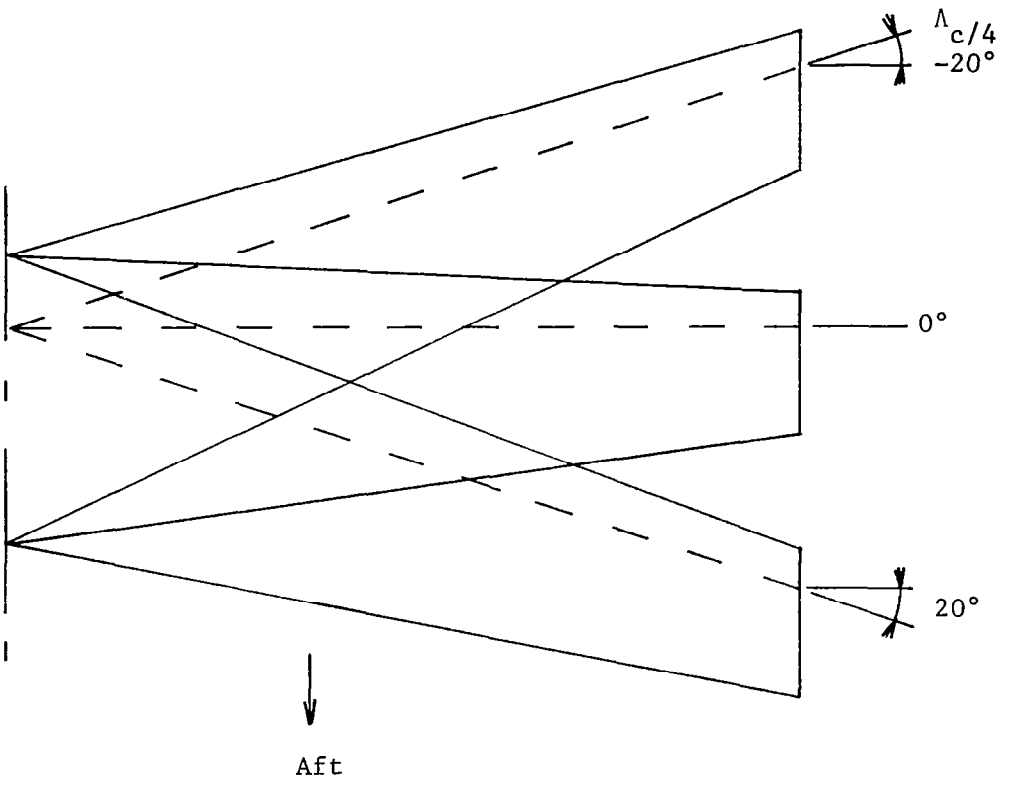

Figure 2.20: Wing Sweep Study

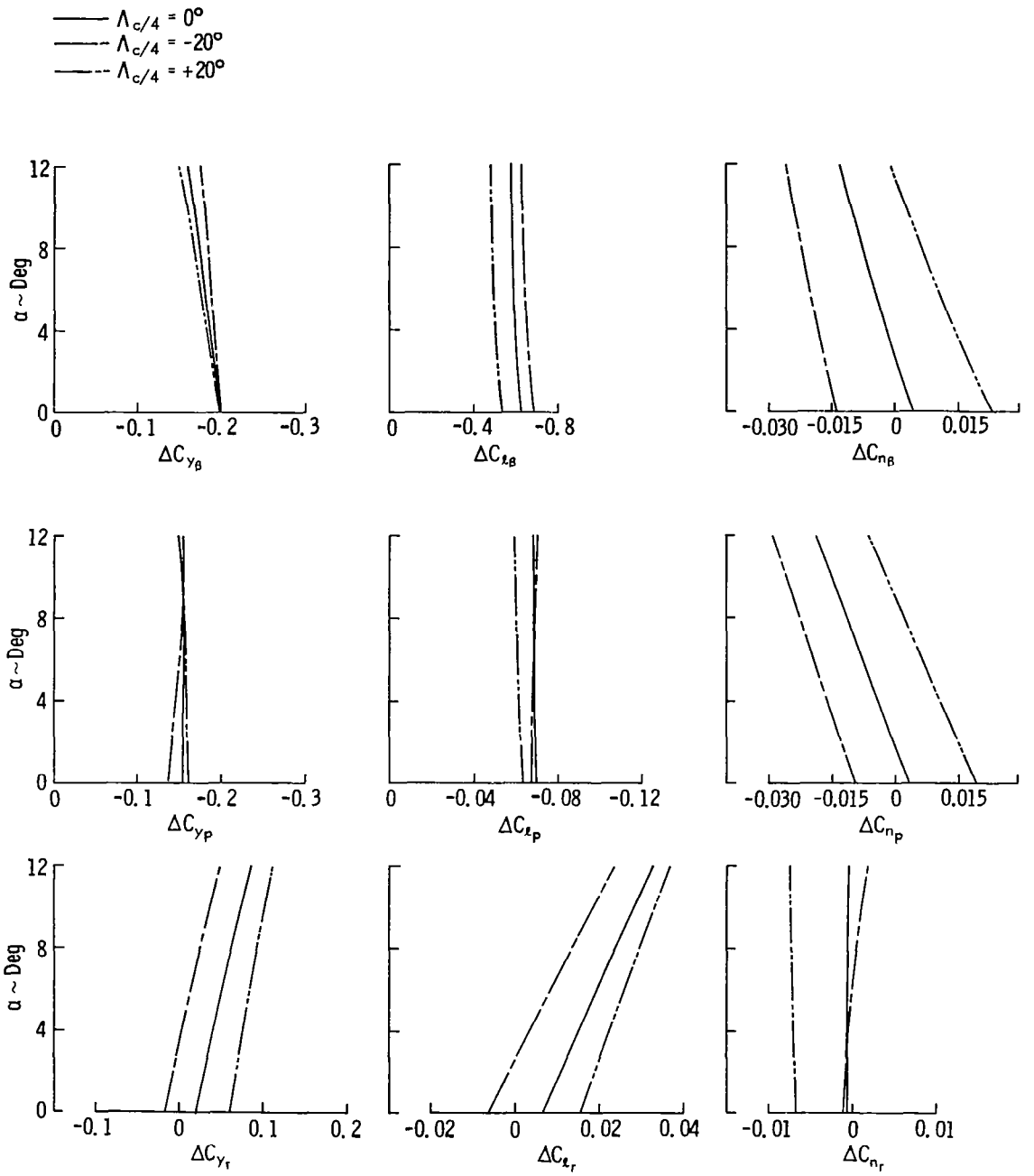

Figure 2.21: Effect of Wing Sweep on Winglet Contribution to Stability Derivatives

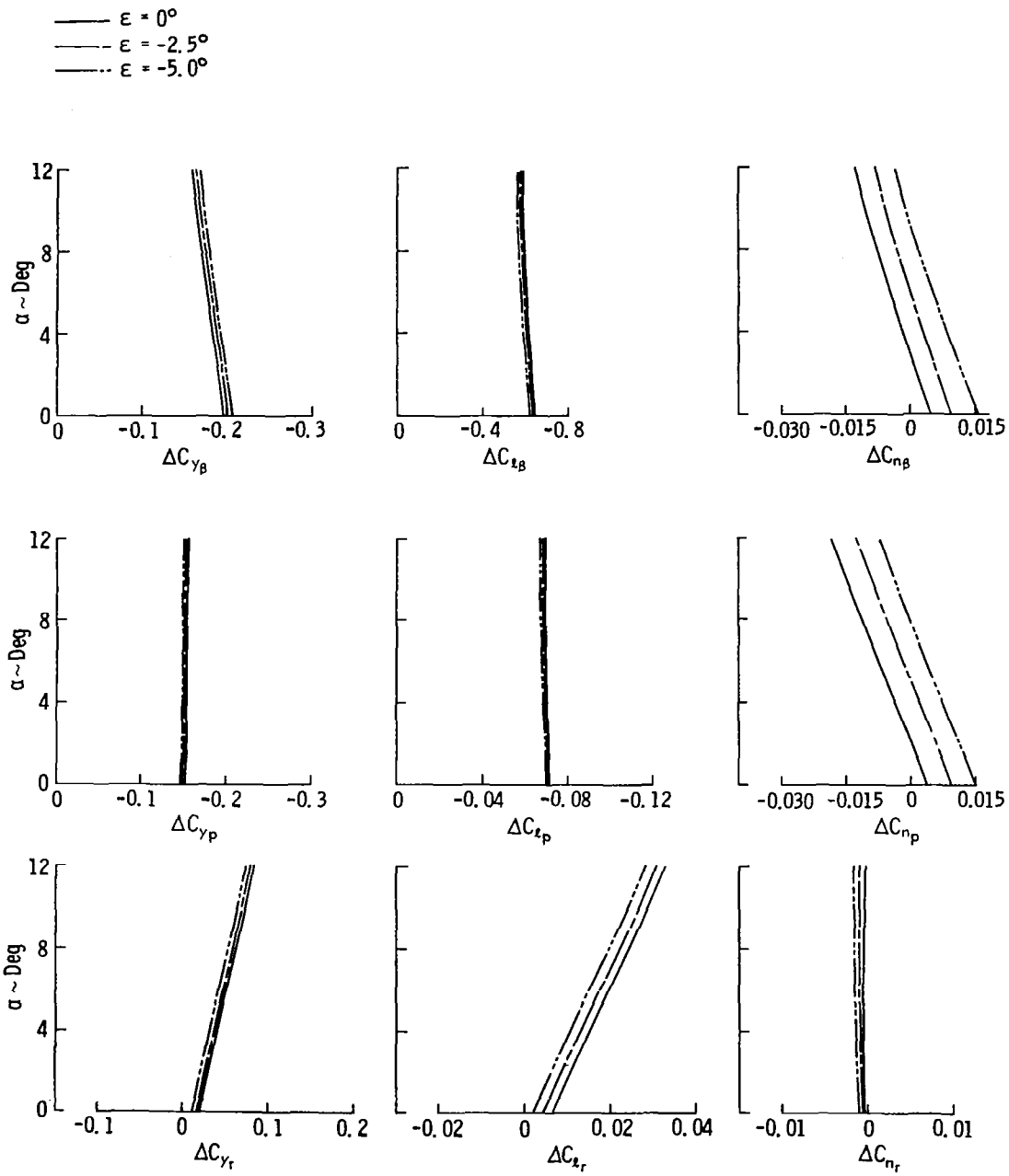

Figure 2.22: Effect of Wing Twist on Winglet Contribution to Stability Derivatives

When washout (negative twist angle) is incorporated in the wing, the loading near the wing tip is reduced. It is clear that due to the decreased outboard aerodynamic loading, the winglet loading is reduced. As a result, the winglet normal force vector will rotate in an aftward direction, producing a more positive yawing moment for a positive sideslip angle, β, or positive roll rate, p.

From the results of Figure 2.22, it can be observed that washout has a negligible influence on the winglet contribution to the other stability derivatives. However, the reduction in lift-induced drag from a winglet has been shown to decrease as washout is increased (Reference 27).

2.2.2.3 Dihedral Angle

The parameter variations in Section 2.2.1 are performed with the baseline wing, which does not have any dihedral. In this study, the baseline wing is rotated +5° about the wing-root, as is shown in Figure 2.23. Winglet dihedral angle is unchanged. The change in dihedral angle also has an effect on the vertical location of the C.G. In the case of 5° dihedral, the C.G. is shifted upward 0.039 b/2.[1]

The results of Figure 2.24 show that the influence of wing dihedral is small, except for the winglet contributions to C_{y_β}, C_{ℓ_β}, and C_{y_p}. The change in C_{ℓ_β} is the most interesting. For low angles of

[1]This value is obtained as follows:

$$\Delta z_{C.G.} = \bar{y_c} \tan\Gamma = \frac{1}{3}\left(\frac{1+2\lambda}{1+\lambda}\right)\frac{b}{2}\tan\Gamma = 0.039\ b/2.$$

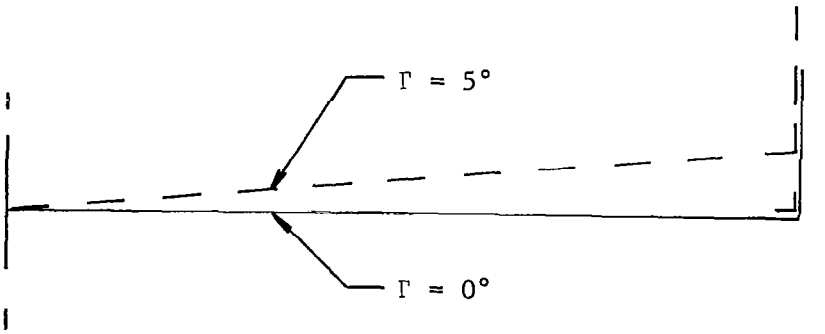

Figure 2.23: Wing Dihedral Angle Study

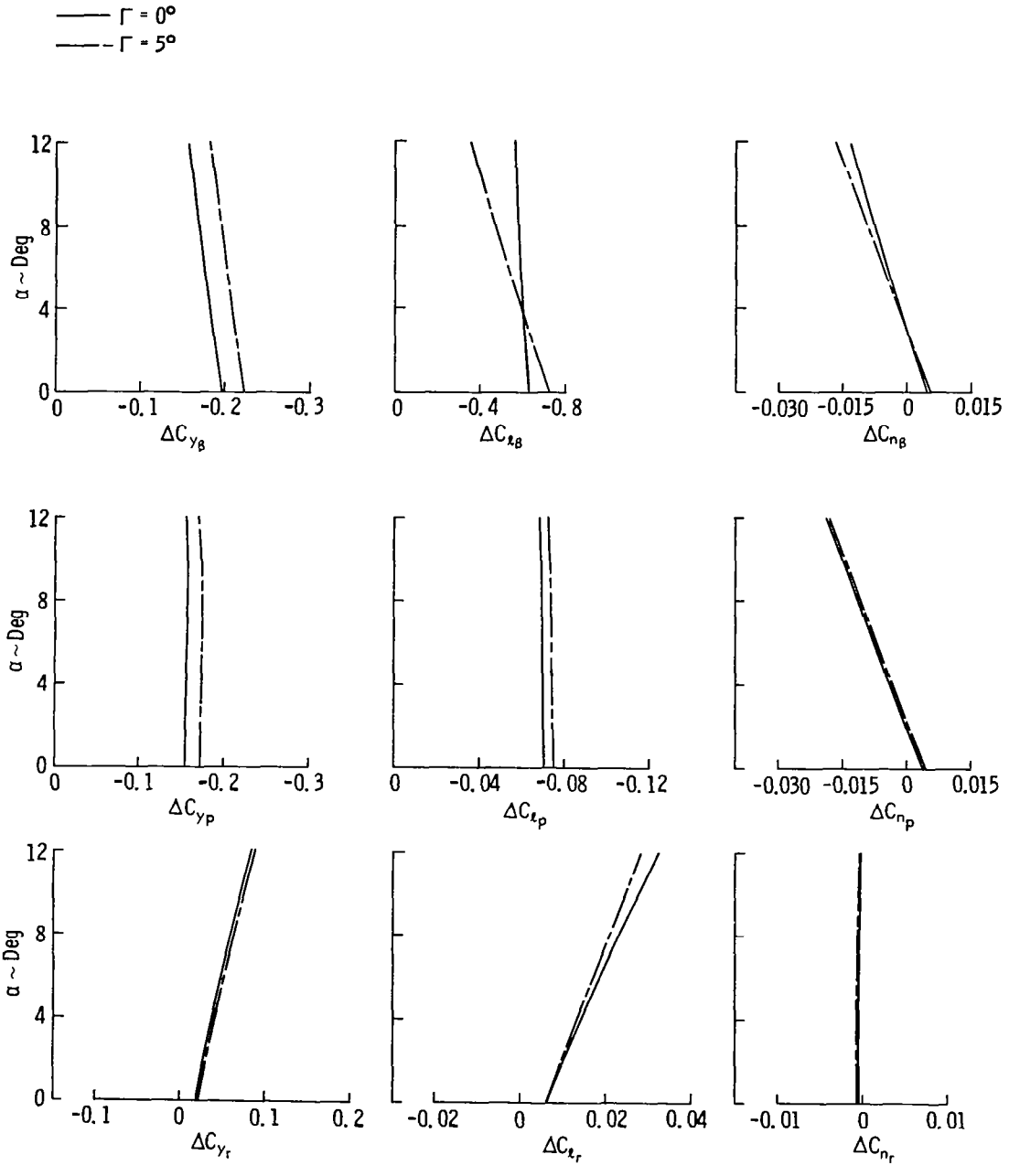

Figure 2.24: Effect of Wing Dihedral on Winglet Contribution to Stability Derivatives

attack, the winglet contribution is more stabilizing compared to the contribution of the winglet on the wing without dihedral. However, with increasing angle of attack, this increment diminishes.

2.2.2.4 Taper Ratio

Three different wings are modeled to study the effects of wing taper ratio on the aerodynamic characteristics. In Figure 2.25 the three wings are sketched. The taper ratios are 0.333, 0.5 (baseline), and 1.0. The wings have identical area, span, and quarter-chord sweep angle. The winglet configurations are also shown in Figure 2.25. The three winglets have the same area, length, quarter-chord sweep angle, and root chord (relative to the wing-tip chord). However, winglet taper ratio changes. The taper ratios are 1.0, 0.5 (baseline), and 0.0, respectively.

In Figure 2.26 the results are plotted. It can be observed that the effects of wing taper on the winglet contributions to the lateral-directional stability derivatives are minor. Therefore, the trends shown in Section 2.2.1 for the baseline (λ = 0.5) wing appear also to be valid for wings with more/less taper.

2.2.2.5 Span

Two wings are used to study the effects of wing span on the stability characteristics. In Figure 2.27 the two wings are sketched. These wings have identical area, taper ratio, and quarter-chord sweep angle. The aspect ratios are 7 (baseline), and 12. The two winglets

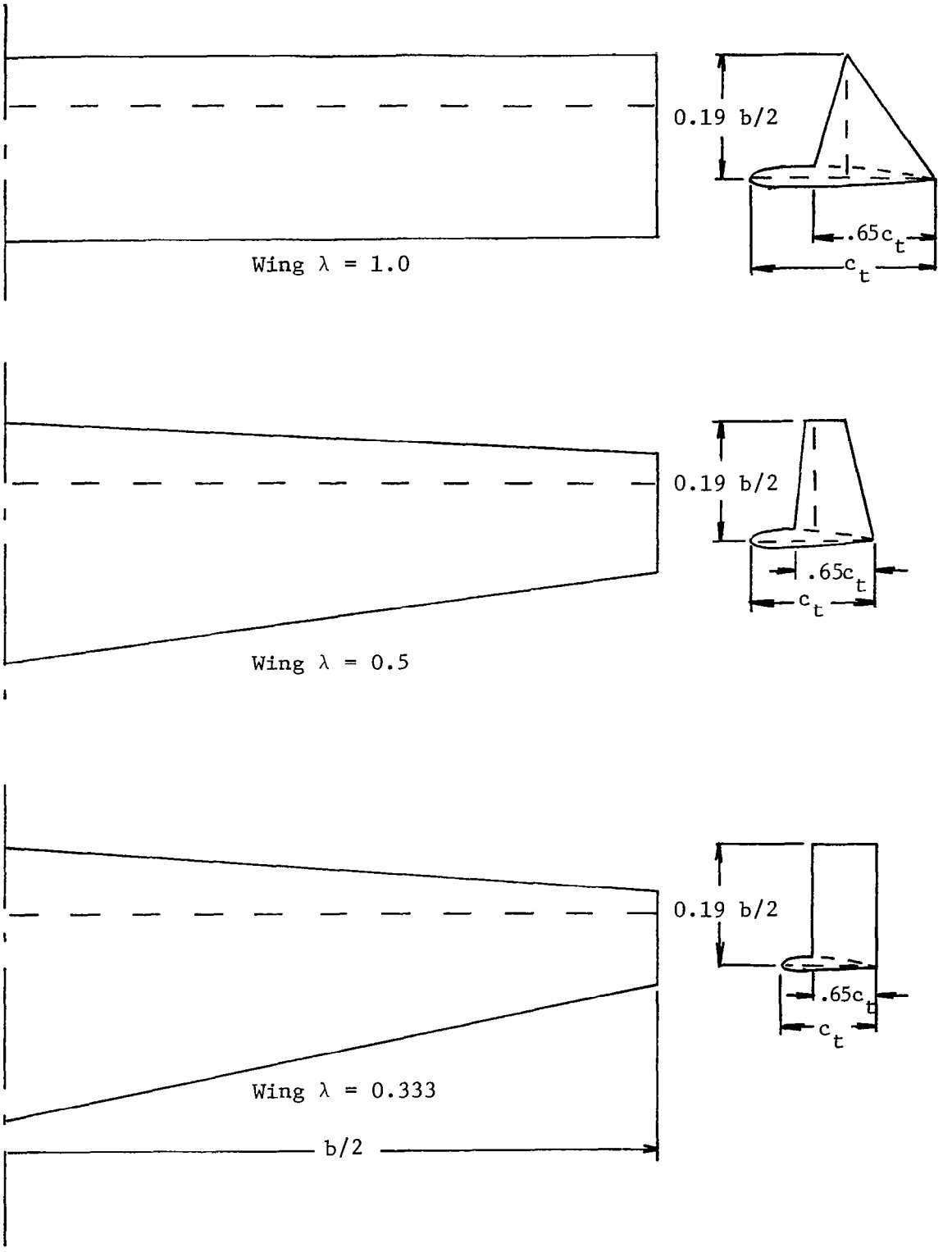

Figure 2.25: Wing Taper Ratio Study

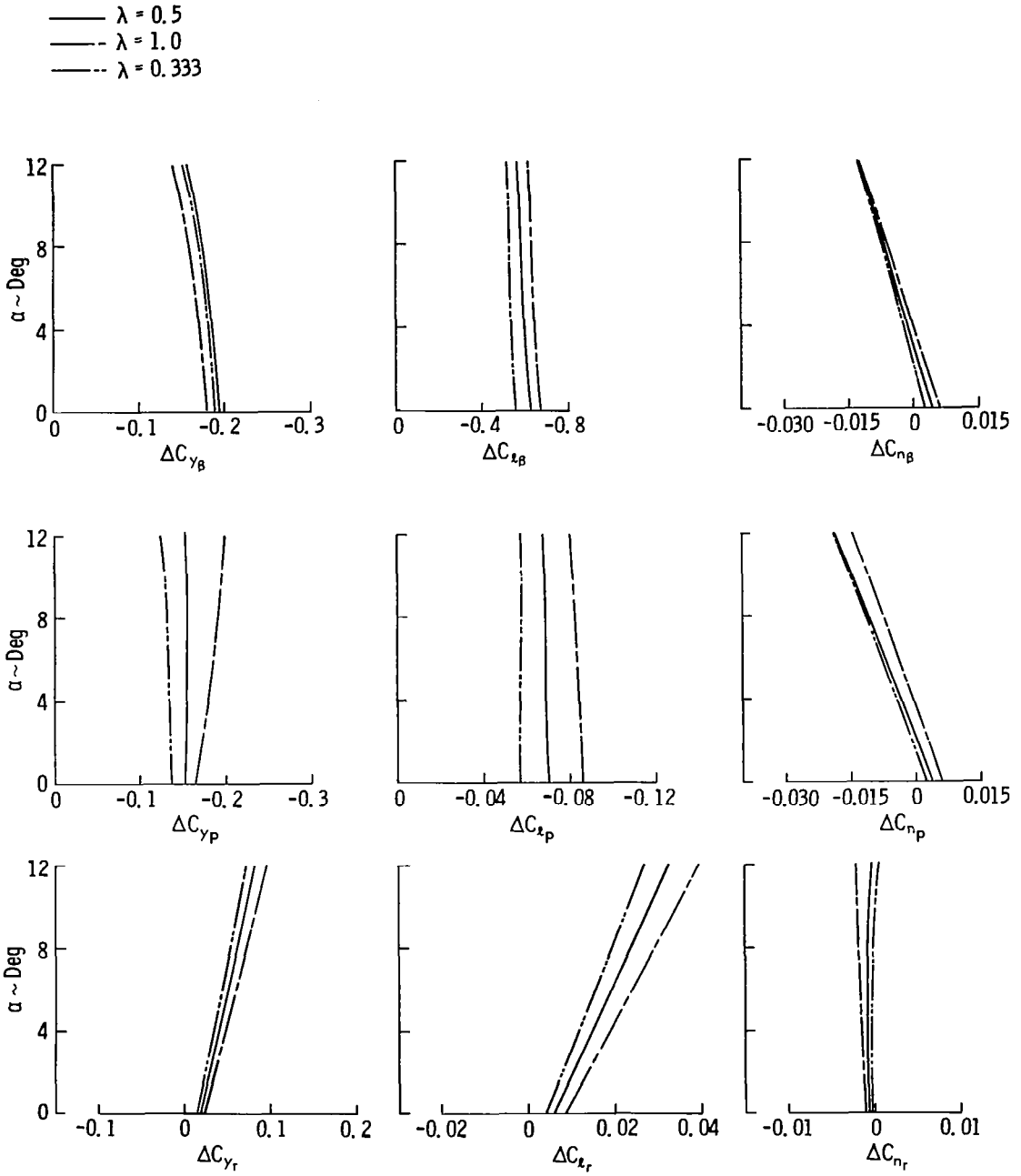

Figure 2.26: Effect of Wing Taper Ratio on Winglet Contribution to Stability Derivatives

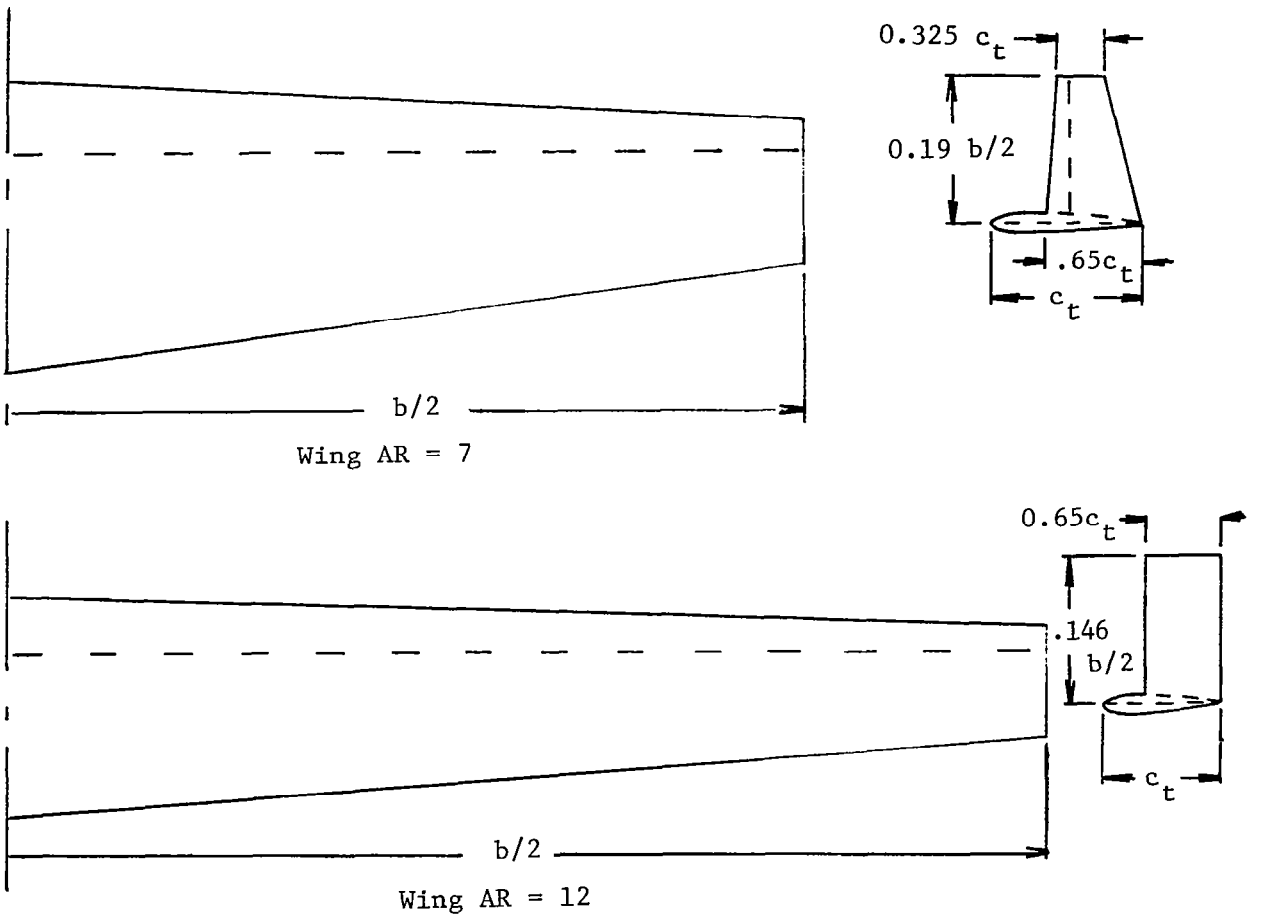

Figure 2.27: Wing Span Study

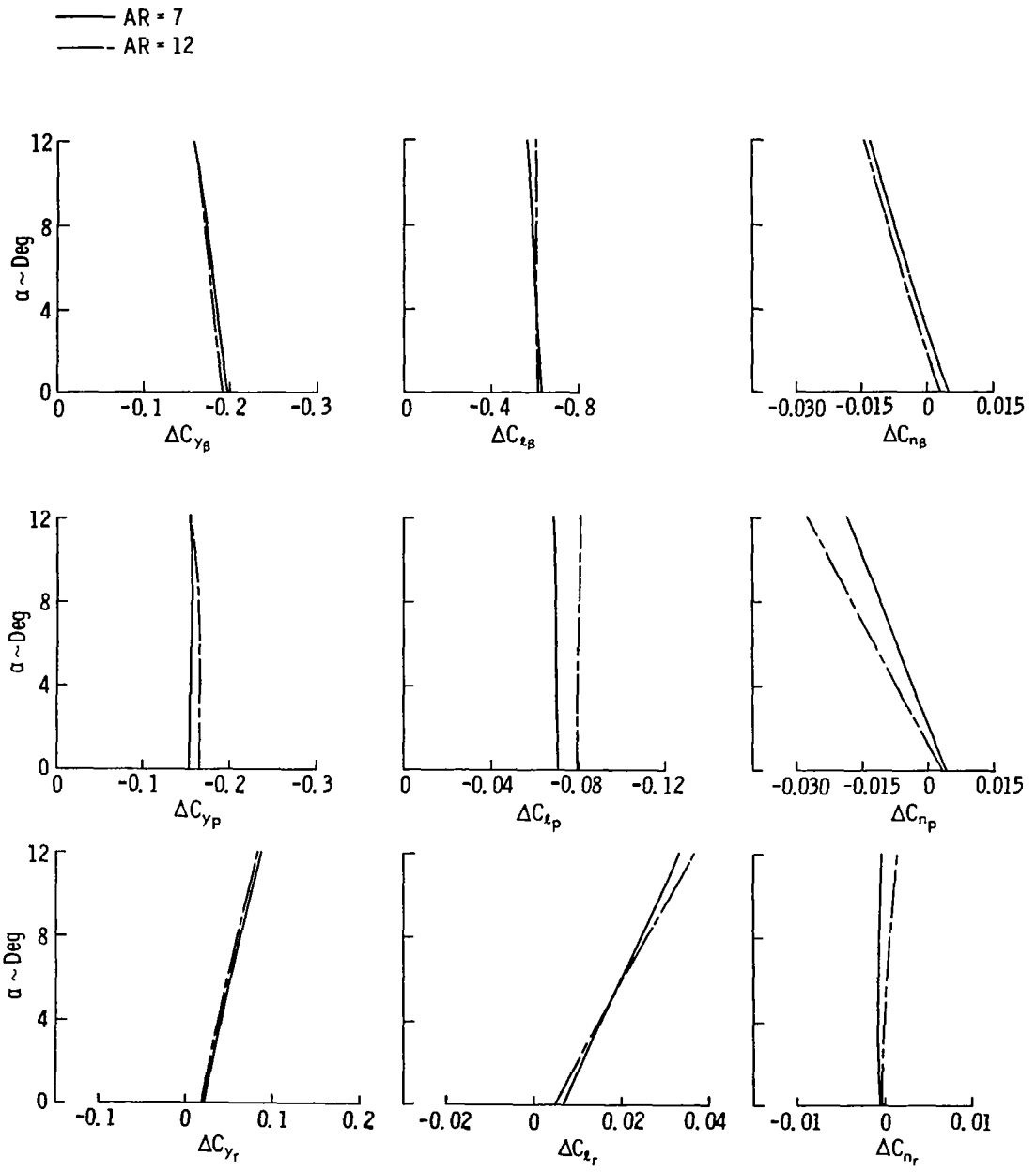

Figure 2.28: Effect of Wing Span on Winglet Contribution to Stability Derivatives

have the same area, length, and root chord (relative to the wing-tip chord). However, winglet taper ratio is modified. The taper ratios are 0.5 and 1.0, respectively.

The results of this study are shown in Figure 2.28. As can be seen, the effects of wing span on the contribution of the winglets to the stability derivatives are small. Consequently, the trends demonstrated in Subsection 2.2.1 for the baseline (AR = 7) wing appear valid also for higher aspect ratio wings.

2.3 Summary

The lifting surface method of Reference 21 has been used to analyze the effects of various winglet parameters on lateral-directional stability derivatives of a general aviation type wing. It is shown that good correlation exists between the results of the lifting surface method (QVLM) and experimental data. The analysis of the effects of various winglet parameters on the stability characteristics is done by way of a parametric study. The most important results of this parametric study are

1. Of all lateral-directional stability derivatives the sideslip stability derivatives C_{y_β}, C_{ℓ_β}, and C_{n_β} are most significantly influenced by winglets. The roll-rate and yaw-rate derivatives are affected to a lesser degree.
2. The increment in dihedral effect due to winglets is significantly reduced as the winglet is moved aftward and/or swept backward. The directional stability increases due to these modifications.

3. Winglet cant angle significantly affects C_{ℓ_β} and C_{ℓ_p} and has a strong effect on lift-induced drag and wing-root bending moment. Outward cant decreases induced drag; but it increases root-bending moment, dihedral effect, and roll damping.

4. The effect of winglet incidence angle on the stability derivatives appears to be small. Therefore, the incidence angle can be optimized for maximum wing-winglet performance without significantly affecting airplane stability and control.

5. Wing sweep and wing twist produce changes in the contribution of the winglet to the yawing moment derivatives. Backward sweep and washout improve directional stability and cause C_{n_p} to become more positive. The other derivatives show only minor changes.

6. The effects of wing span and wing taper ratio on the winglet contribution to the stability derivatives are small. Consequently, the trends demonstrated for the baseline (AR = 7, λ = 0.5) wing appear to be valid also for higher aspect ratio and lower/higher taper ratio wings.

7. Winglet length has an important influence on dihedral effect, induced efficiency, and wing-root bending moment. Increased length produces an increase in induced efficiency, but it also causes an increment in wing-root bending moment and dihedral effect.

CHAPTER 3

AIRPLANE DESCRIPTION AND MODIFICATIONS

A number of devices were designed and built to be flight tested on the agricultural research airplane. This chapter presents a description of the research airplane and these devices. The flight test results obtained with the airplane in various configurations are presented in Chapter 5 and correlated with theoretical predictions where applicable.

3.1 Airplane Description

An Ayres S2R-800 Thrush agricultural airplane was used as a test bed for the Aerial Applications Program. A three-view of the unmodified airplane is shown in Figure 3.1. The airplane has a normal gross weight of 6,000 lbs (26,688 N) and a wing area of 326.6 ft^2 (30.34 m^2). Under Civil Aeronautics Manual (CAM 8), Restricted Category requirements, however, the airplane is certified for operation at a gross weight of 7,800 lbs (36,694 N). The airplane is powered by a Wright-Cyclone R-1300-1 B, seven-cylinder, air-cooled, supercharged, radial engine with a constant speed propeller. This combination provides a take-off power of 800 bhp (597 kW) at 2,600 rpm.

The wing is a constant chord (7.5 ft [2.29 m]), all-metal, full cantilever design, utilizing a NACA 4412 airfoil section. It has 3.5° of dihedral, 1.5° of wing twist (washout), a wing span of 44.4 ft (13.54 m), and an aspect ratio of 6.0.

The horizontal stabilizer, elevator, rudder, and vertical fin are constructed from wire-braced, welded steel tube structure and are covered with fabric.

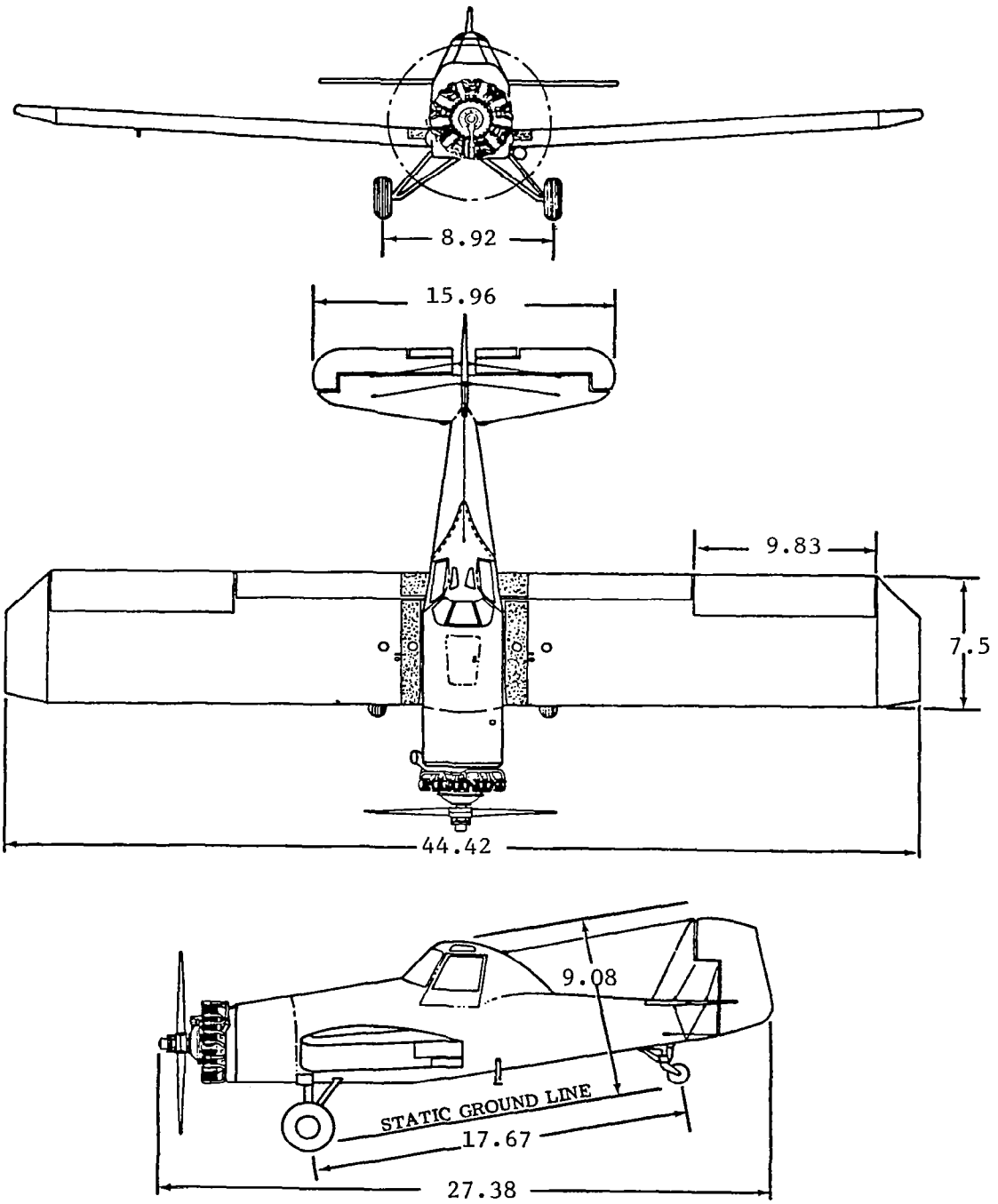

Figure 3.1: Three-View of Unmodified Research Airplane
(Dimensions are in feet.)

The flight controls are of conventional design. The aileron and elevator controls are push rod systems, and the rudder control is achieved through cables. Fixed, ground-adjustable trim tabs are located on the rudder and both ailerons. The elevator trim control has a push rod control system. The airplane has electrically operated plain flaps. The rudder controls are interconnected by springs to the aileron system (a rudder-aileron interconnect). As a result, in flight a wing may be lifted with rudder alone (right rudder results in a downward deflection of the left aileron and an upward deflection of the right aileron).

Throughout the flight test program, streamlined aluminum extrusion spray booms were installed below the wing trailing edge.

3.2 Wing Modification Devices

In this section the wing modification devices which have been used in the research program are described.

3.2.1 Leading Edge Slat

The flight test program has been conducted with inboard leading-edge slats installed. References 18 and 32 present detailed descriptions of the slats and the effects on airplane performance, stability and control, and stalling characteristics. Wind-tunnel results indicate that inboard leading-edge slats eliminate flow separation at the wing-fuselage juncture of the research airplane. This separation creates severe turbulence over the horizontal tail and, as a result,

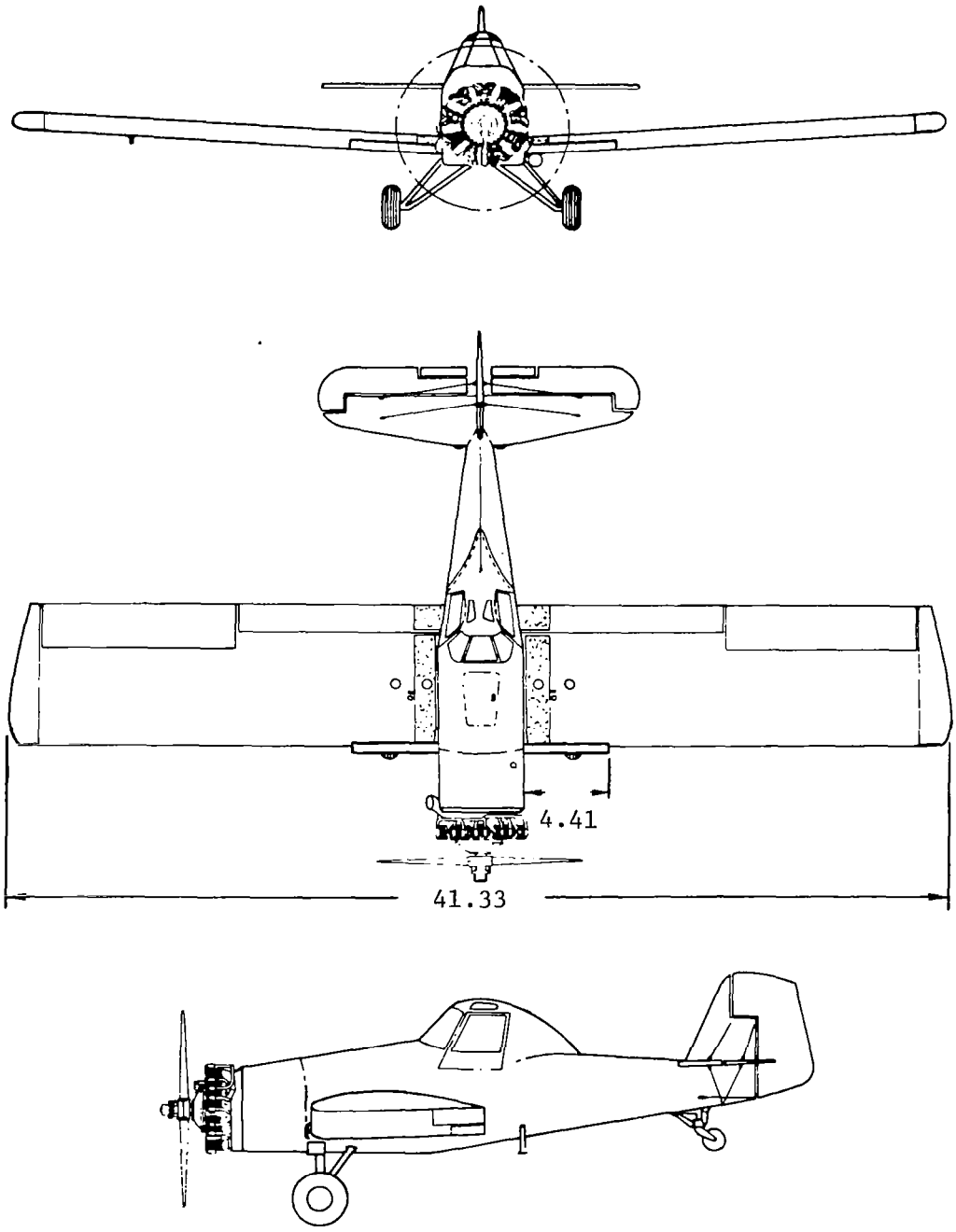

Figure 3.2: Three-View of Airplane in Basic Configuration for Research Flights (Dimensions are in feet.)

Table 3.1: Airplane Geometric and Mass Characteristics

Airplane Configuration	Winglets Off	Winglets On
Weight at takeoff,[1] lb (N)	6194 (27,551)	6484 (28,841)
Moments of inertia, slug-ft^2 (kg - m^2)		
I_x	5023 (6808)	7646 (10,363)
I_y	5277 (7153)	5309 (7196)
I_z	9934 (13,465)	12558 (17,020)
I_{xz}	48 (65)	48 (65)
Wing dimensions:		
Span, ft (m)	41.33 (12.60)	41.08 (12.52)
Area, ft^2 (m^2)	310.0 (28.80)	308.1 (28.63)
Mean aerodynamic chord, ft (m)	7.5 (2.29)	7.5 (2.29)

[1]including pilot, full fuel, hopper empty

horizontal tail vibrations. In Figure 3.2 a three-view of the airplane is shown with the inboard leading-edge slats installed.

3.2.2 Rounded Wing Tip

The tapered metal wing tips (see Figure 3.1) were replaced by rounded fiberglass wing tips in order to obtain an almost identical wing planform area and wing span for the basic airplane compared to the airplane with the various wing tip modifications. As a result, the wing area of the basic airplane is 310.0 ft^2 (28.80 m^2), while the wing span is 41.33 ft (12.60 m). In Figure 3.2 the airplane is sketched with the rounded wing tips installed, and in Table 3.1 the mass and geometric characteristics are listed.

3.2.3 Winglet

The winglets tested were of a modified GA(W)-2 airfoil section and were installed as shown in Figure 3.3. The modifications and the airfoil section coordinates are listed in Reference 1. Each winglet has a root chord approximately equal to 65% of the airplane wing tip chord (5.0 ft [1.52 m]), a span of 5.0 ft (1.52 m), and a taper ratio of 0.56 and is unswept at the 50 percent chord line. The winglets are canted inward 13° from the vertical, are mounted at an incidence of 0°, and are untwisted. Each winglet has an area of 19.5 ft^2 (1.81 m^2) .

The winglets are canted inward instead of outward, as is suggested in Reference 1, to reduce the effective dihedral of the wing. For the same reason the length of the winglet is reduced from 7.5 ft (2.29 m = wing-tip chord length) to 5.0 ft (1.52 m).

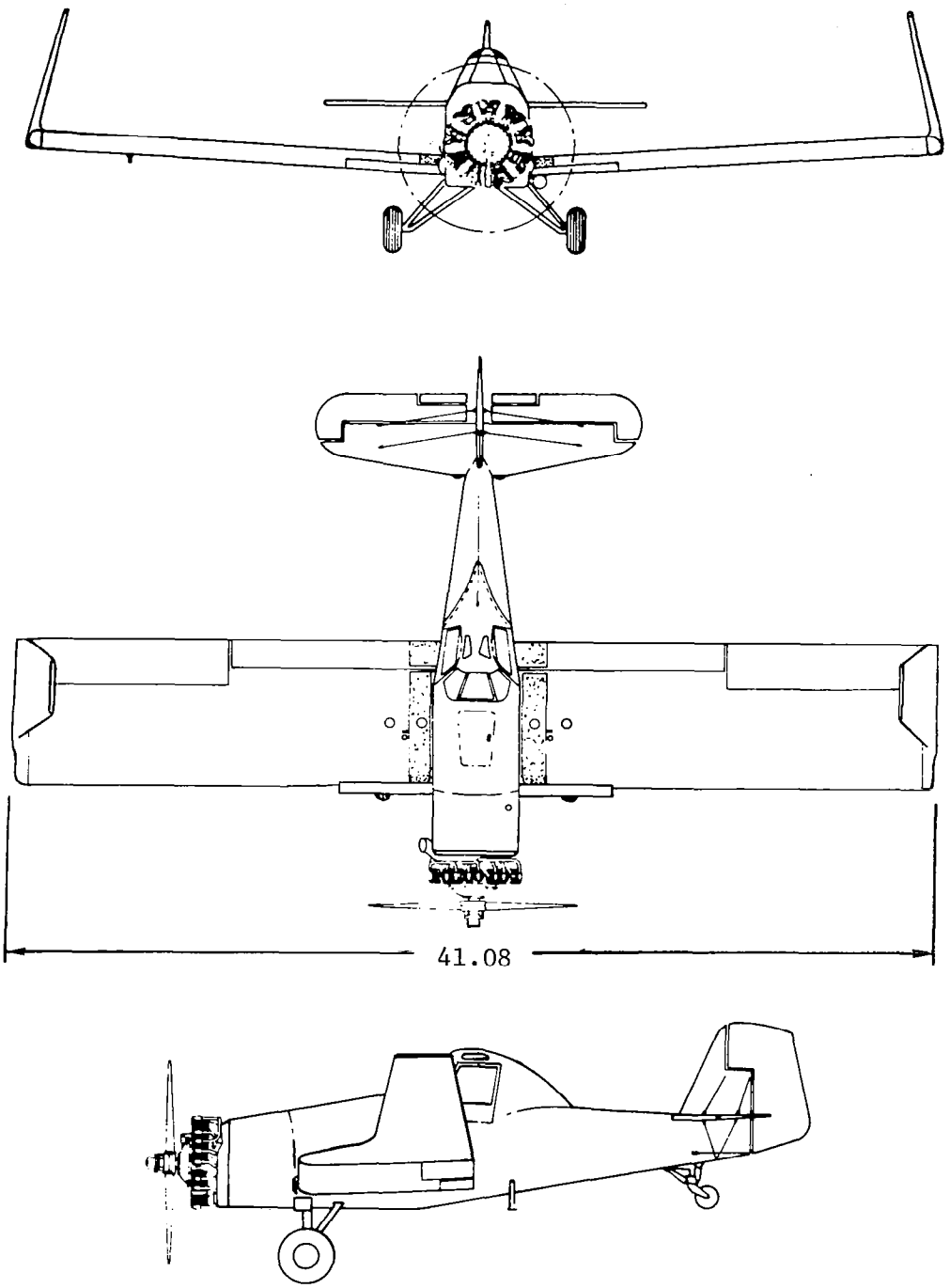

(a) Three-View of Airplane

Figure 3.3: General Layout of Test Airplane with Winglets
(Dimensions are in feet unless otherwise noted.)

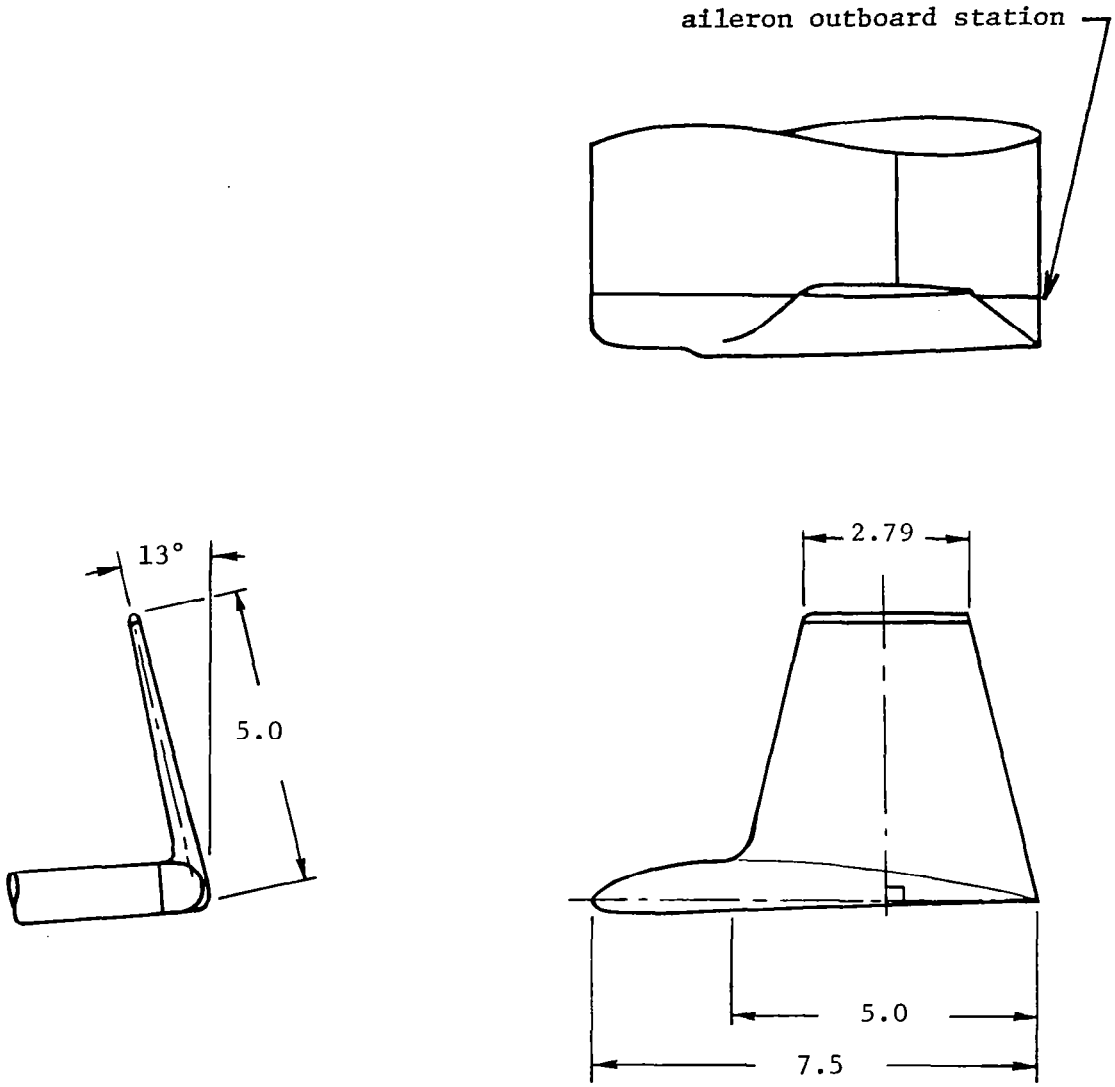

(b) Winglet Detail

Figure 3.3: (Concluded)

In Reference 15 the structural design and integration of the winglets are discussed in more detail. The wing area of the airplane with winglets is 308.1 ft^2 (28.63 m^2), while the wing span is 41.08 ft (12.52 m). Additional mass and geometric characteristics for the winglet-equipped airplane are listed in Table 3.1.

3.2.4 Additional Wing-Tip Modification Devices

Besides the winglet, several other modification devices were considered. Figure 3.4 shows a sketch of a "vortex diffuser" device fitted to the research airplane. The device consists of a winglet-like vane mounted from a boom which trails a wing tip. The vortex diffuser vane has been patented, and a detailed description and design approach can be found in Reference 10.

Another interesting wing-tip device is the "wing-tip sails" concept developed by Spillman at Cranfield Institute of Technology in Great Britain. This device consists of an array of 3 or 4 small winglike extensions, called sails, fitted approximately horizontally to each of the wing tips of an airplane. The device is described in Reference 2. Test results listed in Reference 9 and 14 indicate that the device reduces both airplane lift-induced drag and the amount of spray entrained in the wake of an agricultural airplane and carried out of the target swath pattern by vortex motion.

The vortex diffuser vane as well as the wing-tip sails was planned to be flight tested. However, budgetary constraints made it necessary to cancel these planned tests as part of this project.

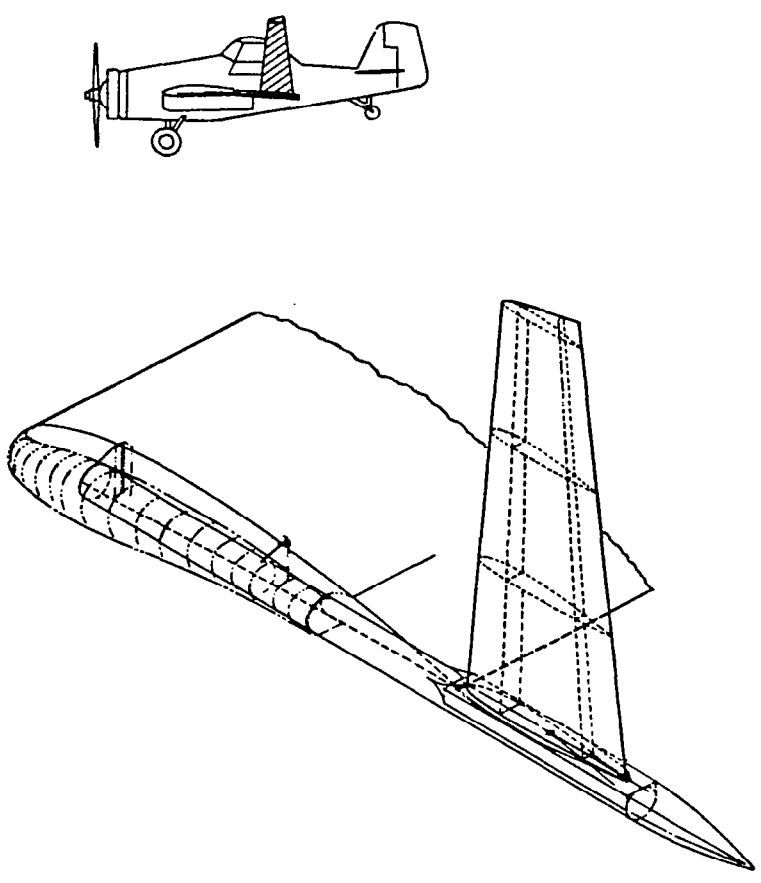

Figure 3.4: Vortex Diffuser Design for Research Airplane (from Reference 10)

CHAPTER 4

FLIGHT TEST PROGRAM AND DATA SYSTEM

This chapter presents the flight test program and its objectives, the flight envelope of the research airplane, a description of the data acquisition system and its accuracy, and data reduction methods.

4.1 Flight Program and Objectives

The flight test program of the research airplane with and without wing-tip-mounted winglets had the objective of determining the effects of winglets on the following:

1. Particle trajectories in the airplane wake
2. Airplane lift and drag characteristics
3. Airplane lateral-directional static and dynamic stability and control characteristics.
4. Winglet aerodynamic loading.

Items 3 and 4 are discussed in this report, while items 1 and 2 are in progress at Langley Research Center and will be reported in the near future.

Four types of flight tests were flown to obtain the flight test data listed in this report.

1. Quasi-steady tests: These tests consisted of performing slow continuous decelerations starting from full power steady state trimmed level flight. Decelerations continued through stall. The tests were performed to calibrate the airspeed system. During these tests a trailing anemometer

was deployed to measure true airspeed. Reference 33 describes this calibration method in more detail.

2. Steady tests: These tests consisted of trimming the airplane for a particular speed with power for level flight. Depending on the type of flight test, at this condition sideslip angles were generated while keeping steady heading. These tests were performed to measure airplane drag characteristics ($\beta = 0°$), winglet aerodynamic loading, and airplane steady heading sideslip characteristics.

3. Perturbation tests: These tests consisted of trimming the airplane with power for level flight and perturbing the trimmed condition with aileron and rudder doublets. The airplane was trimmed at airspeeds between 70 and 115 KIAS. Two different input forms were used to excite the lateral-directional motions, and typical time histories of the inputs are illustrated in Figure 4.1. These tests were performed to estimate lateral-directional stability and control parameters.

4. Roll tests: These tests consisted of trimming the airplane with power for level flight at 80 and 105 KIAS. Two different input forms were used to roll the airplane. The first input form consisted of full aileron deflection and rudder input sufficient to reduce sideslip that retards roll rate (not to produce sideslip that augments roll rate). This test was performed to measure airplane roll characteristics. The second input form was a rudder-pedals-free

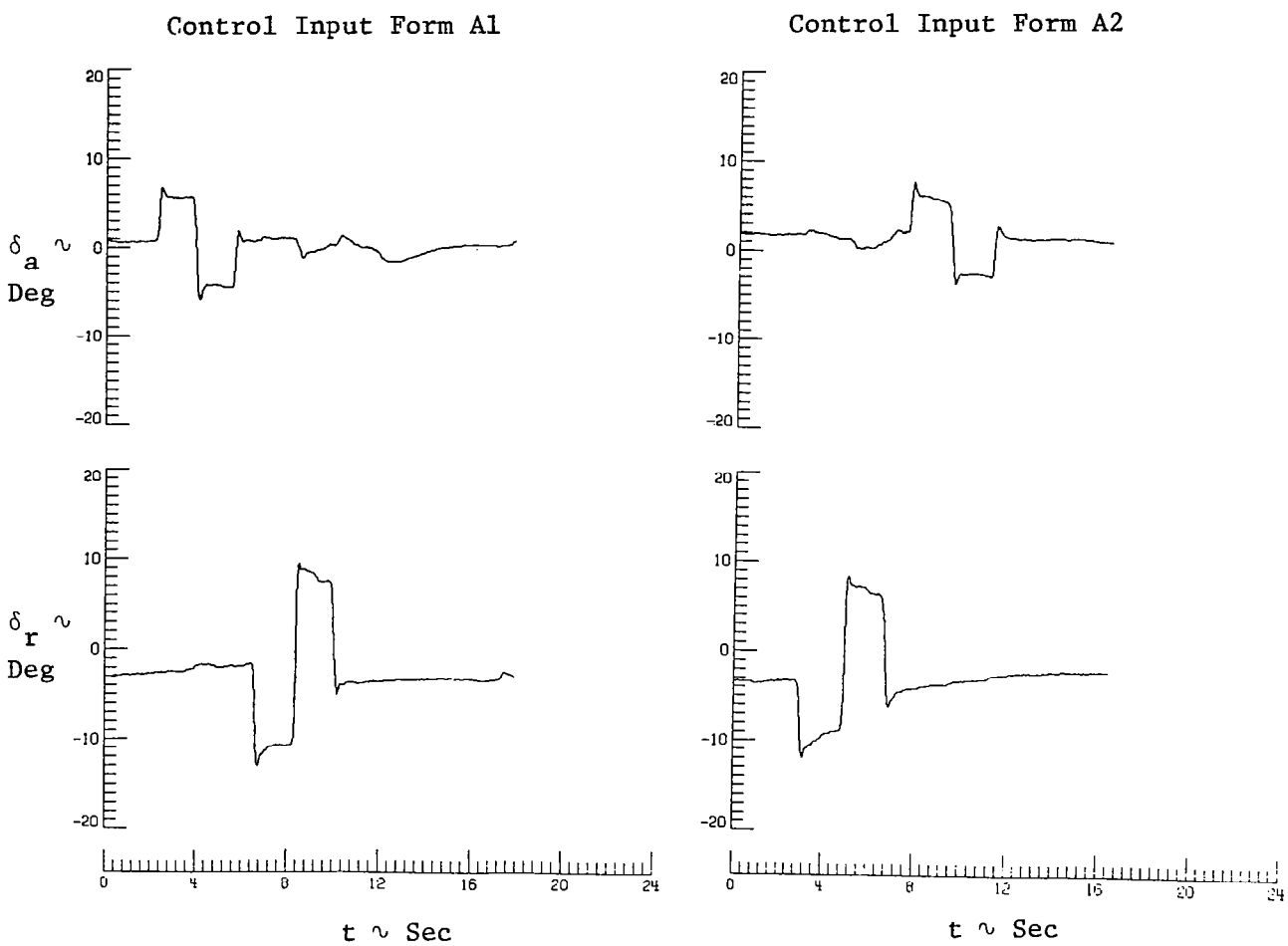

Figure 4.1: Time Histories of Control Input Forms

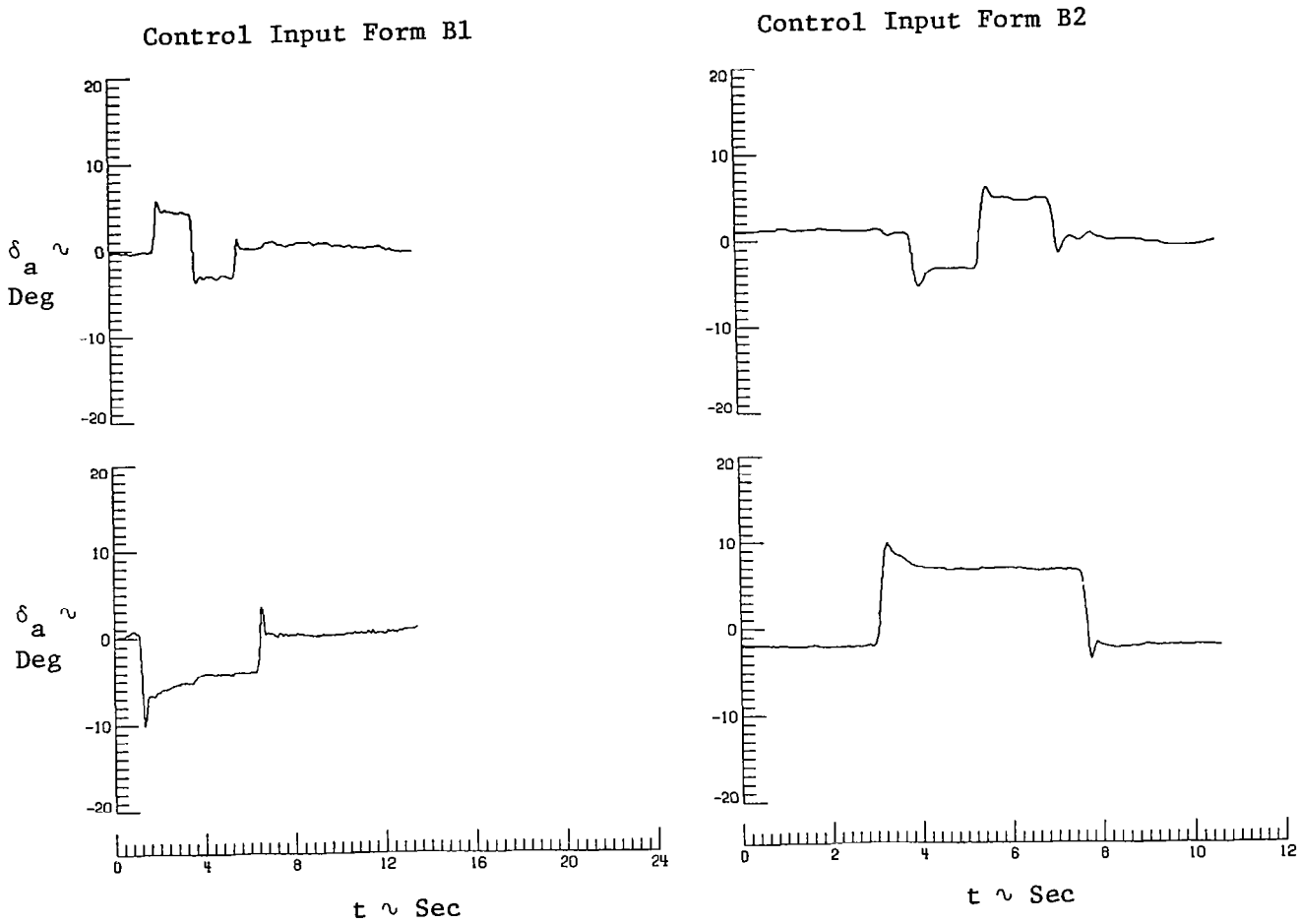

Figure 4.1: (Concluded)

step aileron (full deflection) control input. This test was performed to measure roll rate oscillations and sideslip excursions.

4.2 Flight Envelope

The flight envelope for the research airplane in the basic configuration is the same as for the standard Ayres S2R-800 Thrush. For the airplane with winglets, however, the flight envelope was reduced in order not to exceed the structural limits of the winglets.

Originally the winglets were designed and constructed based on results obtained with an improper load prediction method. Aerodynamic loads analysis based on a lifting surface method (see Chapter 5) revealed that the original method was inadequate to describe the winglet loading. As a result, the winglets required modifications to provide sufficient structural integrity. Also, the flight envelope was reduced compared to that for the basic airplane. For the airplane with winglets, the "never-exceed" airspeed, V_{NE}, is 125 KCAS in combination with a load factor of 2 and a sideslip angle of ±10°, versus 138 KCAS, 2.92 g[1]) and no sideslip angle restriction for the basic airplane.

The C.G. envelope for the basic airplane indicates a forward limit of 22.5 in. (0.57 m) aft of the leading edge and an aft limit of 28.0 in. (0.71 m). This translates into limits relative to the wing MAC of 25.0 percent and 31.1 percent, respectively. As a result of the aft location of a substantial amount of flight test equipment and the

[1]The positive limit load factor is 3.8 at a normal gross weight of 6,000 lbs (26,688 N) or 2.92 at 7,800 lbs (34,694 N).

winglets, the airplane with winglets has a C.G. location for the research flights which is slightly past the aft limit of the basic airplane (28.1 in. for the airplane with winglets, pilot, and full fuel).

4.3 Flight Test Instrumentation

4.3.1 Description

The airplane instrumentation system measured and recorded on magnetic tape the data used in this study. A Piloted Aircraft Data System (PADS) was used to record the data on tape on board the airplane. This system is a digital Pulse Code Modulated (PCM) system, and it has a sampling rate of 80 Hz. The advantage of this system over a Frequency Modulated (FM) system is that a much higher accuracy can be obtained. A disadvantage is, however, that the system has a low pass filter cutoff frequency of approximately 10 Hz. The variables recorded and the range of each sensing instrument are listed in Table 4.1. Following the flight, the data were converted to engineering units to obtain the data used in this study.

During flight tests with the wing-tip-mounted winglets, pressure measurements were obtained on the right winglet. The winglet pressures were recorded on an FM channel and afterwards merged with the PCM channels. Three rows of orifices, each consisting of 14 pressure ports (7 upper- and 7 lower-surface ports) were located at 25, 50, and 75 percent of the winglet span (Figure 4.2). The orifices were flush mounted and connected to a pressure scanning device, which was located in the wing leading edge close to the wing tip. The winglet pressures were referenced to the corrected free streem static pressure.

Table 4.1: Measured Parameters and Accuracies

Parameter	Range	Accuracy (% of full scale)	Units
Time	-	-	sec
Pressure altitude	-990 to 9030	0.3	ft
Vertical speed	±3000	0.4	ft/min
Pitch attitude	±35	0.3	deg
Roll attitude	±90	0.3	deg
Heading	±179	0.3	deg
Pitch rate	±30	0.3	deg/sec
Roll rate	±100	0.3	deg/sec
Yaw rate	±30	0.3	deg/sec
Longitudinal acceleration	±0.5	0.1	g
Normal acceleration	0 to 4	0.1	g
Lateral acceleration	±0.5	0.1	g
Right angle of attack	±35	0.1	deg
Right angle of sideslip	±30	0.1	deg
Left angle of attack	±35	0.1	deg
Left angle of sideslip	±30	0.1	deg
Aileron deflection	±19	0.1	deg
Elevator deflection	-25 to 17	0.5	deg
Rudder deflection	±26.5	1.0	deg
Flap deflection	0 to 27.5	2.5	deg
Longitudinal stick force	±100	0.2	lb
Lateral stick force	±100.	0.2	lb
Rudder pedal force	±150	1.0	lb
Engine rpm	0 to 3000	0.1	rpm
Fuel flow	20 to 100	0.2	U.S. gallon/hr
Manifold pressure	0 to 15	0.5	lb/in^2
Air temperature	0 to 100	0.5	°F
Trailing anemometer[1]	30 to 190	0.5	miles/hr
Propeller blade angle[2]	24 to 38	2.0	deg
Airspeed pressure	0 to 1	0.5	lb/in^2
Radar altimeter	0 to 200	0.3	ft
Differential static pressure[3]	0 to 2.5	0.2	lb/in^2

[1]Operational during airspeed calibration flights when trailing anemometer is attached.

[2]Operational during drag polar flights.

[3]Operational during flights with winglets installed. Recorded on FM track.

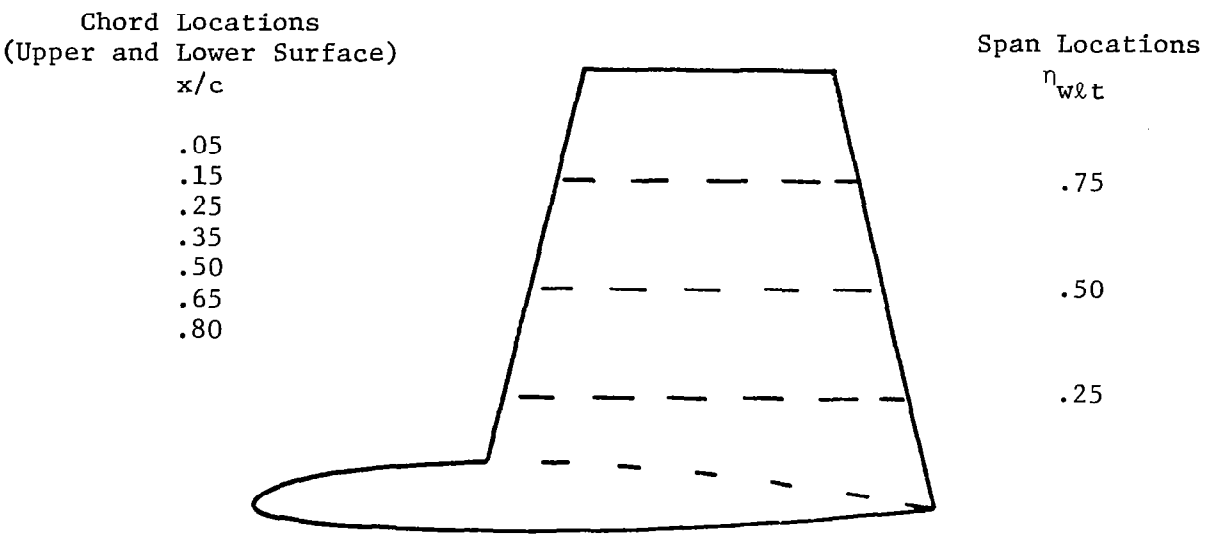

Figure 4.2: Winglet Static-Pressure Orifice Locations

The air data measurements were obtained from two instrument heads mounted on wing-tip booms located near both wing tips. A four parameter transducer instrument head was mounted on the boom located near the right wing tip. The head sensed dynamic pressure, static pressure, angle of attack, and angle of sideslip. The instrument head mounted on the left boom was a three parameter transducer; it sensed static pressure, angle of attack, and angle of sideslip. The booms placed the static pressure ports approximately 1/2 chord length ahead of the wing leading edge.

4.3.2 Accuracy

The accuracies of the PCM channels are listed in Table 4.1, while the calibration of the air data measurements is discussed in the following chapter. The winglet pressure measurements were recorded on an FM channel. According to Reference 34, the combined error of an FM system amounts to about ±2% of full scale. For a 2.5 psi pressure transducer, this results in an estimated error of ±0.05 psi[1].) In addition, the estimated error in the measurement of the free stream static pressure is approximately ±0.008 psi. As a result, for an airspeed of 80 KCAS the average error in the pressure coefficient, C_p, is calculated to be ±0.38. For an airspeed of 125 KCAS, the error in C_p is approximately ± 0.16.

These errors in the measurement of the pressure coefficient can be large relative to the measured C_p and are caused by (1) the 2% error

---

[1] 1 psi = 6,895 N/m^2

generated by the FM data system, and (2) the range of the pressure transducer (0 - 2.5 psi) which is too wide for application on a low-speed airplane. A transducer with a range of 0 - 1.5 psi would substantially improve accuracy of low speed testing such as conducted in this project.

4.4 Data Reduction and Estimation Method

Corrections to the flight data were required before these data could be used for determining lateral-directional response and mode characteristics and for estimating the stability and control parameters, etc. Since the angle of attack and sideslip vanes were mounted on booms located near both wing tips and extended about 1/2 chord length ahead of the wing leading edge, corrections for upwash (see Chapter 5) and angular rates were applied to the measured angle of attack. Angle of sideslip was corrected for angular rates. Airspeed was corrected for position error by applying the position error correction of Subsection 5.1.1. The airspeed was also corrected for density to obtain true airspeed; and since the pitot head was located on the right wingtip boom, angular rates were taken into account to convert airspeed to the airplane C.G. The accelerometer readings were also corrected to the C.G. of the airplane.

The corrected flight data were obtained by applying above corrections and were sampled at the rate of 20 samples per second. The sampled data were used to produce automatic data tabulation, time history plots, plots of various parameters versus sideslip angle, and final digital engineering units data tape for airplane parameter identification. This tape included the following variables: time, true

airspeed, incidence angles (right vanes), angular velocities, attitude angles, linear accelerations, and control surface deflections.

The equation error method was applied to estimate the lateral-directional stability and control parameters using the corrected flight test data. This method, which is based on a least-squares technique, has been used because of its simplicity, while retaining good accuracy. Solutions for the following parameters were obtained:

$$C_{y_o}, C_{y_{\delta_a}}, C_{y_{\delta_r}}, C_{y_p}, C_{y_r}$$

$$C_{\ell_o}, C_{\ell_{\delta_a}}, C_{\ell_{\delta_r}}, C_{\ell_p}, C_{\ell_r}$$

$$C_{n_o}, C_{n_{\delta_a}}, C_{n_{\delta_r}}, C_{n_p}, C_{n_r}$$

In References 35 and 36, the equation error method is discussed in detail. Furthermore, results from the equation error method are compared with parameters determined by the maximum likelihood method. Both Reference 35 and Reference 36 conclude that the estimated values using the two techniques agree in general.

CHAPTER 5

FLIGHT-TEST RESULTS

In this chapter, flight test results are presented for the research airplane with and without winglets. The following characteristics will be discussed in the succeeding sections:

1. Static pressure and angle-of-attack position error calibrations.
2. Winglet pressure and load distributions.
3. Lateral-directional stability and control parameter identification.
4. Lateral-directional characteristics in steady sideslip.
5. Dutch roll mode characteristics.
6. Roll mode characteristics.
7. Lateral-directional response characteristics.

The flight-test results are correlated with theoretical predictions when applicable.

5.1 Position Error Calibrations

5.1.1 Static Pressure

The trailing anemometer method of Reference 33 is used to calibrate the static pressure measuring system of the research airplane. The variation of static pressure error with indicated angle of attack is shown in Figure 5.1. The two calibration curves are obtained for power-on (power for level flight) and flaps-up flight conditions.

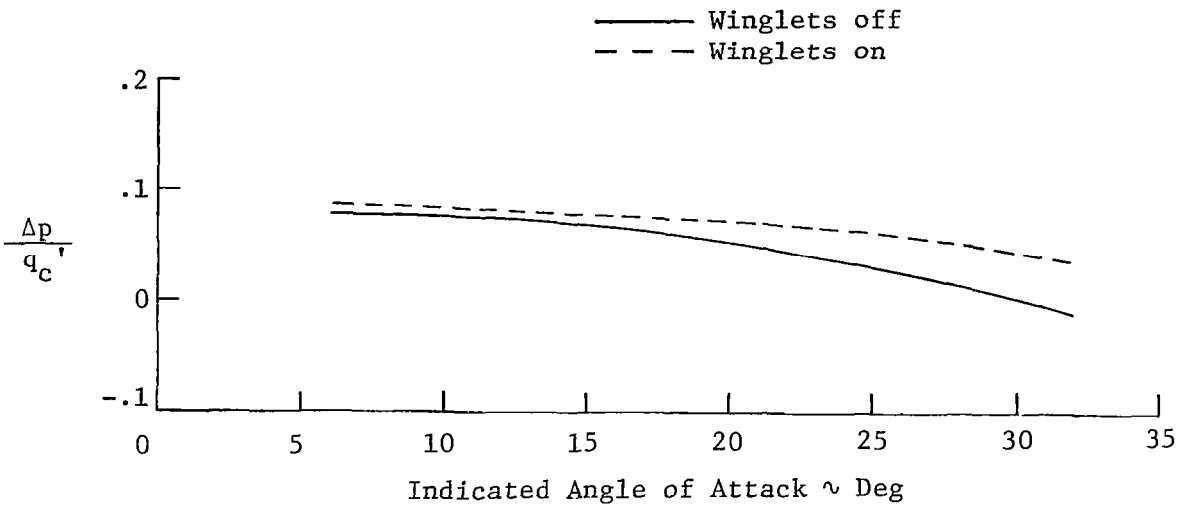

Figure 5.1: Static Pressure Position Error Calibrations

The continuous deceleration variant of the trailing anemometer method is applied to measure the static pressure corrections. This technique is also described in Reference 33.

Calibrated airspeed is calculated by utilizing the correction curves of Figure 5.1 as follows:

$$V_c = V_c' \sqrt{1 + \frac{\Delta p}{q_c'}} \tag{5.1}$$

The altitude (static pressure) measurement is corrected in the following manner:

$$p = p' - \left(\frac{\Delta p}{q_c'}\right) q_c' \tag{5.2}$$

where V_c' and p' are obtained from the pressure probes mounted on the right wing-tip instrument boom.

The results of Figure 5.1 indicate that at low angles of attack, winglet effect on the static pressure measurement is negligible. However, the effect becomes larger with increasing angle of attack. This increment in the ratio $(\Delta p/q_c')$ can be attributed to the rise in aerodynamic loading at the wing tip as a result of the installation of a winglet and the proximity of the winglet to the static pressure orifices. At low angles of attack the winglet is lightly loaded; and, as a result, its effect on $(\Delta p/q_c')$ is small.

During the airspeed calibration flight-tests a number of test runs were performed for sideslip angles of $\pm 5^{o}$ and $\pm 10^{o}$. The quantity of data was insufficient to generate static pressure position error calibration curves for flights with non-zero angle of sideslip. However, the data did indicate the effect to be negligible at low angles of attack.

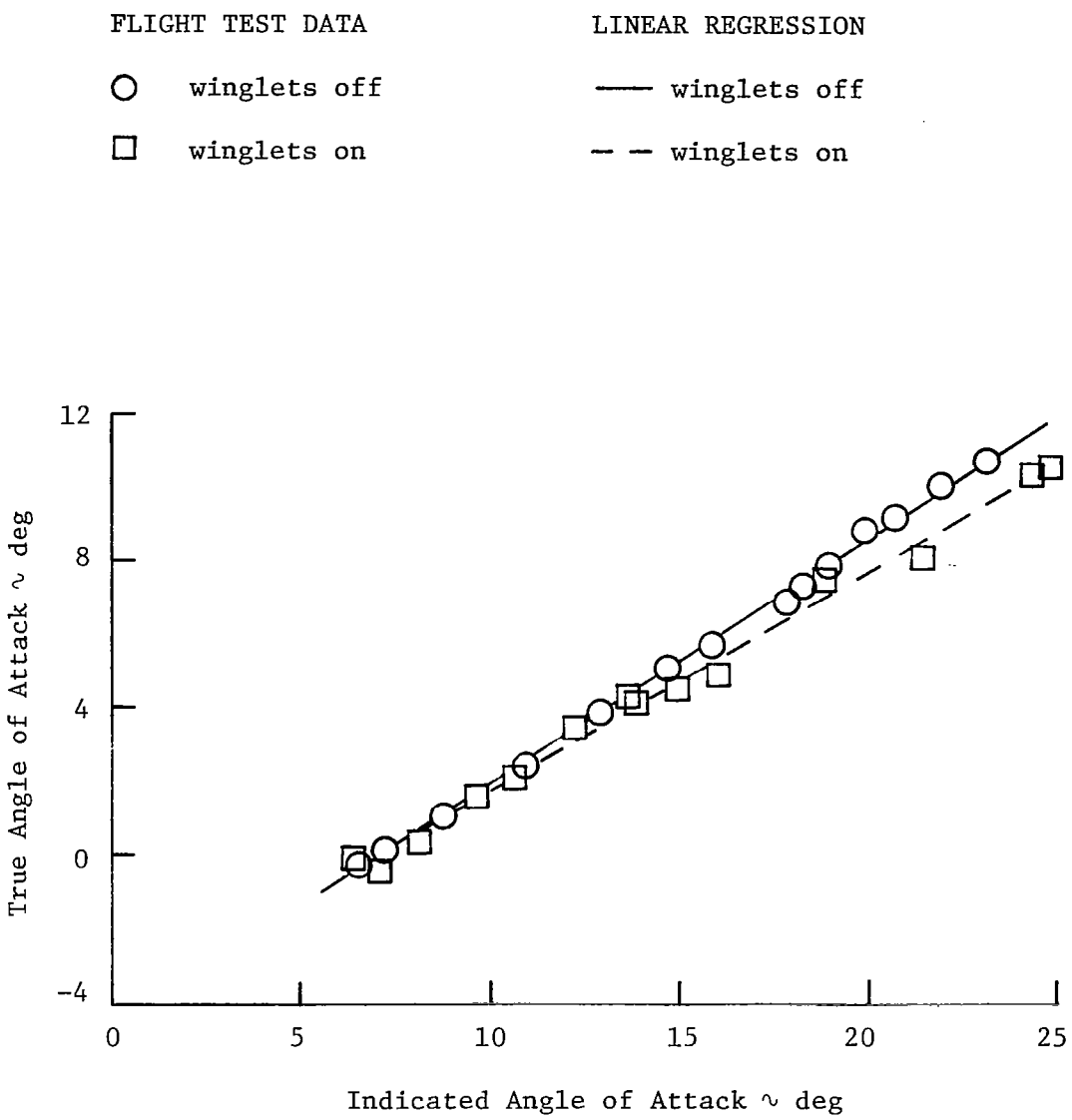

Figure 5.2: Angle of Attack Position Error Calibrations

5.1.2 Angle of Attack

The calibration method used to determine the angle of attack position error is described in Reference 34. This method consists of equating indicated angle of attack to pitch attitude angle in straight and level steady flight conditions.

The calibration curves for the airplane with and without winglets are shown in Figure 5.2. The results indicate that the angle of attack position error is quite large. Also, winglet effect on position error is small at low and medium angles of attack. With increasing angle of attack, however, a continuous rise can be observed in the position error for the airplane with winglets compared to the error for the basic airplane. This increment can be attributed to the enhanced loading at the wing tip produced by the winglet and the proximity of the winglet to the flow angle vanes.

5.2 Winglet Pressure and Load Distributions

The discussion and data presented in this section are limited to a few selected flight conditions. Measured pressure and load distributions are shown for three steady-state, symmetrical flight conditions. For the subject airplane, these conditions represent a high (C_L = 1.32), medium (C_L = 0.72), and low (C_L = 0.48) lift condition. For the second flight condition, angle of sideslip is varied from +10° to -10° in increments of approximately 5° to demonstrate the influence of sideslip angle on winglet pressures and loads. Comparisons with theoretical results are also included.

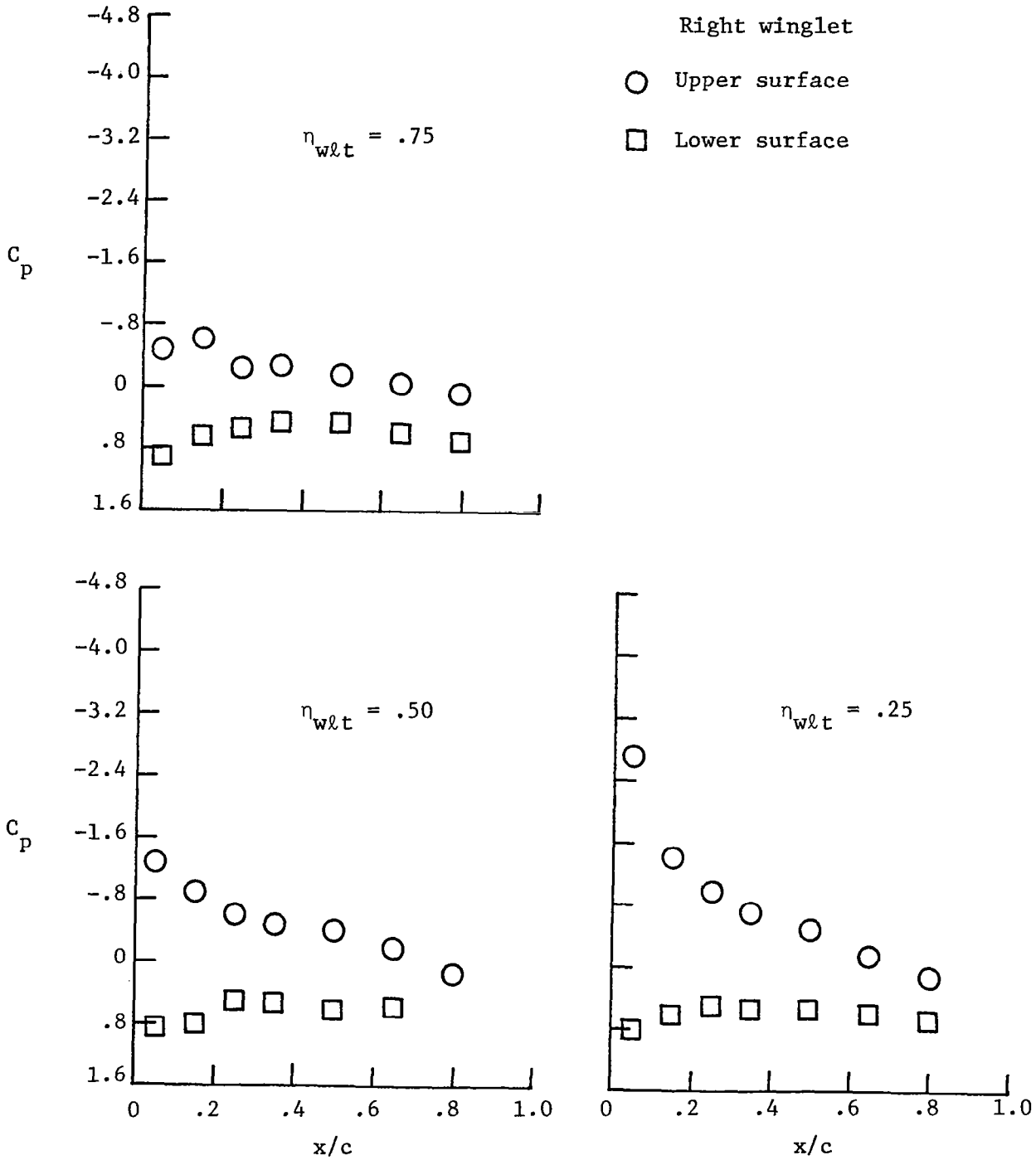

(a) M = 0.11, C_L = 1.32

Figure 5.3: Measured Winglet Pressure Distributions for Steady State, Symmetrical Flight

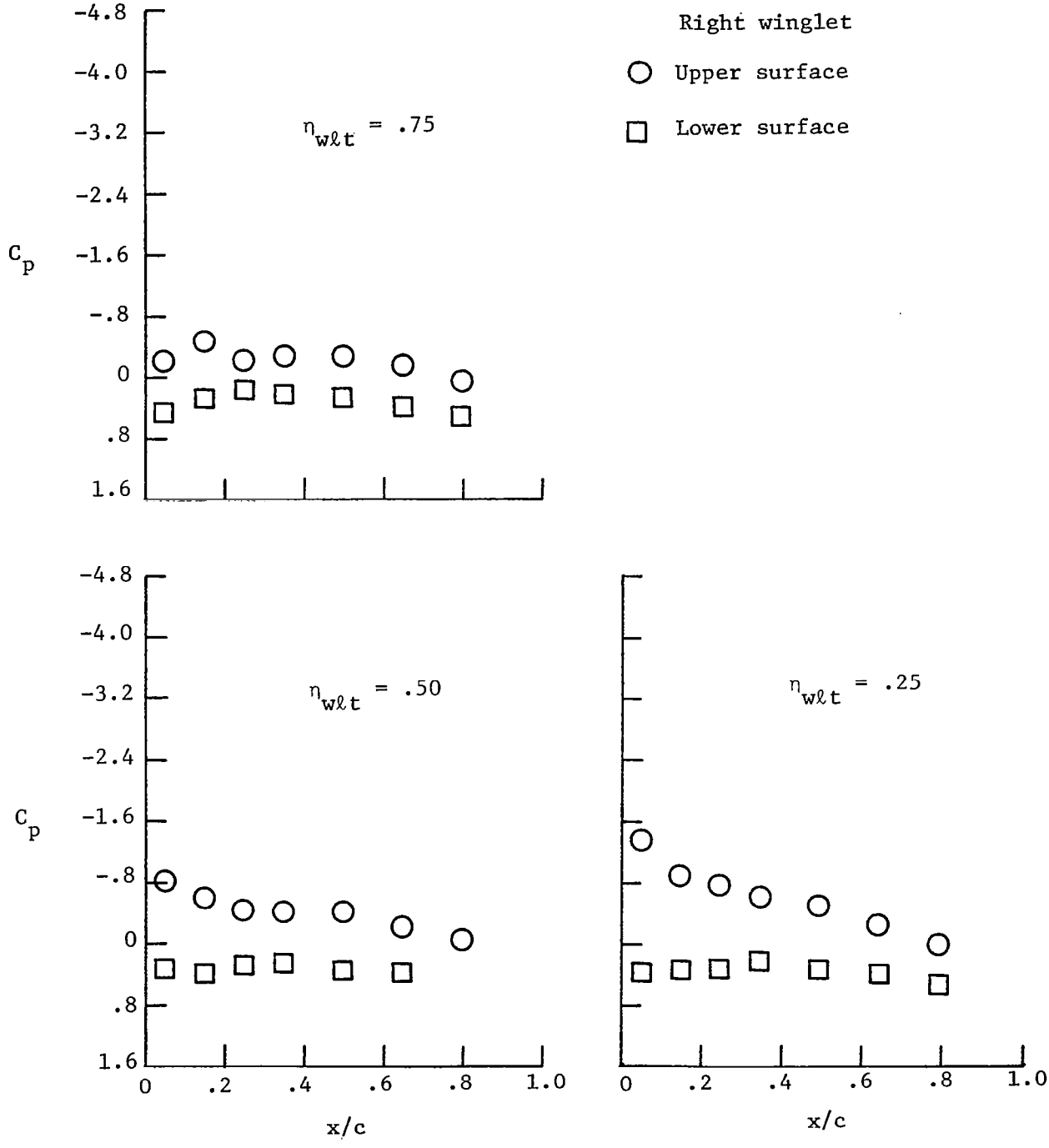

(b) M = 0.15, C_L = 0.72

Figure 5.3: (Continued)

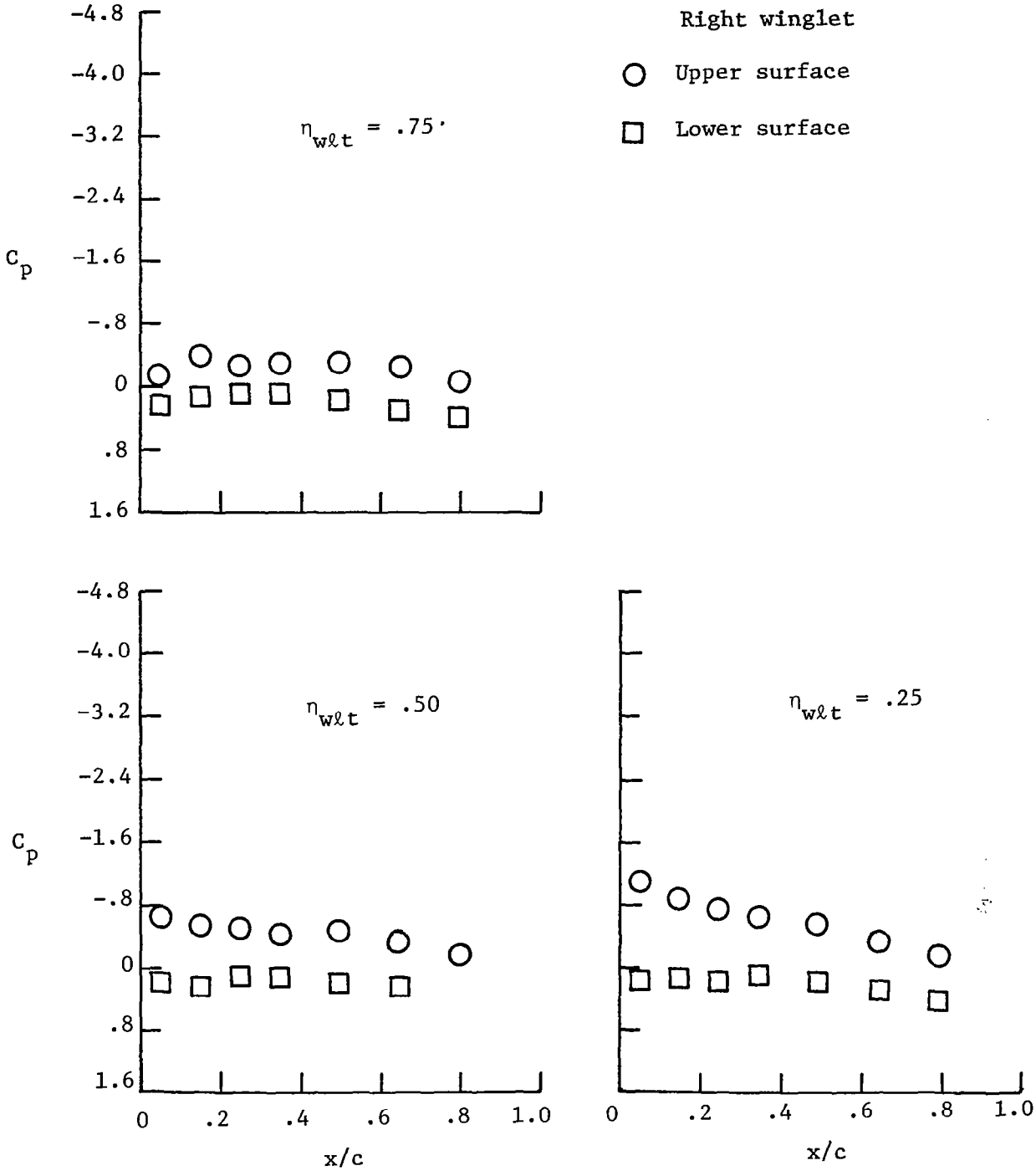

(c) M = 0.18, C_L = 0.48

Figure 5.3: (Concluded)

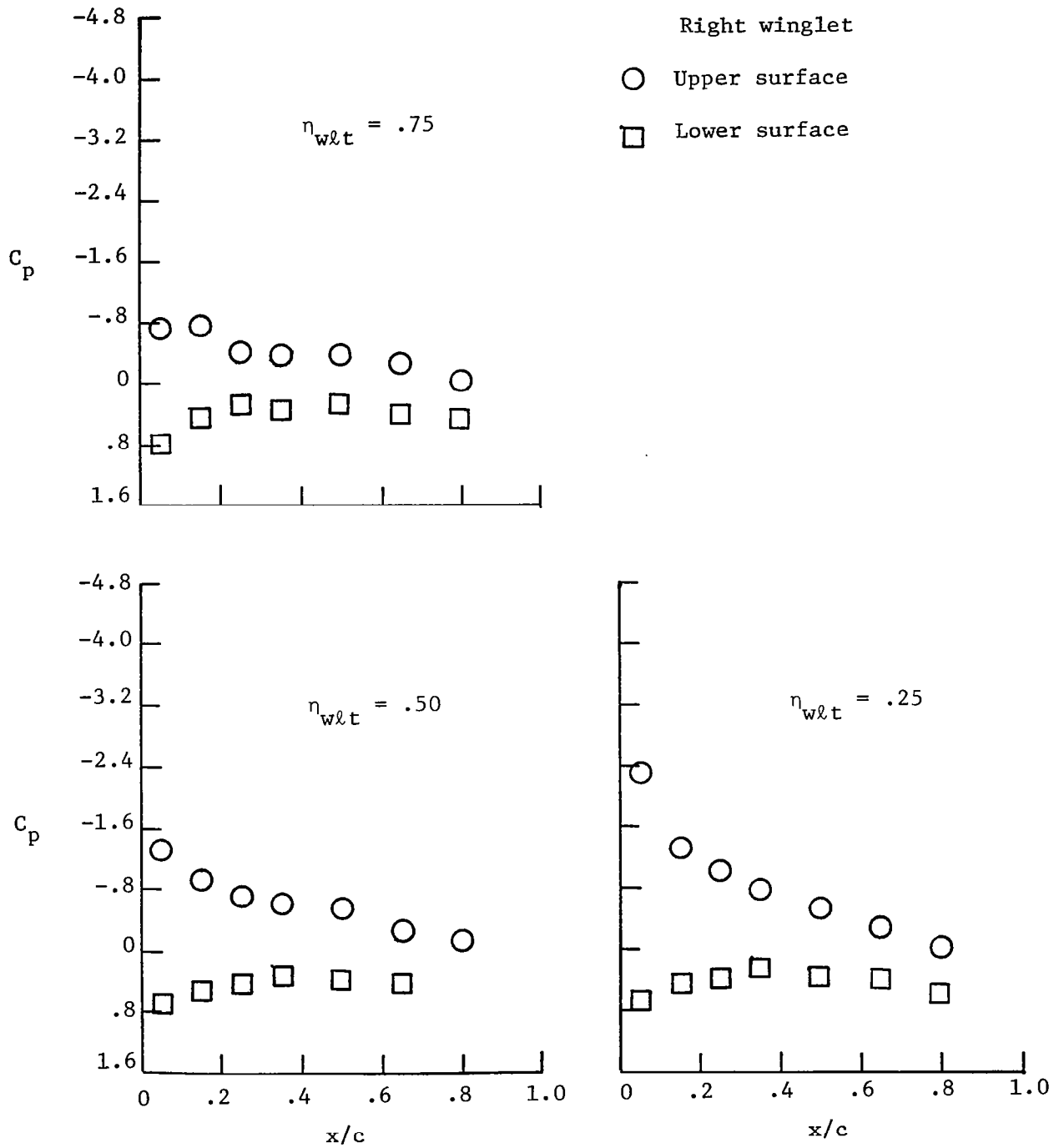

(a) M = 0.14, C_L = 0.74, β = -5.6°

Figure 5.4: Measured Winglet Pressure Distributions for Steady State, Sideslipping Flight

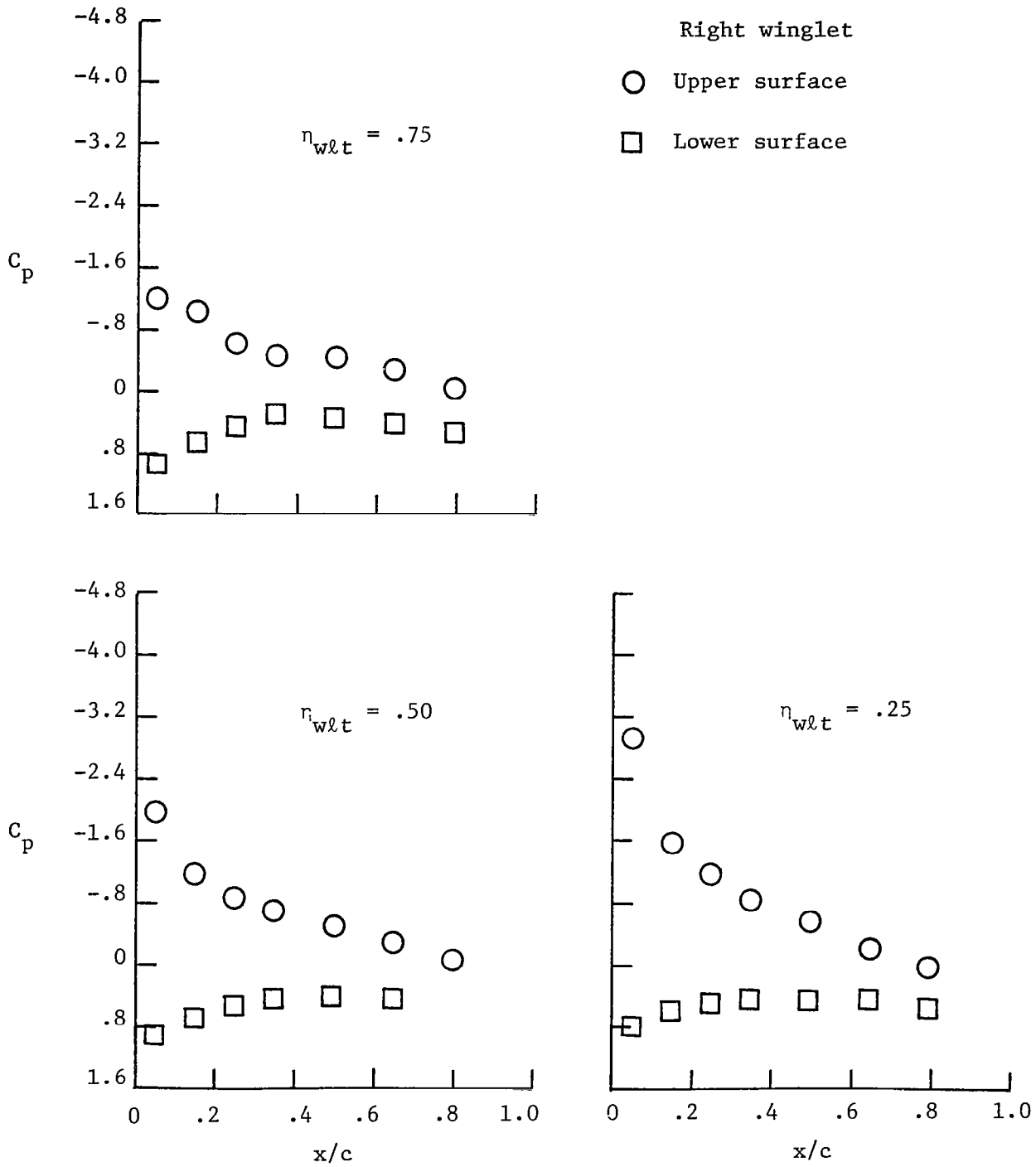

(b) M = 0.14, C_L = 0.74, β = 9.4°

Figure 5.4: (Continued)

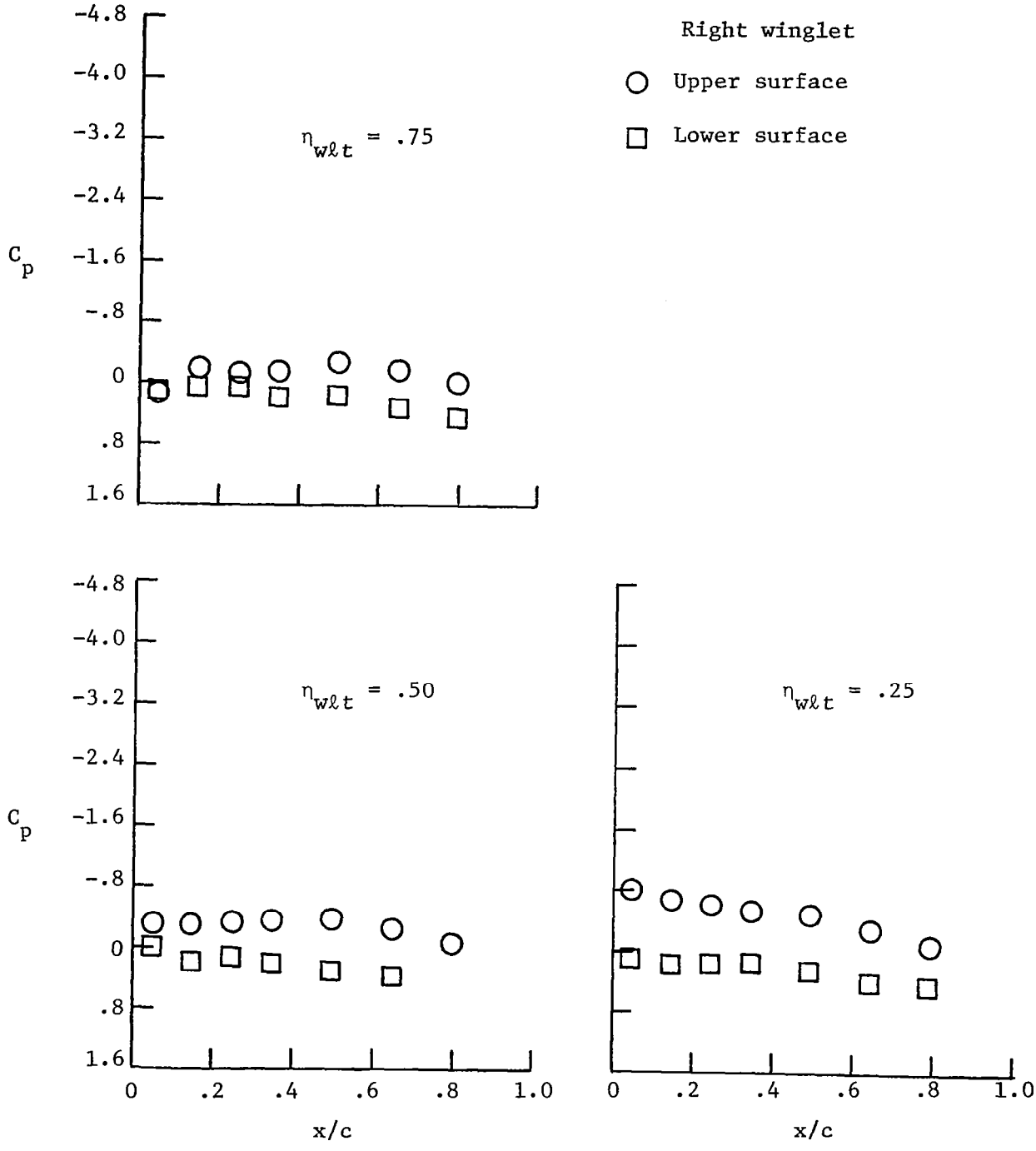

(c) M = 0.15, C_L = 0.68, β = -5.0°

Figure 5.4: (Continued)

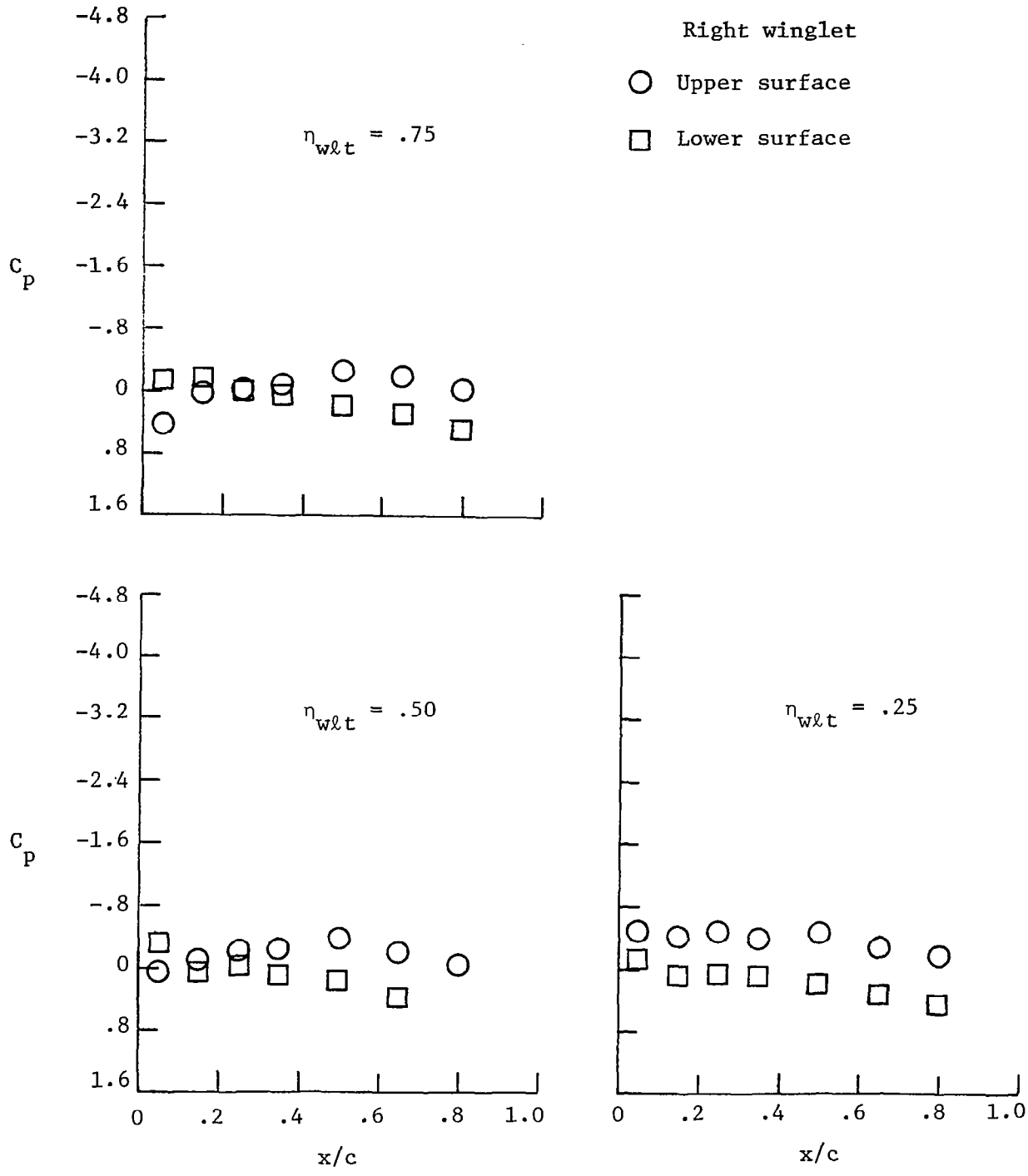

(d) M = 0.15, C_L = 0.68, β = -9.0°

Figure 5.4: (Concluded)

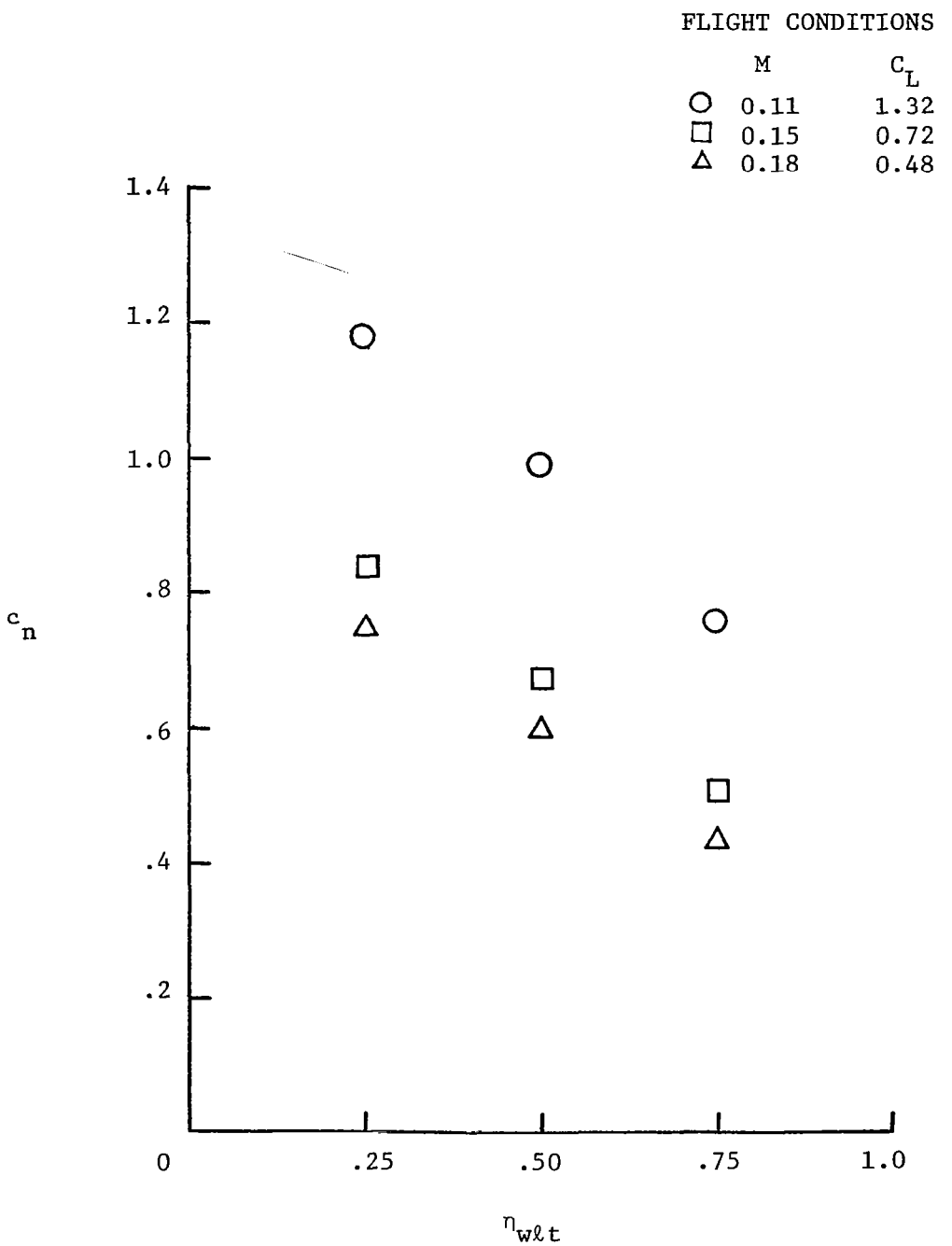

Figure 5.5: Measured Winglet Span Load for Steady State, Symmetrical Flight

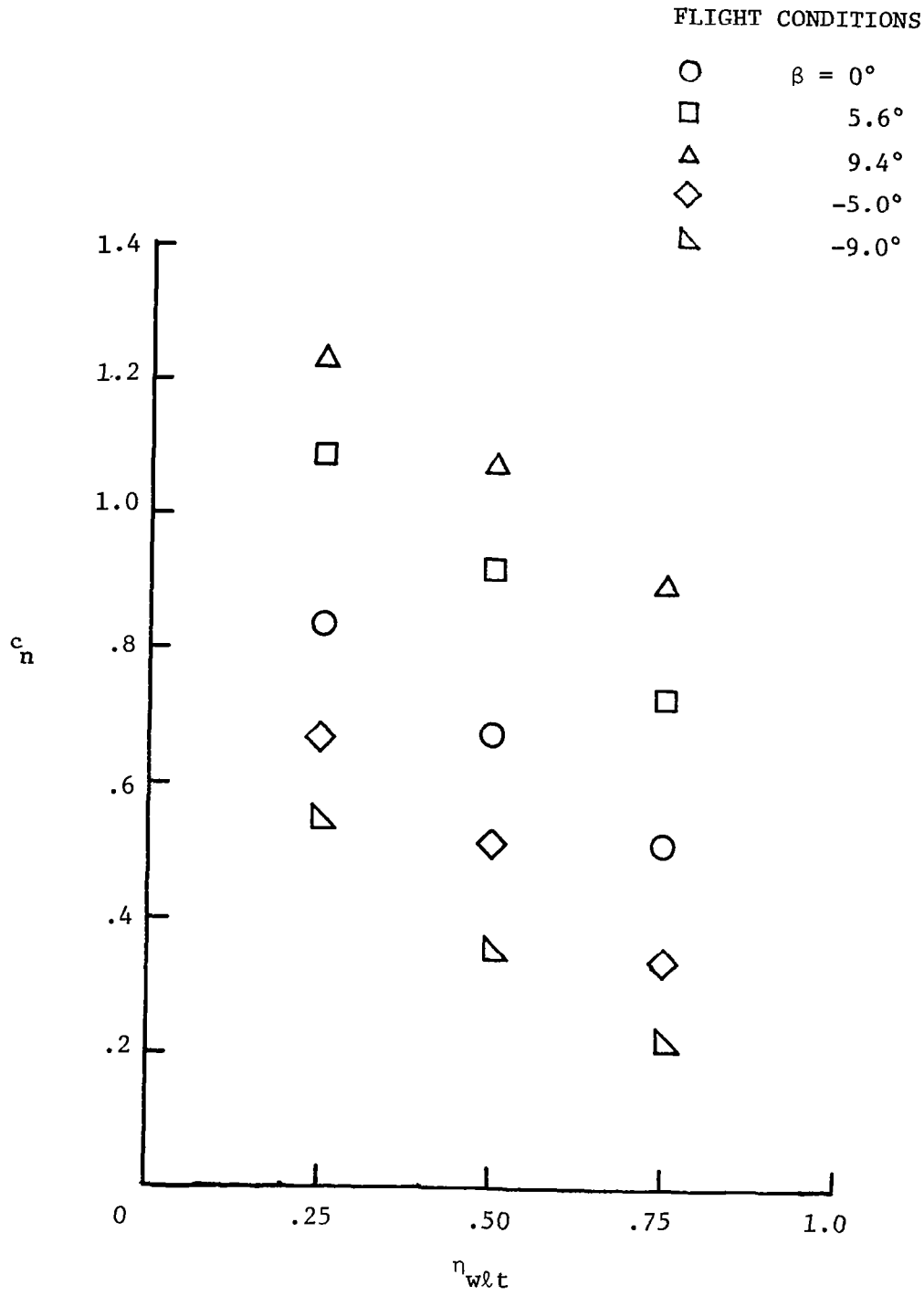

Figure 5.6: Measured Winglet Span Load for Steady State, Sideslipping Flight (M = 0.15, $C_L \simeq 0.72$)

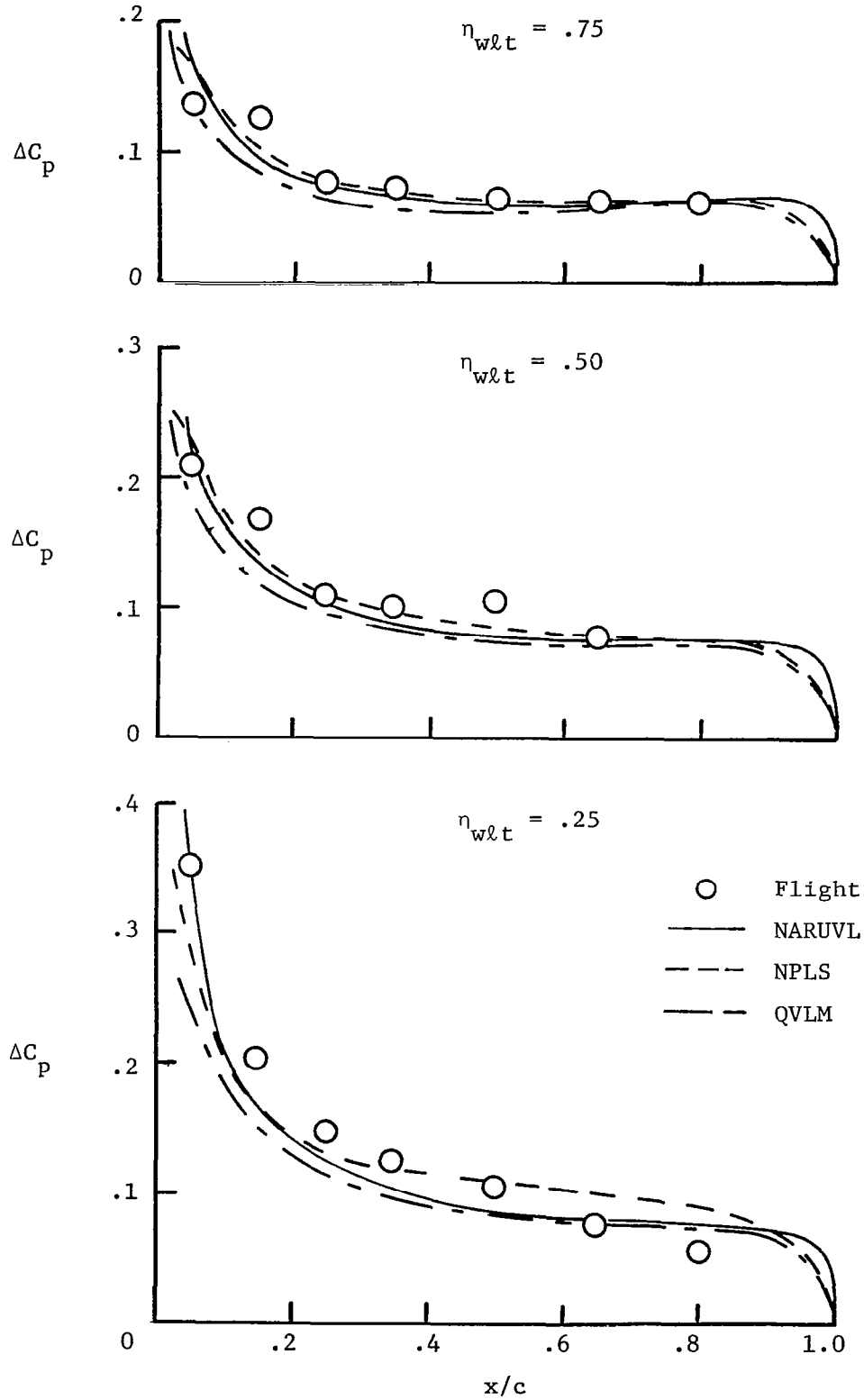

(a) M = 0.11, C_L = 1.32

Figure 5.7: Comparison of Flight Measured and Predicted Winglet Pressure Distribution

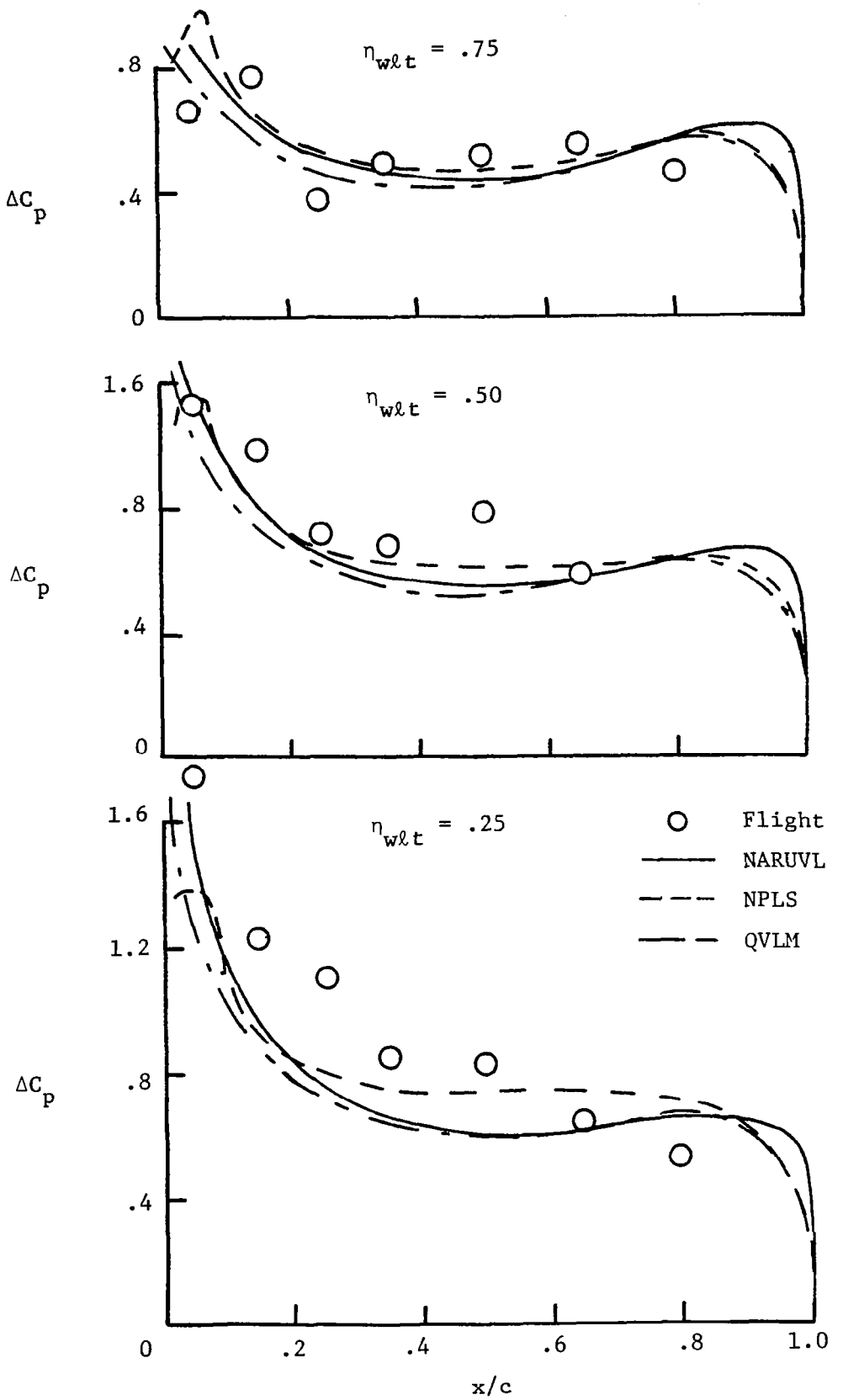

(b) M = 0.15, C_L = 0.72

Figure 5.7: (Continued)

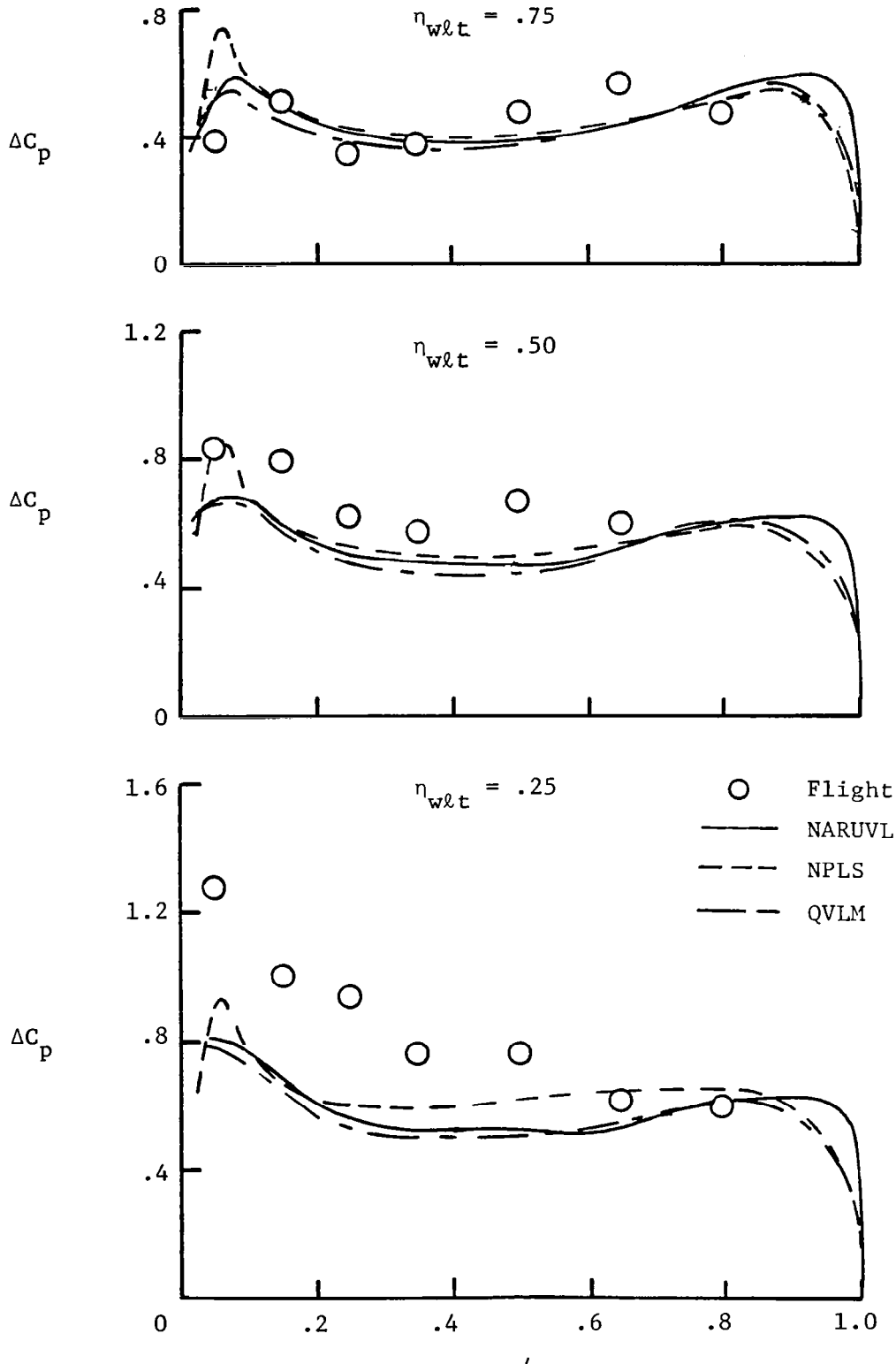

(c) M = 0.18, C_L = 0.48

Figure 5.7: (Concluded)

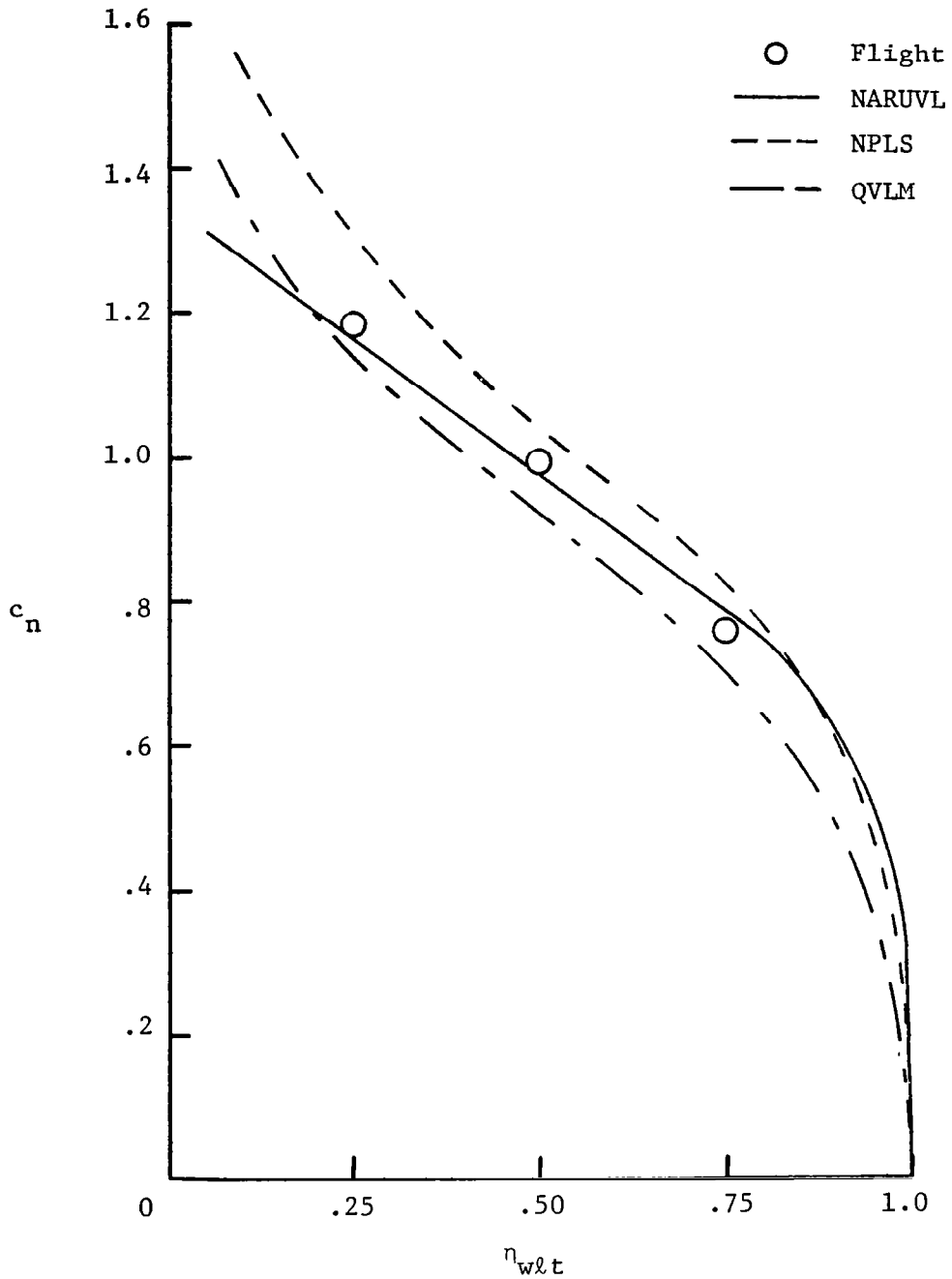

(a) M = 0.11, C_L = 1.32

Figure 5.8: Comparison of Flight Measured and Predicted Winglet Span Loads

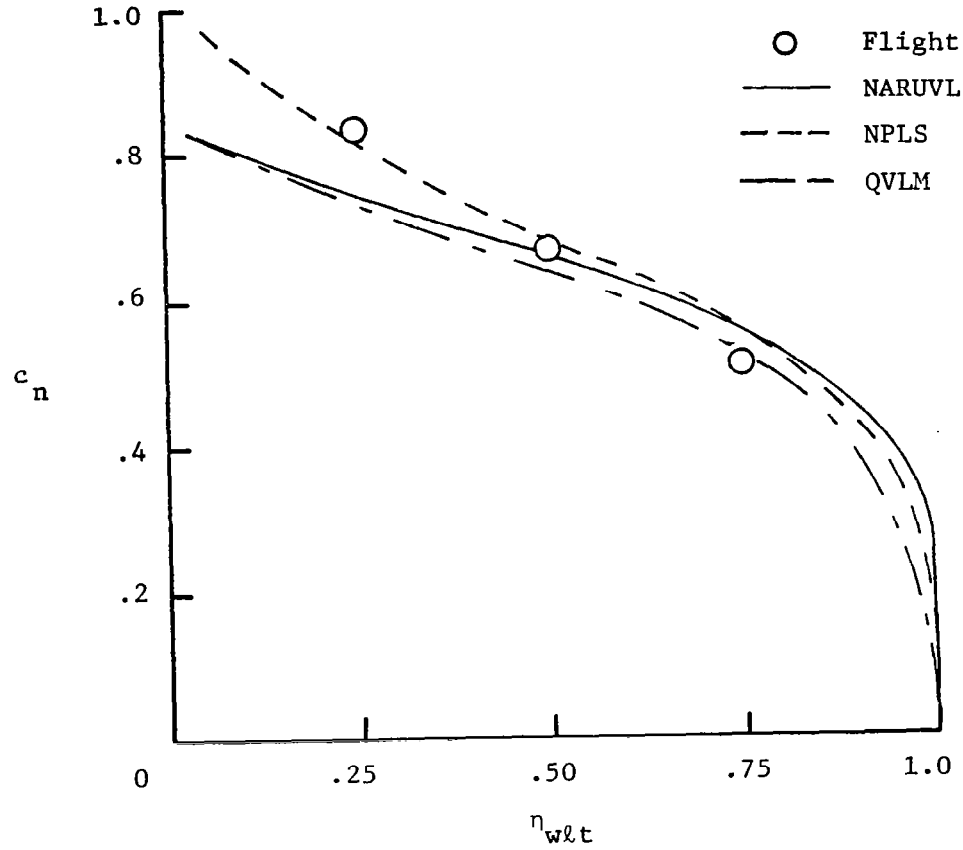

(b) M = 0.15, C_L = 0.72

Figure 5.8: (Continued)

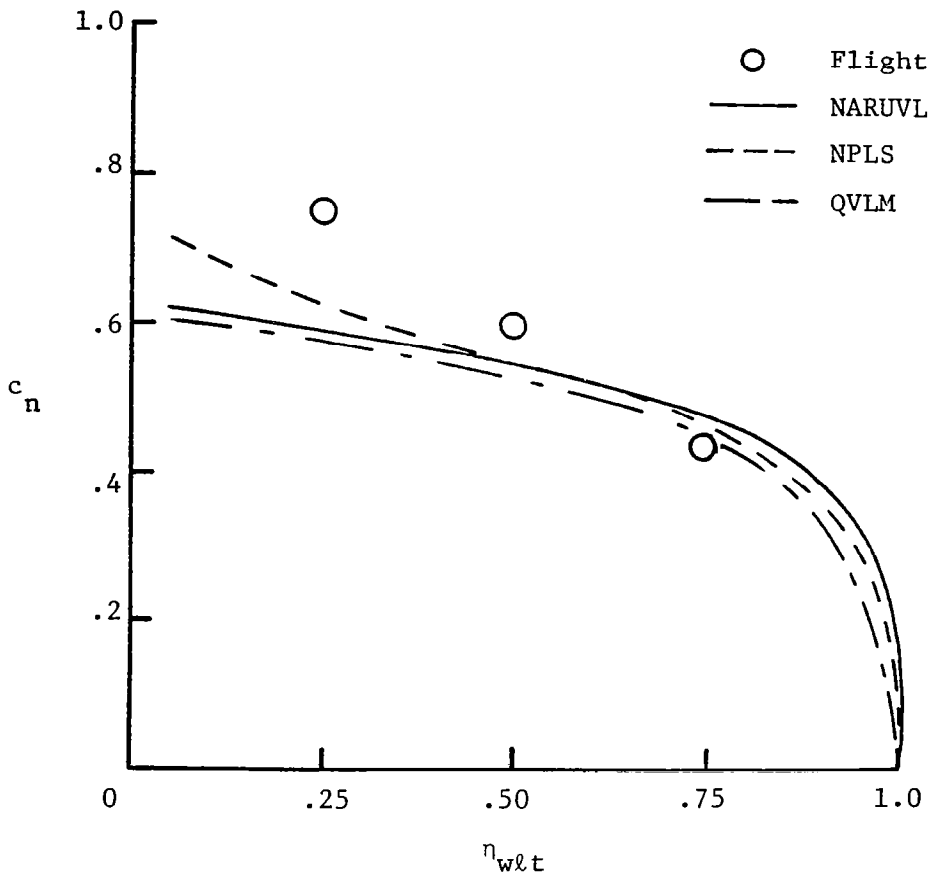

(c) M = 0.18, C_L = 0.48

Figure 5.8: (Concluded)

In Figure 5.3, upper- and lower-surface pressure coefficients at three winglet span stations are plotted for the airplane in steady-state, symmetrical flight. The results clearly indicate the strong effect of airplane angle of attack on the pressures measured on the upper surface of the winglet close to the leading edge and the wing-winglet juncture.

The effects of angle of sideslip on the winglet pressure coefficients are shown in Figure 5.4. The pressures are measured on the right winglet. Consequently, a positive increase in angle of sideslip results in higher winglet loading, as is also indicated by the results of Figure 5.4. At large negative sideslip angles, the front part of the winglet generates a negative (outward) lift, as can be seen in Figure 5.4d.

Figures 5.5 and 5.6 present winglet span load distributions for the airplane in symmetrical and sideslipping steady-state flight, respectively. These results are obtained from the data of Figures 5.3 and 5.4 through numerical integration.

Comparisons of in-flight measured and predicted winglet pressure differentials (ΔC_p) are shown in Figure 5.7. Three lifting surface methods are applied to predict the aerodynamic loading on the winglet: (1) the North American Rockwell United Vortex Lattice Method (NARUVL, Reference 23), (2) the Douglas Nonplanar Lifting Systems Method (NPLS, Reference 22), and (3) the Quasi-Vortex-Lattice Method (QVLM, Reference 21).

As can be seen in Figure 5.7a, the pressure differential comparisons at 25, 50, and 75 percent of the winglet span are in good agree-

ment with the theoretical predictions. At lower lift coefficients, However, the methods underpredict the aerodynamic loading near the wing-winglet juncture (see Figures 5.7b and 5.7c).

In Figure 5.8 comparisons are shown between measured and predicted winglet span loads. Again, all three methods show good agreement with the flight data except at low lift coefficients, at which the loading near the wing-winglet juncture is underpredicted. This underprediction of the loads may be the result of a non-uniform flow field near the wing tip while the lifting surface methods assume the flow field to be uniform.

5.3 Lateral-Directional Stability and Control Parameters

This section presents stability and control derivatives of the basic airplane and the airplane equipped with winglets. The equation error method is used to estimate the values of the stability and control derivatives from flight test data. The data reduction and estimation method both are described in Chapter 4, while geometric and mass characteristics for the airplane in both configurations are presented in Chapter 3.

The results for the airplane with and without winglets are presented in Figure 5.9. The data include four types of input forms for both rudder and aileron deflection. Time histories of the different input forms are shown in Chapter 4. In Figure 5.9 solid symbols represent the data for the winglet-equipped airplane, while open symbols represent the airplane without winglets. Also, the estimated values are fitted by linear or quadratic polynomials.

A significant amount of scatter can be observed for most derivatives. This scatter is partly due to the different control input forms applied. However, it is impossible to select the best estimates

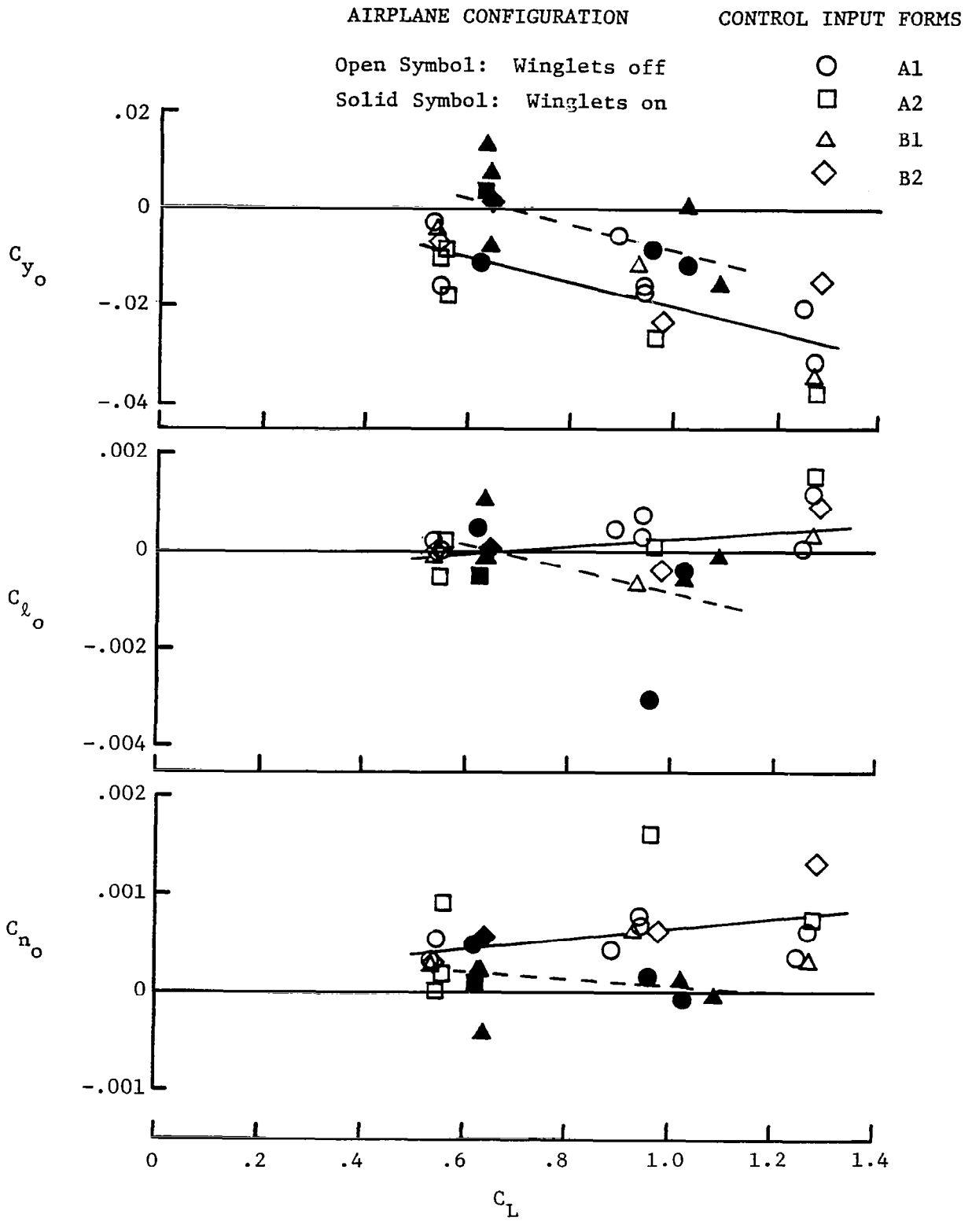

Figure 5.9: Estimated Lateral-Directional Parameters

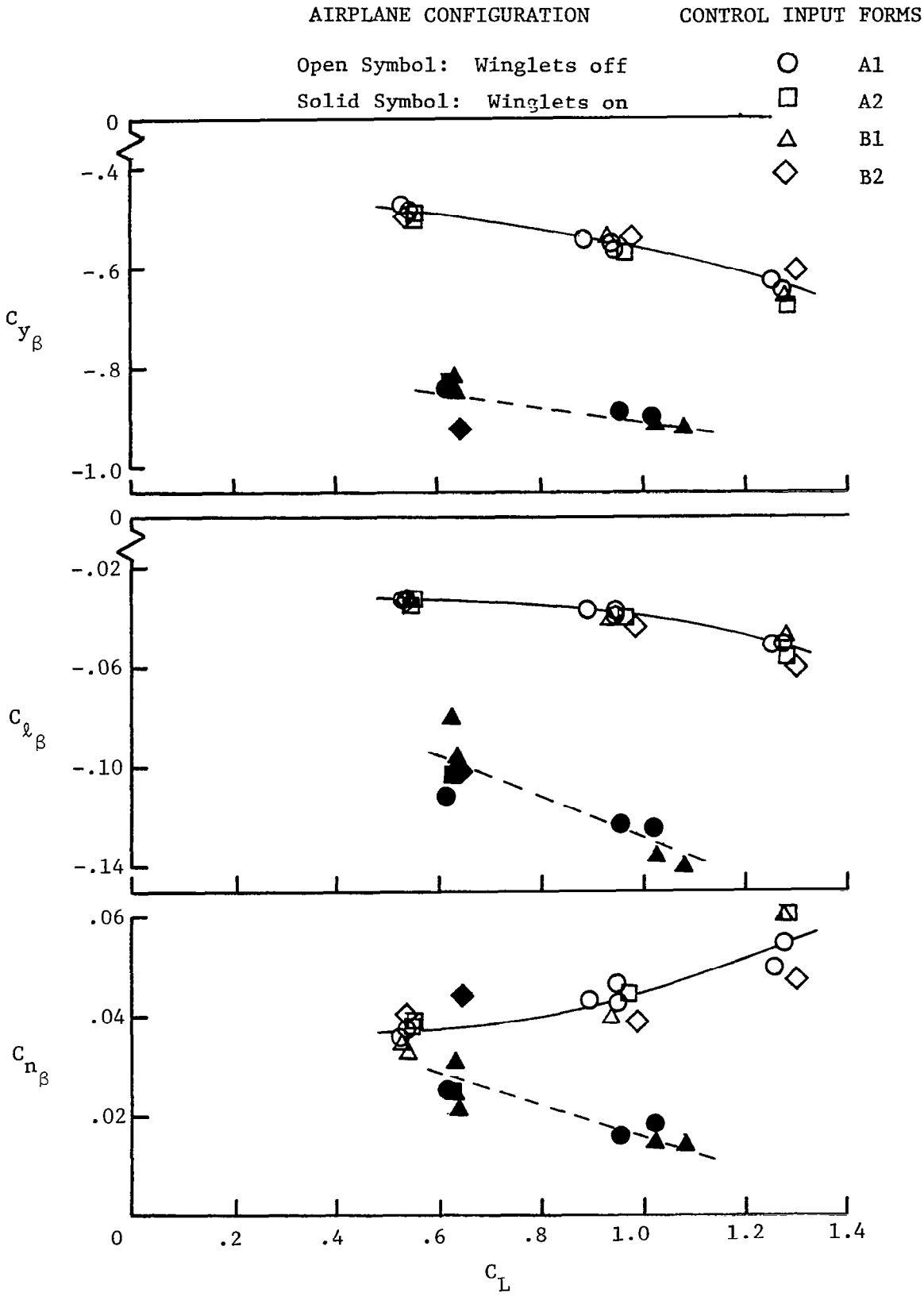

Figure 5.9: (Continued)

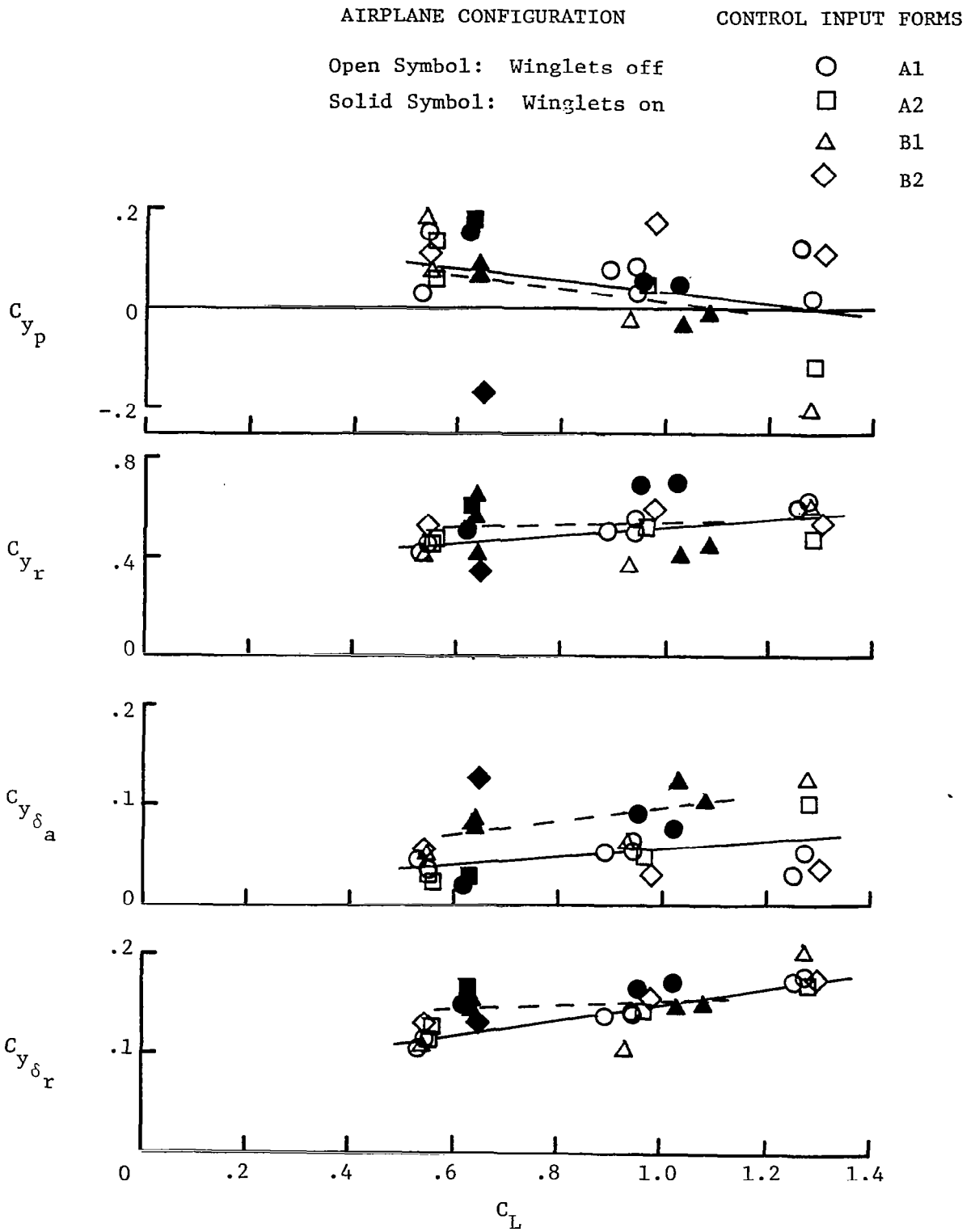

Figure 5.9: (Continued)

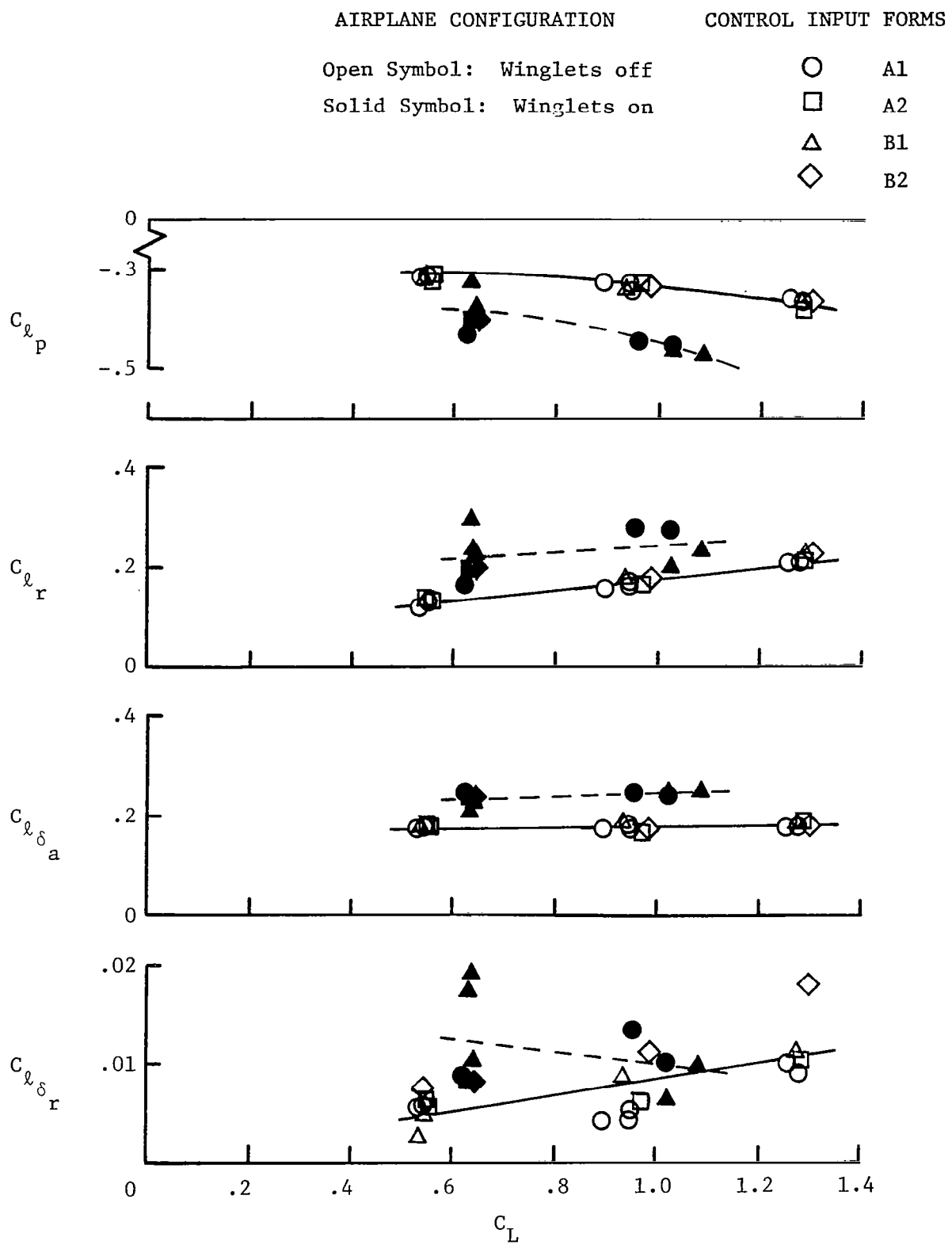

Figure 5.9: (Continued)

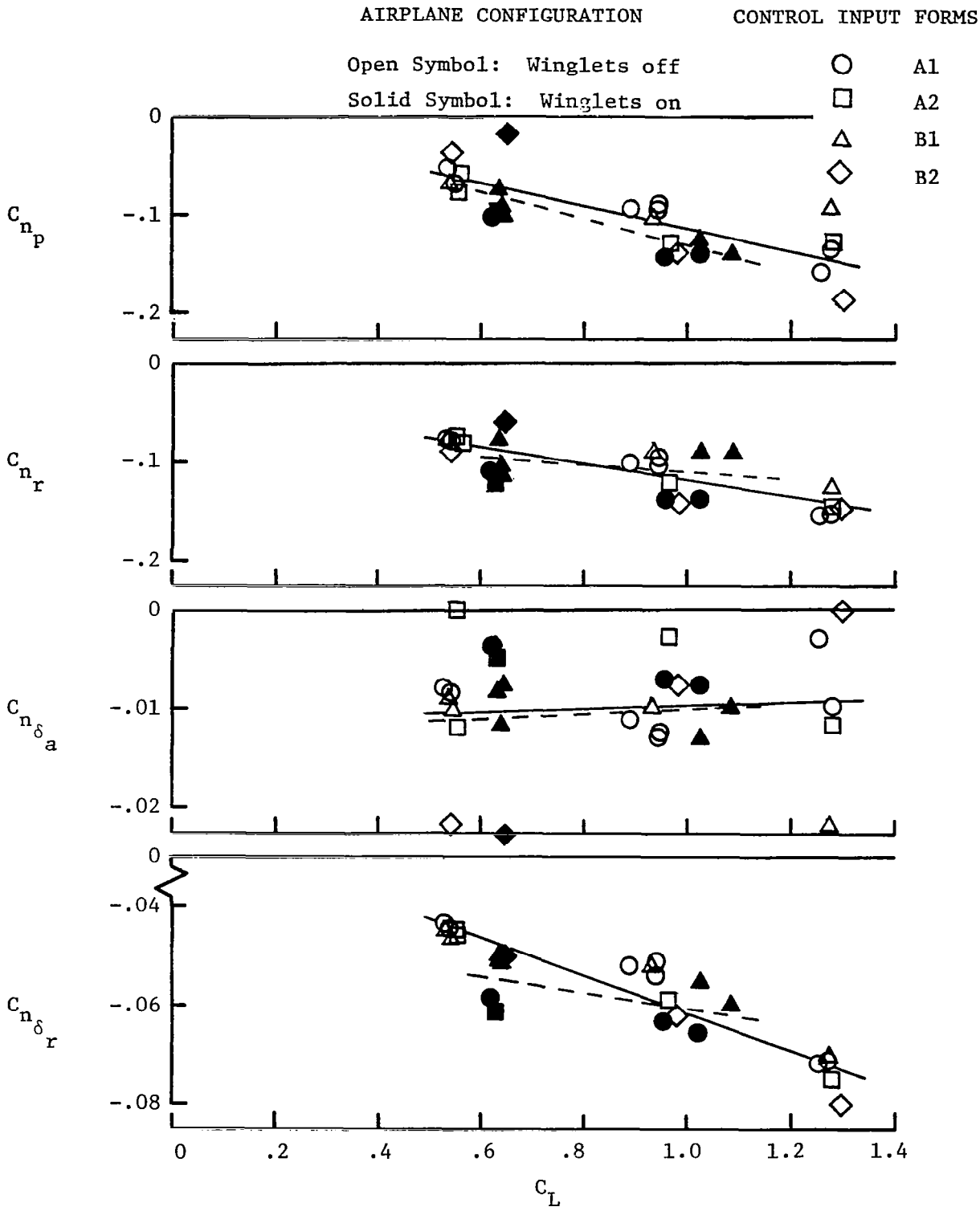

Figure 5.9: (Concluded)

from the flight test data. This problem is discussed in References 35 and 37. A comparison of the basic airplane results with those of other straight wing general aviation airplanes (e.g., References 35 and 36) indicates similar trends and magnitudes for the different lateral-directional stability and control derivatives. This comparison also reveals that the variability in the data of the various derivatives is also approximately the same. From the data of Figure 5.9 can be observed that the variability in the estimated values of the winglet-equipped airplane is higher. It appears that this is caused by an increase in the control input form sensitivity as a result of the addition of the wing-tip-mounted winglets.

The effects of winglets on the various lateral-directional stability and control derivatives are discussed in the following subsections. A physical explanation of the various effects of winglets on lateral-directional stability derivatives can be found in Chapter 2 (Sub-Subsection 2.2.1.1).

The stability and control derivatives are referenced to the airplane body axes.

5.3.1 Sideslip Stability Derivatives

The side force derivative due to sideslip, C_{y_β}, is well estimated as indicated by the small amount of scatter in the data. The increment in C_{y_β} produced by the winglets is approximately 60%.

The rolling moment derivative due to sideslip, C_{ℓ_β}, is augmented by about 250 percent due to winglets. This increase has a signficant effect on the flying qualities of the airplane, as can be expected.

The variability in the estimated values of the basic airplane is very small. More scatter can be observed in the data for the winglet-equipped airplane.

Winglets appear to have a destabilizing influence on the directional stability of the airplane. This destabilizing effect becomes larger with increasing angle of attack. With increasing angle of attack, winglet loading increases; and, consequently, the winglet normal force vector will rotate forward, which results in a destabilizing influence on C_{n_β}.

5.3.2 Roll-Rate Stability Derivatives

The side force derivative due to roll rate, C_{y_p}, is not well determined, as is indicated by the scatter of the estimated values. The linear fit through both sets of data shows very good agreement. This indicates that the effect of winglets on C_{y_p} is negligible.

The roll damping derivative, C_{ℓ_p}, is very well determined. The estimated values do not show much variability. Winglets produce an increase in roll damping, due to a higher wing-tip loading.

The yawing moment due to roll rate, C_{n_p}, is hardly affected by the addition of winglets, as indicated by the good agreement between the linear fits through the data of both configurations.

5.3.3 Yaw-Rate Stability Derivatives

The side force due to yaw rate derivative, C_{y_r}, is generally not a very important stability parameter. The effect of winglets on this de-

rivative is very small, as indicated by the agreement of the linear curve fits through both sets of flight data.

A slight increment can be observed in the rolling moment derivative due to yaw rate, C_{ℓ_r}, as a result of installation of winglets. The estimated parameters of the basic airplane display significantly less variability than those of the winglet-equipped airplane.

The scatter in the data of the yaw damping derivative, C_{n_r}, masks possible winglet effects. However, the influence of winglets on yaw damping appears to be small, as indicated by the results shown in Figure 5.9.

5.3.4 Lateral Control Derivatives

The side force derivative due to lateral control, $C_{y_{\delta_a}}$, is generally negligible. However, an exception may occur when the lateral control device is located close to a vertical surface (Reference 38). The aileron control surfaces of the subject airplane are situated very near to the winglets. Therefore, a change can be expected in the magnitude of this derivative. The results of Figure 5.9 indicate that $C_{y_{\delta_a}}$ is not very well estimated. However, a comparison of the linear fits through the data reveals that winglets increase the level of side force due to lateral control by approximately 60 percent. Positive aileron deflection is defined as left aileron deflected downward and the right aileron upward. As a result, the left (right) winglet will experience a lower (higher) pressure at its upper surface. The sum of these effects is a positive increment in side force due to a positive aileron deflection, and vice versa.

The rolling moment due to lateral control, $C_{\ell_{\delta_a}}$, is very well determined. The effect of winglets on aileron effectiveness is similar to the effect on roll damping showing slightly increased aileron effectiveness. As a result, only minor changes can be observed in the roll performance of the airplane.

The yawing moment due to lateral control parameter, $C_{n_{\delta_a}}$, is not very well determined, as can be observed from the significant amount of scatter in the data. The subject airplane displays adverse yaw due to aileron, and winglets appear to have virtually no effect on the level of adverse yaw. This agrees with the results listed in Reference 20.

5.3.5 Directional Control Derivatives

It is clear that for most airplane configurations the effect of winglets on the directional control derivatives should be small. The influence of winglets on the side force due to rudder, $C_{y_{\delta_r}}$, is small, as can be observed from the data in Figure 5.9.

The roll derivative due to rudder control, $C_{\ell_{\delta_r}}$, is not very well determined, as indicated by the variability in the data. However, References 35 and 36 also indicate that $C_{\ell_{\delta_r}}$ is not a well-determined parameter. For the winglet-equipped airplane, the slightly negative trend in $C_{\ell_{\delta_r}}$ with increasing C_L can be attributed to the two outlying data points at $C_L \simeq 0.60$. Except for these two data points the effect of winglets on this derivative appears to be small.

The scatter in the estimated values of the yawing moment due to rudder control derivative, $C_{n_{\delta_r}}$, is very similar to the pattern displayed in the yaw damping data. Winglet effect on this derivative is masked as a result of the scatter in the data. A comparison of the linear curve fits for the airplane in both configurations appears to indicate a slight change in the trend of $C_{n_{\delta_r}}$ versus C_L. However, the total effect is small.

5.4 Lateral-Directional Flying Qualities

A short flight-test program has been conducted to evaluate the effects of winglets on the flying qualities of the research airplane. The characteristics of the airplane in both configurations are (winglets on and off) measured for a cruise (105 KIAS and power for level flight) and a power approach type condition (80 KIAS and power for level flight).

5.4.1 Steady Heading Sideslips

It is clear from the analytical predictions of Chapter 2 and the flight measured parameters in Section 5.3 that stability and control derivatives can be affected significantly by the installation of winglets. The steady heading sideslip method is a suitable flight test technique to verify the changes in sideslip stability and lateral-directional control derivatives due to winglets.

The lateral-directional steady state, straight-line flight equations of motion can be written as follows (see References 38 and 39):

$$C_{y_o}' + C_{y_\beta}\beta + C_{y_{\delta_a}}\delta_a + C_{y_{\delta_r}}\delta_r = (-mg\ \sin\phi)/\bar{q}S \qquad (a)$$

$$C_{\ell_o}' + C_{\ell_\beta}\beta + C_{\ell_{\delta_a}}\delta_a + C_{\ell_{\delta_r}}\delta_r = 0 \qquad (b) \qquad (5.3)$$

$$C_{n_o}' + C_{n_\beta}\beta + C_{n_{\delta_a}}\delta_a + C_{n_{\delta_r}}\delta_r = 0 \qquad (c)$$

For symmetrical airplane configurations, symmetrical power conditions, and small bank angles the following expressions can be developed for the variation of aileron position, rudder position, and bank angle with sideslip angle:

$$C_{y_\beta} + C_{y_{\delta_a}}\frac{\partial\delta_a}{\partial\beta} + C_{y_{\delta_r}}\frac{\partial\delta_r}{\partial\beta} + C_L\frac{\partial\phi}{\partial\beta} = 0 \qquad (a)$$

$$C_{\ell_\beta} + C_{\ell_{\delta_a}}\frac{\partial\delta_a}{\partial\beta} + C_{\ell_{\delta_r}}\frac{\partial\delta_r}{\partial\beta} = 0 \qquad (b) \qquad (5.4)$$

$$C_{n_\beta} + C_{n_{\delta_a}}\frac{\partial\delta_a}{\partial\beta} + C_{n_{\delta_r}}\frac{\partial\delta_r}{\partial\beta} = 0 \qquad (c)$$

These expressions will be used in the following discussions.

5.4.1.1 Rudder Deflection and Force

In Figure 5.10, rudder deflection required for steady heading sideslip is plotted for the airplane flying at 80 KIAS and 105 KIAS. The flight data indicate that winglets significantly diminish rudder deflection required for a given steady heading sideslip angle.

From Equation (5.4) the following expression can be derived for the rudder deflection versus sideslip gradient:

$$\frac{\partial \delta_r}{\partial \beta} = \frac{-\frac{C_{n_\beta}}{C_{n_{\delta_r}}}\left(1 - \frac{C_{n_{\delta_a}}}{C_{\ell_{\delta_a}}}\frac{C_{\ell_\beta}}{C_{n_\beta}}\right)}{\left(1 - \frac{C_{n_{\delta_a}}}{C_{\ell_{\delta_a}}}\frac{C_{\ell_{\delta_r}}}{C_{n_{\delta_r}}}\right)} \tag{5.5}$$

The denominator of the right-hand side of this expression is approximately equal to one. The results of Section 5.3 indicate that winglets have a stabilizing effect on dihedral effect, while the directional stability is reduced. These two changes combined with adverse yaw due to aileron ($C_{n_{\delta_a}} < 0$) produce a reduction in the gradient $\partial\delta_r/\partial\beta$, as shown in Figure 5.10. For the winglet-equipped airplane at 80 KIAS and sideslip angles smaller than 10°, the gradient is nearly zero. For larger sideslip angles, directional stability slightly improves; and, consequently, the gradient becomes steeper.

In Figure 5.11 in-flight measured variations of rudder pedal forces with sideslip are plotted. Rudder forces display the same trend as rudder deflections.

An interesting effect which can be observed from the flight data is the continuous need for right rudder (positive rudder force, negative rudder deflection) to maintain a zero sideslip steady heading flight attitude. This is caused by the propeller slipstream effect on the sidewash angle and the dynamic pressure at the tail.

An additional observation which can be made is that for the winglet-equipped airplane, the rudder is not fully deflected. During the maneuver, the pilot restricted rudder deflection to prevent stal-

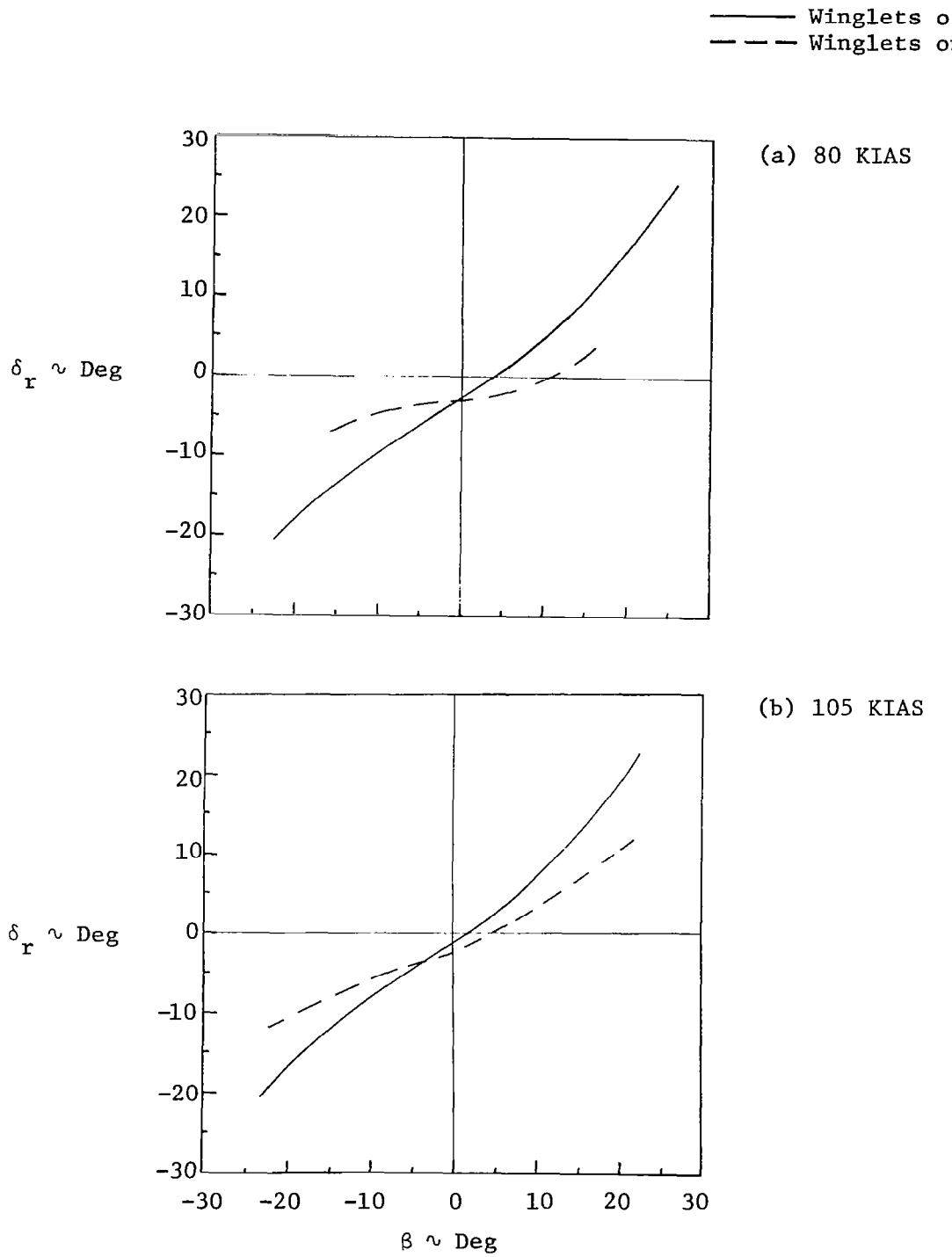

Figure 5.10: Effect of Winglets on Rudder Deflection Required in Steady Heading Sideslip

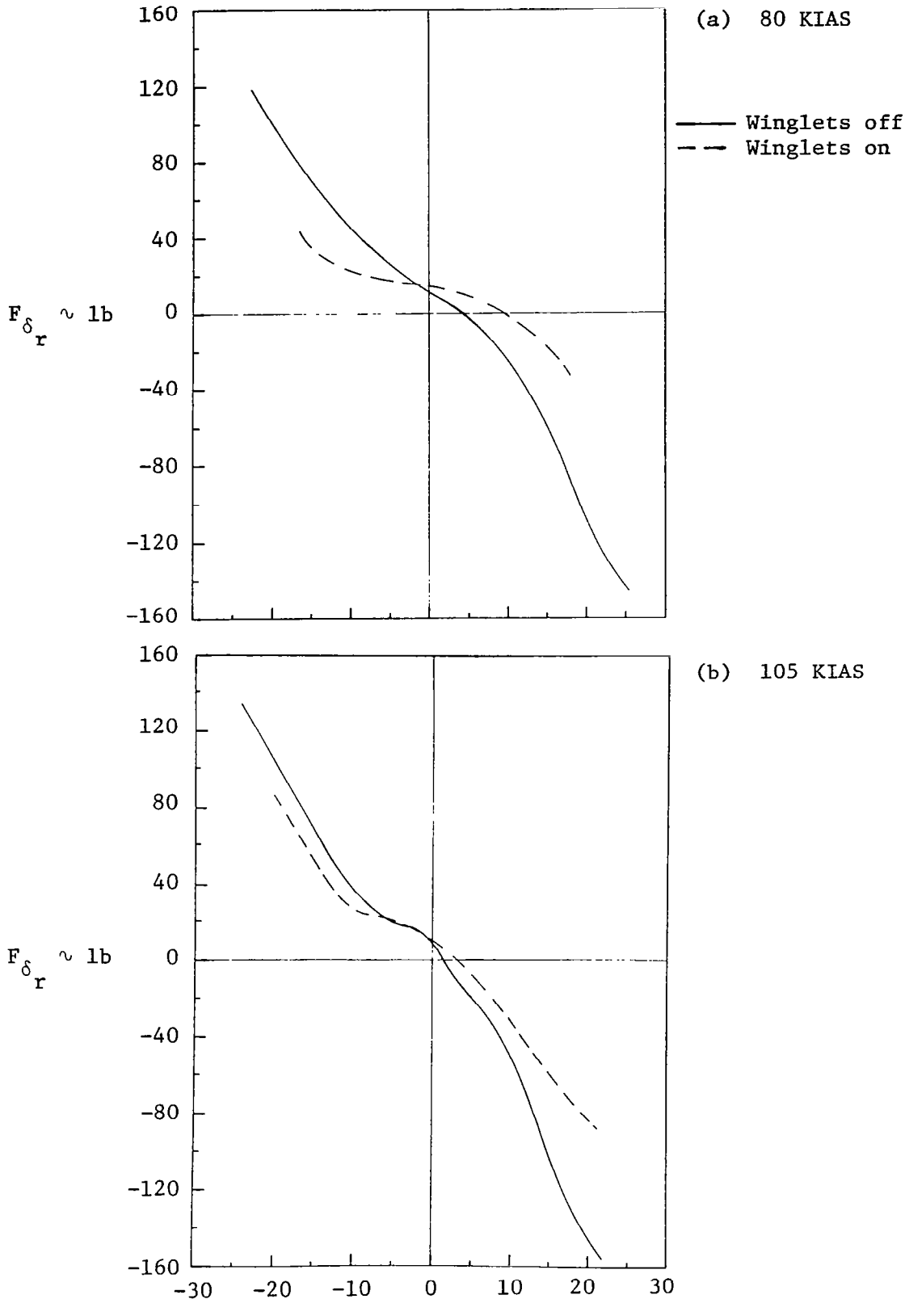

Figure 5.11: Effect of Winglets on Rudder Pedal Force Variation with Steady Heading Sideslip

ling of the upwind winglet. In Section 5.4.1.5, the effects of winglet stall on the lateral-directional characteristics in steady heading sideslip will be discussed.

5.4.1.2 Aileron Deflection and Force

From Equation (5.4) the following expression can be derived for the gradient of aileron deflection versus sideslip:

$$\frac{\partial \delta_a}{\partial \beta} = \frac{-\frac{C_{\ell_\beta}}{C_{\ell_{\delta_a}}} \left(1 - \frac{C_{\ell_{\delta_r}}}{C_{n_{\delta_r}}} \frac{C_{n_\beta}}{C_{\ell_\beta}}\right)}{\left(1 - \frac{C_{n_{\delta_a}}}{C_{\ell_{\delta_a}}} \frac{C_{\ell_{\delta_r}}}{C_{n_{\delta_r}}}\right)} \tag{5.6}$$

Again, the denominator of the right-hand side of this expression is approximately one. At the same time, the rudder control derivatives can be considered to be virtually unaffected by winglets. Consequently, it is clear that a reduction in directional stability and an increase in dihedral effect produce an increment in aileron required for steady heading sideslip. This explanation correlates well with the in-flight measured data shown in Figure 5.12. The total winglet effect results in an increase in gradient of more than 100 percent.

The aileron stick forces are plotted in Figure 5.13. The airplane flight control system has an important influence on these forces. In Chapter 3, it is mentioned that the airplane has a rudder-aileron interconnect. This interconnect feeds rudder forces into the aileron control system. Therefore, the total winglet effect is a slight increase in the aileron force gradient. A by-product of this increase

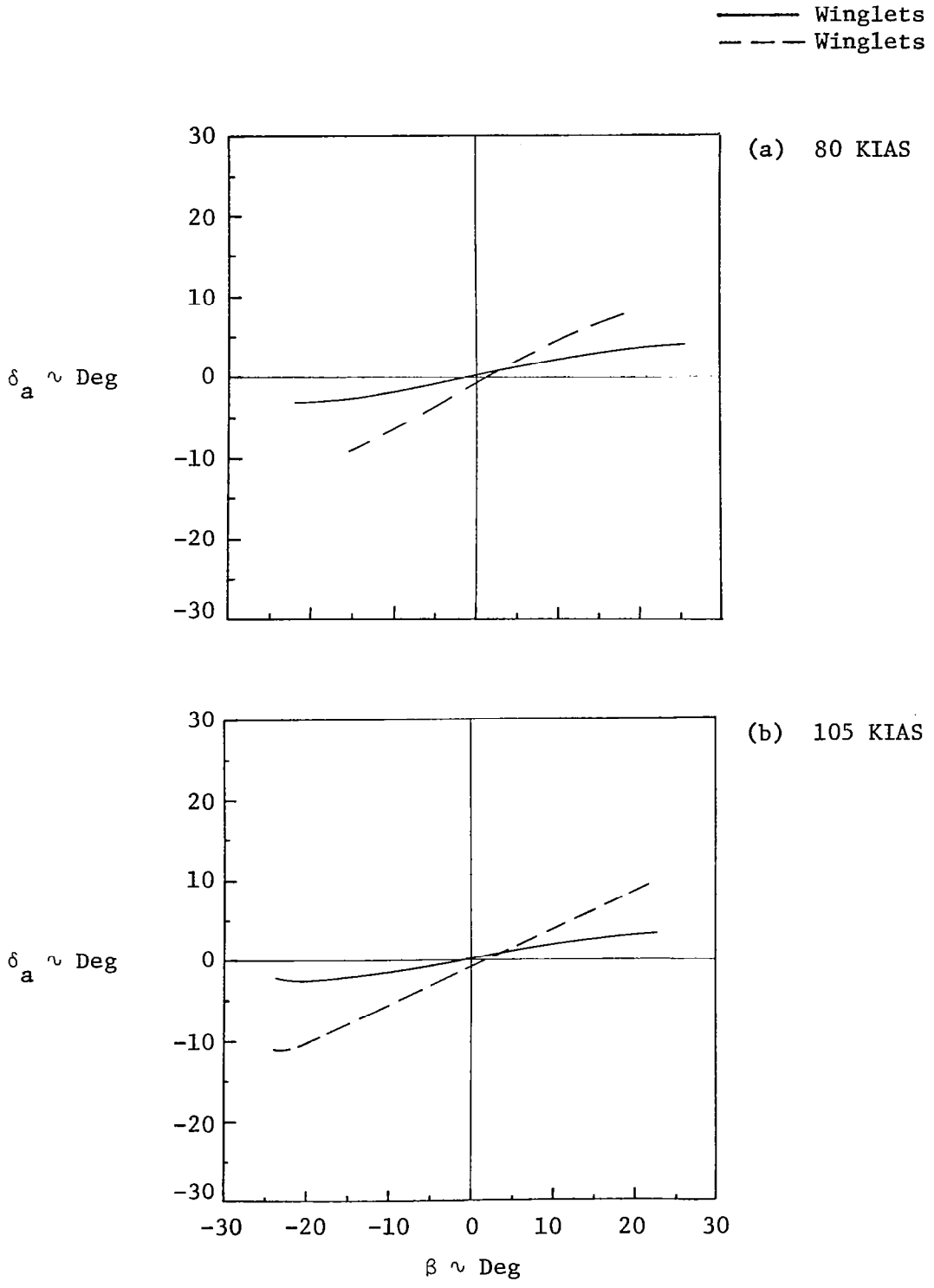

Figure 5.12: Effect of Winglets on Aileron Deflection Required in Steady Heading Sideslip

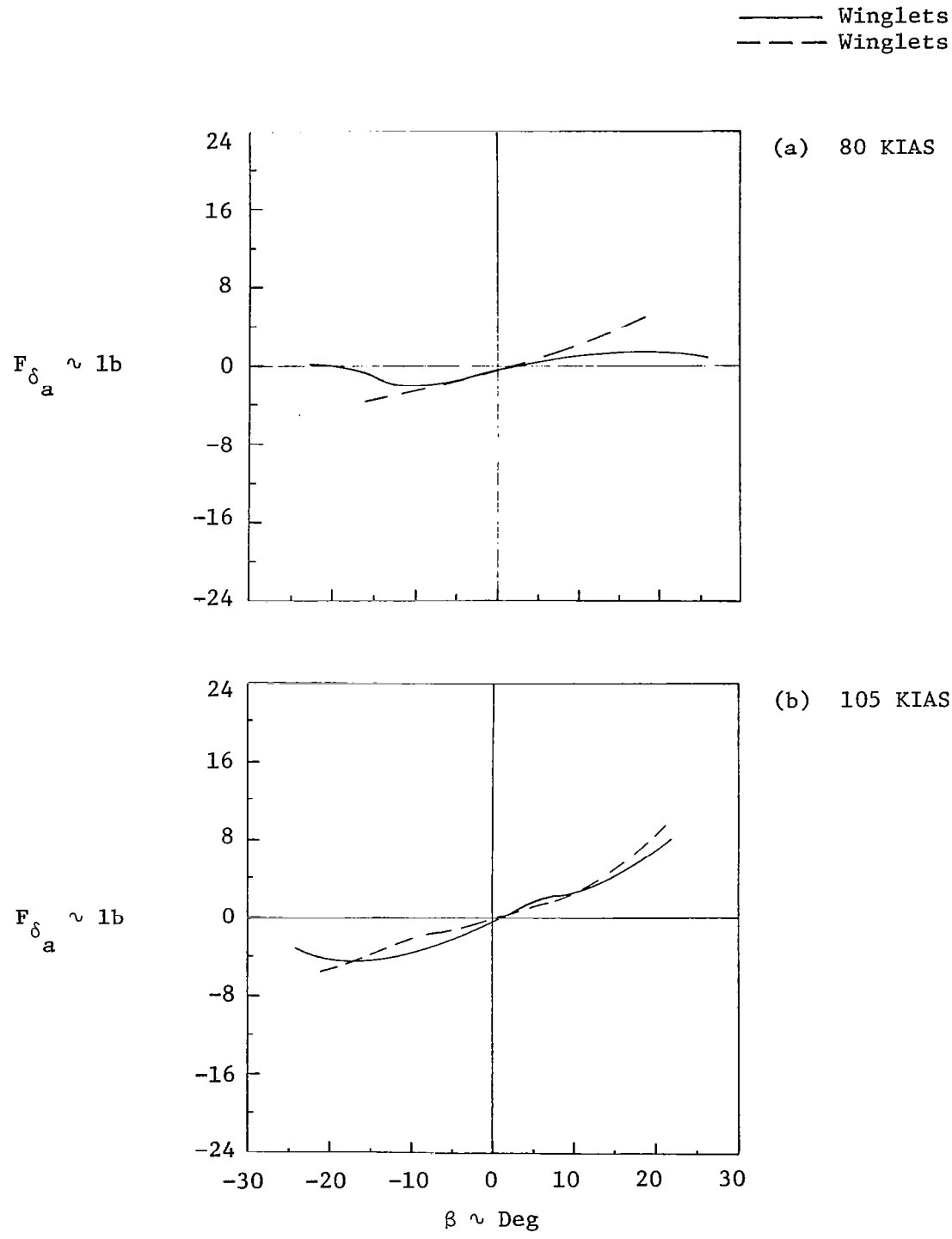

Figure 5.13: Effect of Winglets on Aileron Stick Force Variation with Steady Heading Sideslip

in aileron deflection requirements for trim is a decrease in cross-wind component allowable for landing (Reference 54).

5.4.1.3 Elevator Deflection and Force

Pitching moments are generated by sideslip angles due to changes in airflow characteristics at the wing and the horizontal tail. Elevator deflection and elevator stick force are plotted as function of angle of sideslip in Figures 5.14 and 5.15, respectively. A nose-down pitching moment can be observed with sideslip for the airplane in both configurations. This is caused by the move of the horizontal tail out of the high energy propeller slipstream when sideslip is induced. Therefore, the elevator must be deflected upward for the horizontal tail to generate the same down force.

A comparison of the δ_e versus β plots for the two flight conditions indicates that a more downward (positive) elevator deflection is required with increasing airspeed, as expected.

The plots also indicate that winglets produce a small positive increment in C_{m_o}. Consequently, for a given flight condition a more positive elevator deflection is required for the winglet-equipped airplane. This positive increment in C_{m_o} is caused by the inward cant of the winglets.

5.4.1.4 Bank Angle

The relationship for bank angle variation with sideslip angle can be developed, e.g., from Equation (5.4a) and can be stated as follows:

$$\frac{\partial \phi}{\partial \beta} = - \frac{1}{C_L} \left(C_{y_\beta} + C_{y_{\delta_r}} \frac{\partial \delta_r}{\partial \beta} + C_{y_{\delta_a}} \frac{\partial \delta_a}{\partial \beta} \right) \qquad (5.7)$$

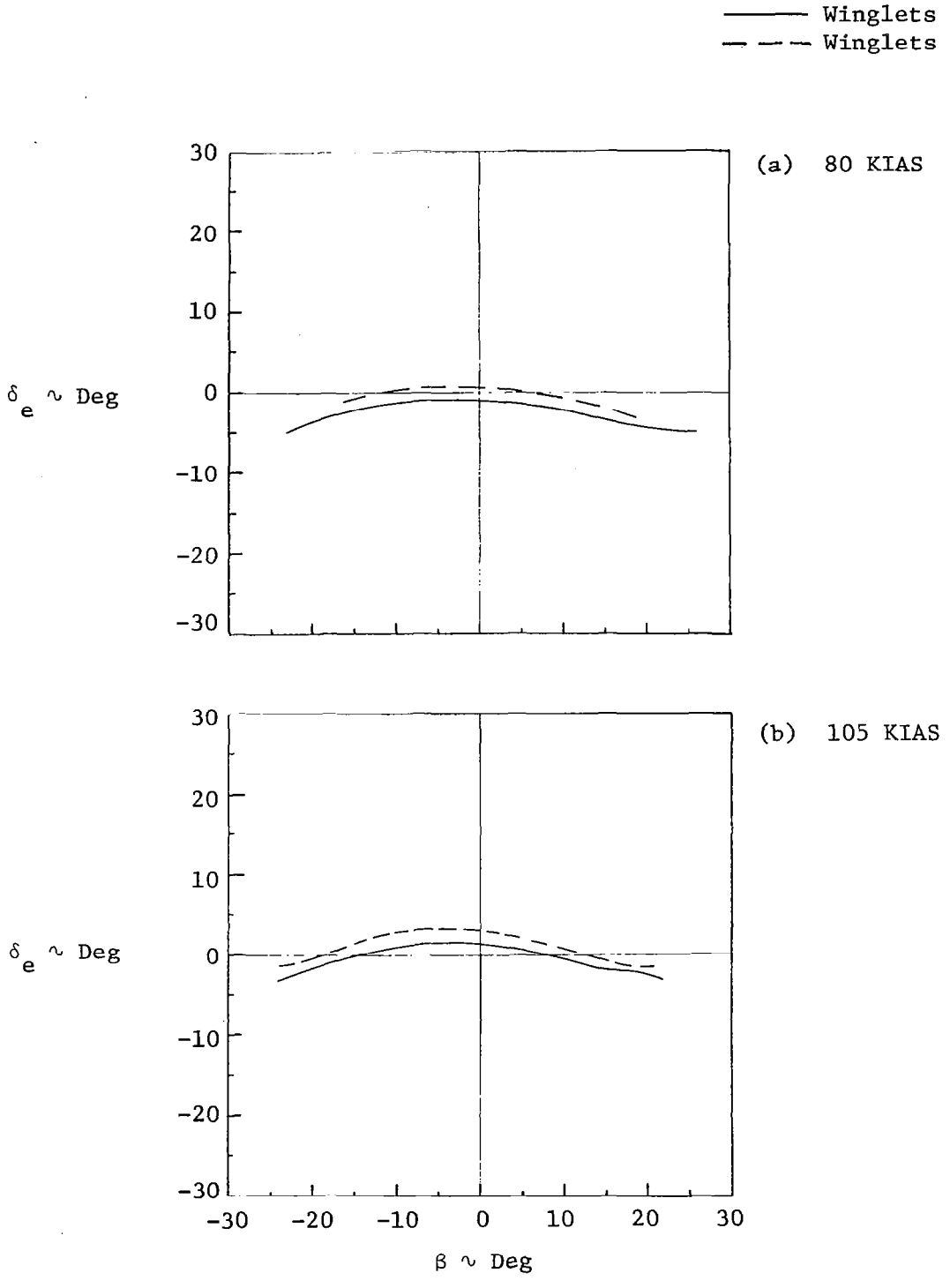

Figure 5.14: Variation of Elevator Deflection with Steady Heading Sideslip for the Airplane with and without Winglets

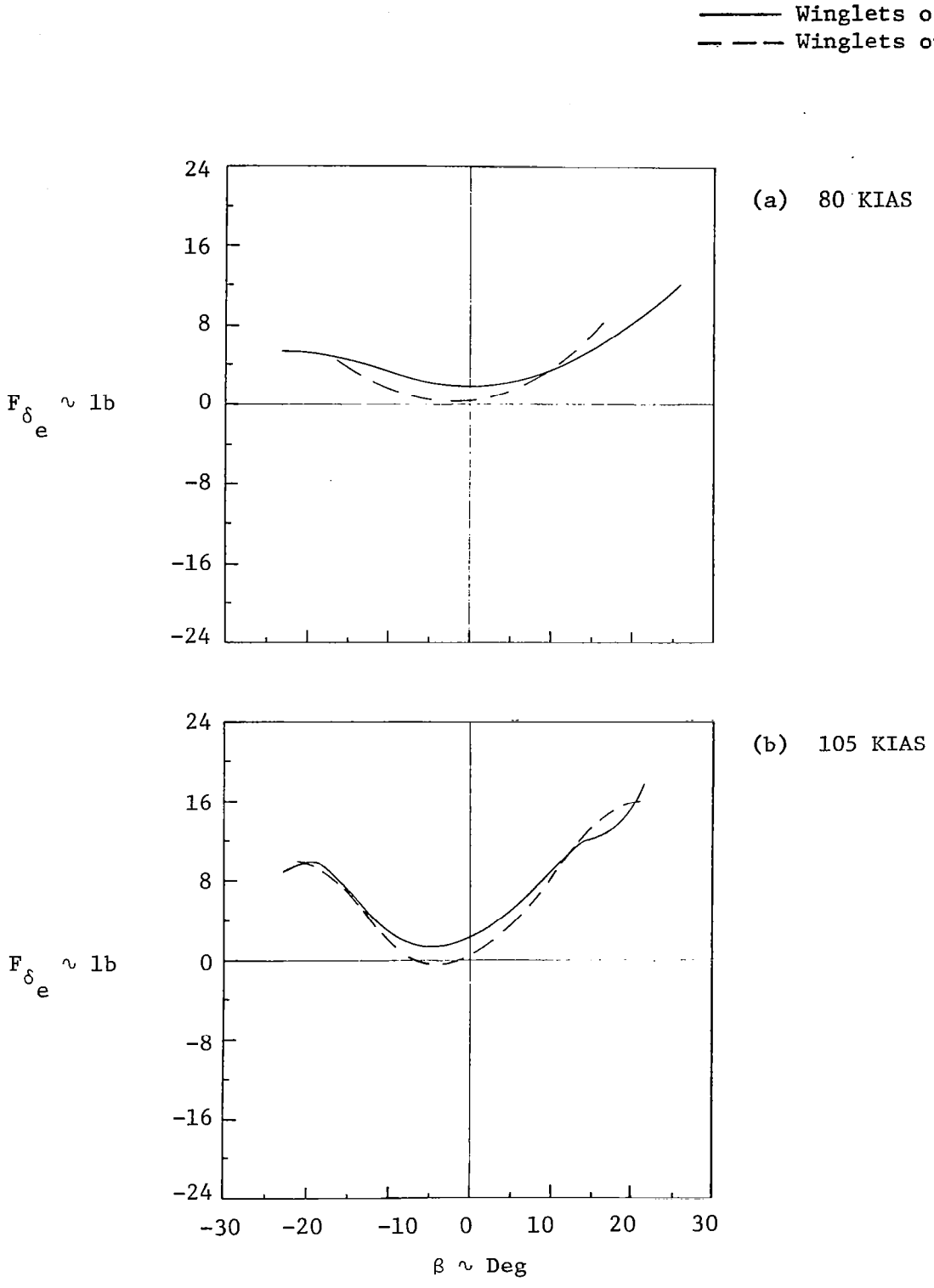

Figure 5.15: Variation of Elevator Stick Force with Steady Heading Sideslip for the Airplane with and Without Winglets

The dominant parameter in this equation is C_{y_β}. Winglets produce a large increase in C_{y_β}, and as a result the gradient of bank angle versus sideslip becomes steeper. This conclusion agrees with the in-flight results shown in Figure 5.16. Airplane lift coefficient reduces with increased airspeed. Consequently a reduction in the gradient can be noted when comparing the plots for the two flight conditions.

In Table 5.1 the measured relationship between sideslip angle and bank angle, aileron deflection, and rudder deflection are compared with those predicted using the lateral-directional stability derivatives estimated from transient data and listed in Section 5.3. The analytical form of these relationships is derived in Appendix B of Reference 35. Good correlations are shown between both sets of data, except for $\partial\beta/\partial\delta_a$ for the airplane with winglets. The results of Table 5.1 appear to verify to some extent the estimates in Section 5.3 of the derivative C_{y_β}, and the combination of derivatives $C_{\ell_{\delta_a}}/C_{\ell_\beta}$ and $C_{n_{\delta_r}}/C_{n_\beta}$.

5.4.1.5 Aileron Stick Force Reversal

A topic not discussed in the earlier subsections is the influence of winglet stall on the lateral-directional characteristics in steady heading sideslips. The previous results show that with increasing sideslip angle a continuous increase in aileron deflection and rudder deflection is required. The same is true for aileron stick force and rudder pedal force. These trends are also demonstrated in Figure 5.17.

Table 5.1: Measured and Predicted Aileron, Rudder, and Bank Angle Gradients in Steady Heading Sideslip

Measured[1]

Configuration	Winglets off		Winglets on	
Flight Cond.	80 KIAS	105 KIAS	80 KIAS	105 KIAS
C_L	0.98	0.63	1.03	0.60
$\partial\beta/\partial\phi$	2.13	1.38	1.32	0.87
$\partial\beta/\partial\delta_a$	5.0	6.15	1.82	2.13
$\partial\beta/\partial\delta_r$	1.38	1.33	5.0	2.35

Predicted[2]

Configuration	Winglets off		Winglets on	
Flight Cond.	80 KIAS	105 KIAS	80 KIAS	105 KIAS
C_L	0.98	0.63	1.03	0.60
$\partial\beta/\partial\phi$	2.07	1.54	1.17	0.77
$\partial\beta/\partial\delta_a$	4.76	6.15	1.93	2.64
$\partial\beta/\partial\delta_r$	1.44	1.38	5.39	2.13

[1]From Figures 5.10, 5.12, and 5.16 for sideslip variation of ±10°

[2]Data of Figure 5.9 and method presented in Appendix B of Reference 35.

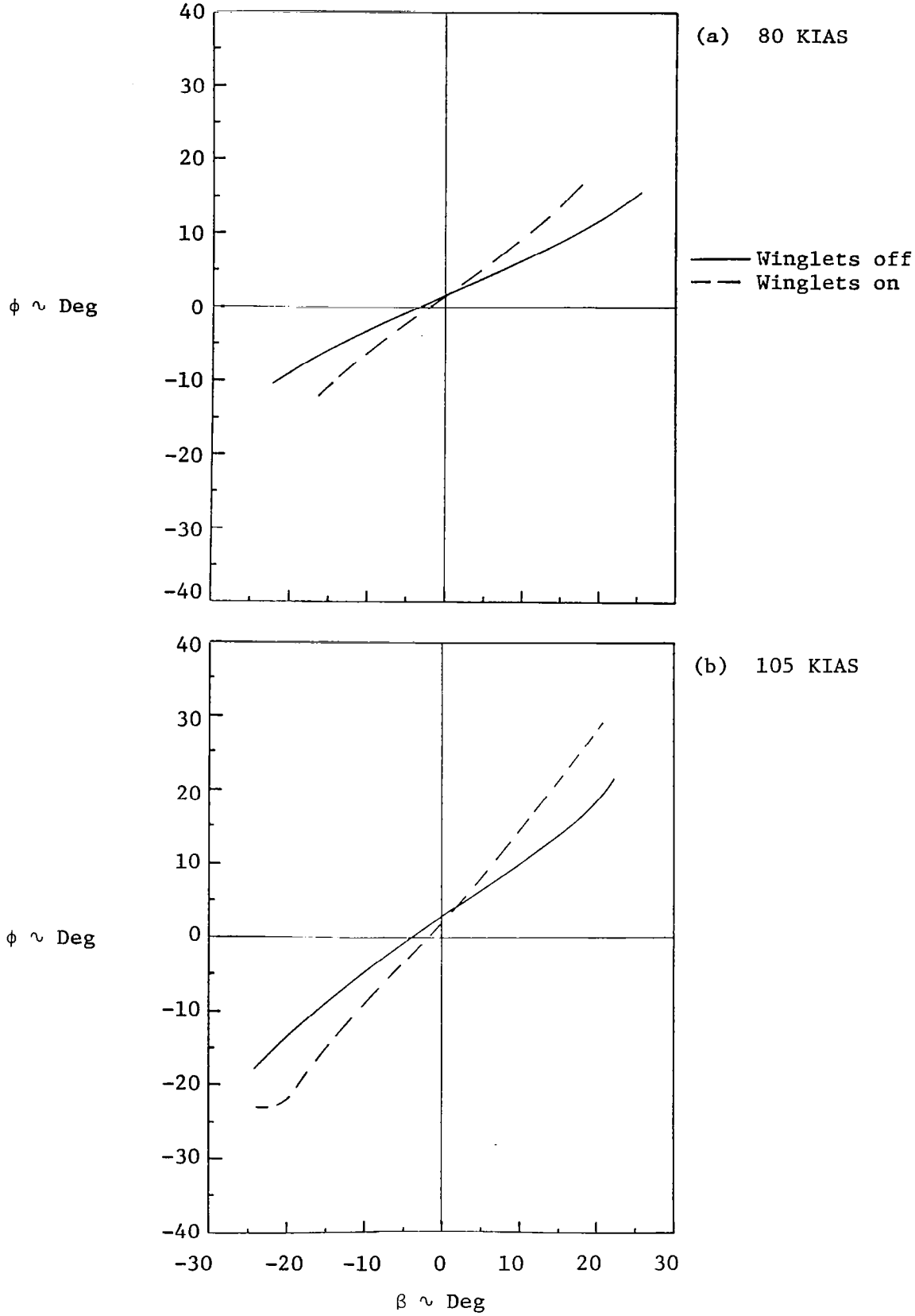

Figure 5.16: Effect of Winglets on Bank Angle Required for Steady Heading Sideslip

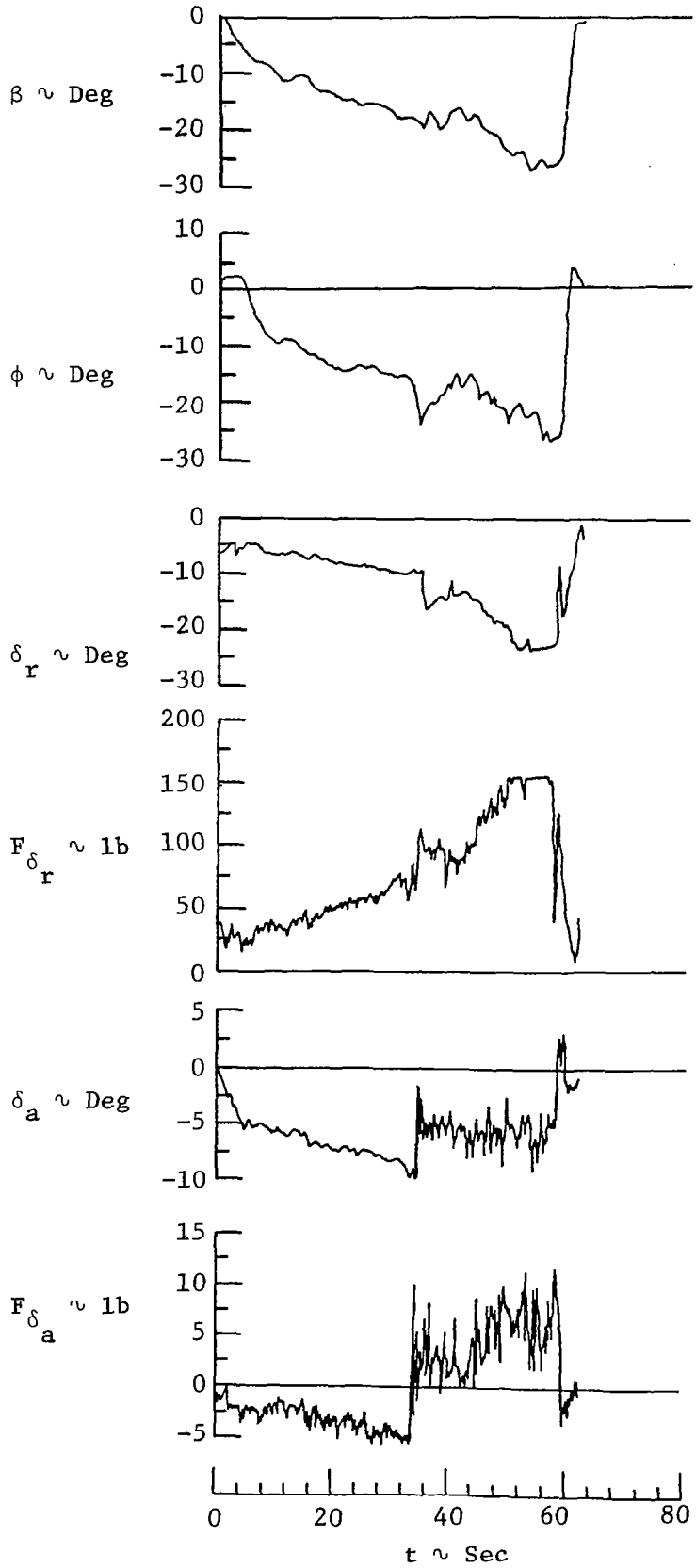

Figure 5.17: Time Histories of Steady Heading Sideslip Maneuver for Airplane with Winglets (h = 7300 ft, 90 KIAS, W $\simeq$ 6400 lb)

In Figure 5.17, time histories are presented for a continuously increasing steady heading sideslip ($\beta < 0$). From t = 0 sec. until t = 35 sec., a steady increase can be observed in angle of sideslip, aileron deflection and force, and rudder deflection and force. At t = 35 sec. an abrupt change is displayed in aileron stick force and deflection. A reversal can be noted in aileron force direction. At the same time, aileron position reduces in magnitude but does not change in sign. From t = 35 sec. through t = 56 sec., sideslip is again increased continuously until maximum rudder deflection is reached and the maneuver is terminated.

The aileron stick force reversal coincides with the onset of flow separation over the wing tip. This separation is induced by the completely stalled upwind winglet. For the subject airplane, the distance between the aileron tip chord and the winglet is only a couple of inches. As a result, the region of separated flow extends over part of the upper surface of the upwind aileron. The two main effects of separated flow over the wing tip and aileron are

(1) a change in aileron hinge moments (consequently, the aileron displays a tendency to float upward toward the stop instead of downward);

(2) a reduction in wing dihedral effect (therefore, aileron deflection required for a given steady heading sideslip is reduced).

Although part of the aileron encounters separated flow, the airplane is still controllable, as shown by the time histories. However, it is clear that flow separation over the aileron is undesirable and may not be certifiable.

In Reference 17, the identical phenomenon is observed on a twin-engine, high wing airplane. On that airplane a boundary layer fence is installed, which confines the region of separated flow to the immediate vicinity of the winglet, allowing the aileron to remain effective. An alternative solution is to design the wing tip and winglet in a manner such that sufficient distance is kept between the winglet and aileron to prevent separated flow from extending over the aileron.

5.4.2 Dutch Roll Mode

The damping ratio, ζ_D, undamped natural frequency, ω_{n_D}, and roll-to-yaw ratio, $(\phi/\beta)_D$, of the Dutch roll motion are measured for the airplane in both configurations. The results are listed in Table 5.2. For the winglet equipped airplane, two sets of data are shown for each of the test conditions. Comparison of the data indicates excellent repeatability of the test results. The rudder pulsing technique was used to excite the Dutch roll motion for the airplane with winglets. The steady sideslip release method was applied for the basic airplane[1]. The latter test technique did not excite the Dutch roll motion satisfactorily; and therefore, only one test run produced quantitative results. Although the quality of these results is lower, they are also listed in Table 5.2.

A comparison of the Dutch roll mode characteristics for the winglet-equipped airplane and the basic airplane shows that the influence of winglets on the Dutch roll characteristics of the subject airplane is

[1]Both test techniques are described in Reference 39.

Table 5.2: Dutch Roll Mode Characteristics

Winglets on:

Trim speed (KIAS)	ω_{n_D} (rad/sec)	ζ_D	$(\phi/\beta)_D$
80	1.236	0.210	1.520
80	1.235	0.205	1.500
105	1.322	0.210	1.558
105	1.329	0.215	1.533

Winglets off:

Trim speed (KIAS)	ω_{n_D} (rad/sec)	ζ_D	$(\phi/\beta)_D$
80	1.231	0.190	1.081

small. The roll-to-yaw ratio increased due to the installation of winglets. This increment is expected because the numerator of $(\phi/\beta)_D$ is very much a function of C_{ℓ_β} (see page 466 of Reference 38). Consequently, more positive dihedral effect due to winglets results in an increase in the roll-to-yaw ratio.

5.4.3 Roll Characteristics

The time constant of the rolling motion, T_R, the steady state roll rate, P_{ss}, and the roll performance (time required to roll 30°, 45°, and 60°) are measured for the airplane with and without winglets. Full lateral control deflection is applied. Rudder is deflected sufficiently to reduce sideslip that retards roll rate (not to produce sideslip that augments roll rate). Rolls are performed in both directions to demonstrate asymmetrical effects (e.g., engine torque). The results of the measurements are listed in Table 5.3.

A combination of two circumstances makes it difficult to measure accurately the roll characteristics of the airplane. First, large stick deflection is required for maximum aileron deflection. Consequently, it is difficult for the pilot to generate an acceptable lateral control step input. Second, the airplane has a short time constant. Therefore, some variability can be observed in the data of Table 5.3.

The results show that the influence of winglets on roll mode time constant is small. This parameter is approximately equal to the negative inverse of the dimensional roll damping derivative, L_p. Although an increase in C_{ℓ_p} can be noted due to winglets (see Section 5.3), L_p

Table 5.3: Roll Performance and Mode Characteristics

Winglets on:

Trim speed (KIAS)	Roll direction	T_R (sec)	P_{ss} (deg/sec)	Time to roll (sec) 30°	45°	60°
80	L → R	.40	51.2	1.03	1.33	1.61
80	R → L	.54[1]	-48.5	1.15	1.45	1.76
105	L → R	.38	65.2	0.90	1.13	1.37
105	R → L	.40	-63.5	0.93	1.17	1.42

Winglets off:

Trim speed (KIAS)	Roll direction	T_R (sec)	P_{ss} (deg/sec)	Time to roll (sec) 30°	45°	60°
80	L → R	.39	56.7	0.95	1.20	1.45
80	R → L	.42	-61.9	0.91	1.14	1.38
105	L → R	.41	76.4	0.83	1.03	1.23
105	R → L	.39	-83.9	0.79	0.98	1.16

[1]Long rolling moment time constant caused by relatively slow aileron input.

appears to be less affected. Apparently, the increase in C_{ℓ_p} is cancelled by the increase in airplane moment of inertia about the X axis.

Maximum steady state roll rate and roll performance are slightly degraded as a result of winglets. However, the total effect appears to be small.

5.4.4 Roll Rate Oscillations and Sideslip Excursions

The problem of Dutch roll excitation as it affects roll control of airplanes is usually studied in terms of the transfer function relating bank angle and aileron deflection:

$$\frac{\phi(s)}{\delta_a(s)} = \frac{K_{\phi_{\delta_a}}(s^2 + 2\zeta_\phi \omega_{n_\phi} s + \omega_{n_\phi}{}^2)}{(s + 1/T_S)(s + 1/T_R)(s^2 + 2\zeta_D \omega_{n_D} s + \omega_{n_D}{}^2)} \qquad (5.8)$$

In Referenced 40, 41, and 42 excellent discussions concerning this problem are presented; and it is shown that the amount of Dutch roll execution that a pilot will tolerate in step aileron rolls is highly dependent upon the position of the zero in relation to the Dutch roll pole of the ϕ/δ_a transfer function. A typical representation is plotted in Figure 5.18; and it shows a region of acceptable displacement of the zero from the pole defined by a constant pilot rating contour. The size of this region is very much a function of roll time constant and Dutch roll damping and frequency. In Figure 5.19, an analytical example taken from Reference 20 demonstrates the effect of $\omega_{n_\phi}/\omega_{n_D}$ on the roll response characteristics.

The undamped natural frequency of the numerator of the ϕ/δ_a transfer function can be approximated as follows:

$$\omega_{n_\phi}{}^2 \simeq \omega_{n_D}{}^2 - \frac{N_{\delta_a}}{L_{\delta_a}} \left(\frac{Y_\beta}{V} L_r + L_\beta\right) \tag{5.9}$$

This approximation is used to gain physical insight into the problem and should not be used in practice. In the previous section it is shown that the effect of winglets on the Dutch roll undamped natural frequency is fairly small. The above expression shows that for airplanes with adverse yaw due to aileron ($N_{\delta_a} < 0$), an increase in the stability of Y_β and L_β will result in a reduction of ω_{n_ϕ}. Consequently, an increase in the stability of these derivatives due to winglets will increase the level of roll rate oscillations.

Following a rudder-pedals-free step aileron control input (maximum deflection), the ratio P_2/P_1 is measured, where P_2 is roll rate at first minimum following the first peak P_1. The 45°-45° rolls are performed in both directions. This maneuver follows closely the one described in Section 3.3.2.2 of Reference 43. The results of this in-flight maneuver are listed in Table 5.4.

The data of Table 5.4 show that winglets increase the level of roll rate oscillations, as indicated by the reduction in the ratio P_2/P_1. In Table 5.4 the parameter $\Delta\beta$ represents the sideslip excursion during the maneuver described earlier. The increment in sideslip excursion degrades airplane flying qualities because it increases pilot difficulty in quickly and precisely taking up a given heading.

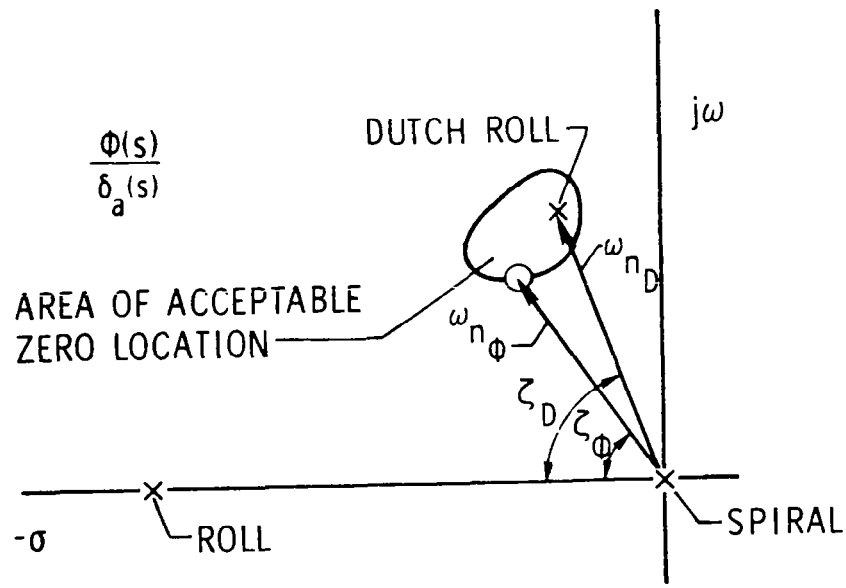

Figure 5.18: Complex Plane Representation of the ϕ/δ_a Transfer Function

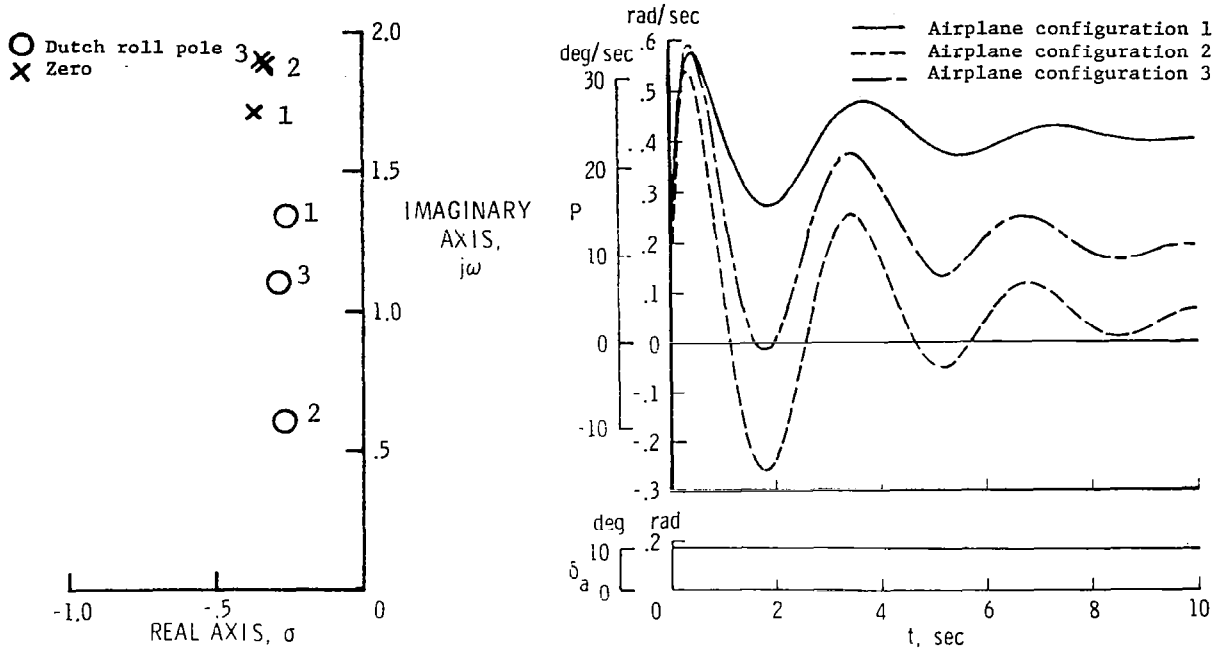

Figure 5.19: Roll Rate Response due to an Aileron Step Input for Various Locations of ϕ/δ_a Transfer Function Zero and Dutch Roll Pole (from Reference 20)

Table 5.4: Roll Rate Oscillations and Sideslip Excursions

Winglets on:

Trim speed (KIAS)	Roll direction	P_2/P_1	$\Delta\beta$ (deg)
80	L → R	.366	33.0
80	R → L	.336	33.3
105	L → R	.542	23.1
105	R → L	.537	25.0

Winglets off:

Trim speed (KIAS)	Roll direction	P_2/P_1	$\Delta\beta$ (deg)
80	L → R	.892	23.0
80	R → L	.951	27.9
105	L → R	.897	-
105	R → L	.924	17.8

Two observations can be made from Equation (5.9). First, a reduction in dihedral effect due to winglets will reduce the increase in roll rate oscillations. This can be done in various ways, as shown by the results of the parametric study in Chapter 2. Second, an aileron-rudder-interconnect (ARI) can be added to the airplane control system. An ARI will cause a reduction in the adverse yawing moment due to aileron ($N_{\delta_a} \simeq 0$) with, as a result, a smaller difference between ω_{n_D} and ω_{n_ϕ}. Reference 8 presents an evaluation of the effect of winglets on the flying qualities of a light general aviation airplane with an ARI installed.

5.5 Summary

The results presented in this chapter indicate that winglets have a significant influence on position error calibration and lateral-directional stability and control of the subject airplane.

1. Static pressure and angle of attack position error become larger with increasing airplane angle of attack as a result of enhanced aerodynamic loading at the wing tips due to the winglets and proximity of the winglets to the flow measuring sensors.
2. Winglet aerodynamic loading is very much dependent on airplane angle of attack and angle of sideslip. The results obtained with the lifting surface methods of References 21, 22, and 23 show fair to good agreement with in-flight measured winglet loading.
3. Airplane stability and control derivatives are estimated from flight data using the equation error method. The data

show that airplane sideslip stability derivatives are most significantly influenced by winglets. The other lateral-directional stability and control derivatives show much smaller changes due to winglets. A comparison of the estimated stability and control derivatives for the airplane without winglets with the derivatives of two other straight wing general aviation airplanes indicates similar trends and magnitudes.

4. Results obtained during a flight evaluation of the effect of winglets on airplane flying qualities show fair to good agreement with predicted results using the derivatives estimated from transient flight-test data.

5. For large sideslip angles, flow separation over the upwind wing tip and aileron appears to produce aileron stick force reversal. This separation is induced by the completely stalled upwind winglet.

6. Winglets produce an increment in Dutch roll roll-to-yaw ratio. Dutch roll damping and frequency are hardly affected.

7. Airplane roll mode time constant and (coordinated) roll performance display small changes due to winglets. Roll performance appears to be slightly more sluggish as a result of winglets. However, this reduction in roll performance is small.

8. Winglets cause a significant increment in the level of Dutch roll excitation following a step aileron input. This increment results in a high level of roll rate oscillations and larger sideslip excursions.

CHAPTER 6

WINGLET DESIGN CONSIDERATIONS

The design of wing-tip-mounted winglets is discussed in detail by Richard T. Whitcomb in Reference 1. In Reference 27, a parametric study on the relative advantages of wing-tip extensions and winglets confirms most of the recommendations of Reference 1 and provides additional design information, for a wide range of wings. Furthermore, in Reference 28, a large number of winglet parameters are studied to determine the effects on the longitudinal aerodynamic characteristics and loading of a wing for a first generation jet transport. These three publications provide the designer with background information and guidelines for the design of winglets in terms of lift-induced drag, root-bending moments, and sectional force coefficients. However, the effects of wing-tip-mounted winglets on airplane stability and control are hardly discussed. For transport and business jet aircraft, the influence of these surfaces on airplane stability and control are generally small (References 44 and 45). In addition, this type of aircraft is normally equipped with an automatic flight control system (AFCS). Conversely, for general aviation and agricultural airplanes, the changes in airplane stability and control due to winglets can be significant, as demonstrated by the data presented in this report. Also, these airplanes generally do not have an AFCS to improve airplane flying qualities.

A final consideration is that cruise Mach number and Reynolds number for transport jets are higher than for low-speed general avi-

ation airplanes. This can affect the decision concerning which winglet airfoil section to choose.

In this chapter, a discussion is presented of the considerations involved in the design of winglets for low-speed general aviation and agricultural airplanes. This discussion is based on results presented in this report and on data and design considerations listed in References 1, 27, and 28. The following considerations along with the application of a lifting surface method (e.g., Reference 21 or 22) should make the design process of winglets more efficient.

6.1 Airfoil Section[1]

Past winglet designs have made frequent use of turbulent airfoil sections similar to the NASA low-speed family of airfoils (formerly GA(W) airfoil family). Details of this type of airfoil can be found, e.g., in References 46 and 47. The most important factor favoring these airfoils is their desirable high-lift, low-speed characterictics.

Currently, a resurgence is occurring in natural laminar flow (NLF) airfoil and wing research. This trend is exemplified by the recent publications pertaining to NLF (References 48, 49, 50, and 51). Two recent research results in this area should be taken into consideration when a winglet is being designed: (1) the feasibility of NLF on practical airframe surfaces at large values of transition Reynolds number, and (2) the ability to design low-drag NLF airfoils while retaining the desirable low-speed, high-lift characteristics of the low-speed turbulent flow airfoils.

---

[1]The author acknowledges Dr. B. J. Holmes' valuable contributions to this section.

The design constraints for a winglet NLF airfoil are considerably different than for a wing. On a wing, the extent of laminar flow that can be designed into the airfoil is limited by pressure recovery considerations for the fully turbulent case where separation may be a problem. This means in part that sectional maximum lift coefficient is not allowed to decrease with transition fixed near the leading edge. This requirement is set by safety considerations relative to stall speed and degraded airplane longitudinal stability and control due to extensive separation. The same concern may not be important for a winglet airfoil, because of the relatively small effect on airplane aerodynamics due to any separation which might occasionally exist on an NLF winglet in the fully turbulent case. Thus, instead of limiting the laminar boundary-layer runs to 40 or 50 percent chord, as is the practical limit for wing airfoil sections, a winglet NLF airfoil might safely support much more laminar flow. Substantial reduction in winglet profile drag would result from the increased laminar runs.

A second constraint often placed on a wing airfoil design is the amount of negative pitching moment allowed. Maximum allowable pitching moment for an NLF winglet airfoil would likely be much greater than for a wing. Due to the approximate vertical position of the winglet, the winglet is loaded in its plane by the winglet pitching-moment loads. This results in a minimal weight penalty for larger pitching moments.

In addition, with the winglet having a fixed geometry, one element design (no leading-edge or trailing-edge high-lift devices), aft loading due to large camber, is less of a constraint. Thus, long laminar boundary-layer runs can be sought while flexibility is maintained in camber shape to meet high-lift requirements.

The potential benefit of tailoring a winglet for maximum feasible laminar boundary layer results from the smaller profile drag losses the winglet must overcome to produce a thrust in the direction of flight. With sufficiently low winglet profile drag, the airplane lift coefficient at which drag polar crossover occurs (winglets off versus on) may be outside the airplane flight envelope. A winglet with these characteristics would provide net performance gains throughout the flight envelope.

Additional research is required to verify the above-stated advantages of NLF airfoil sections on winglets.

6.2 Winglet Location

The location of the winglet in relation to the leading-edge of the wing and lateral control surfaces has an important effect on winglet induced efficiency, airplane stability and control, and structural and aeroelastic considerations.

Flight test results presented in Reference 17 and in this report demonstrate that sufficient distance should be kept between winglet and outboard aileron. In the case of winglet stall, this will prevent separated flow from extending over the aileron and cause significant nonlinear effects in airplane lateral control.

Results listed in Reference 28 and in Chapter 2 of this report indicate that an aftward shift of the winglet decreases lift-induced drag and dihedral effect and improves directional stability for the wing-winglet configuration. These trends tend to make an aft location of the winglet preferable.

However, if the winglet is moved aft, attachment of this device to the wing becomes a greater problem, since the structural box of the winglet moves aft of the usual rear spar location of the wing. In addition, winglet center of gravity moves aft in relation to the elastic axis of the wing. If the wing with winglet is the critical flutter structure in the airplane, then the above-mentioned modification may cause a reduction in the maximum flutter speed of the airplane.

6.3 Winglet Sweep

In Reference 1, Whitcomb states: "For satisfactory winglet effectiveness at supercritical design conditions, the effective sweep of these surfaces should be approximately the same as that of the wing." The foundation for this design guideline is that backward sweep of the winglet minimizes the level of interference and compressibility drag in the wing-winglet juncture by offsetting the velocity fields of both lifting surfaces.

Backward sweep of the winglets also tends to minimize the increment in dihedral effect due to winglets and produces a slight increase in directional stability and yaw damping, as demonstrated in Chapter 2 of this report. The influence of backward sweep on induced drag and wing-root bending moment is small until the sweep angle becomes very large ($\approx 60°$). Therefore, it appears that for unswept wing configurations, backward sweep of the winglet should be applied because it minimizes the increase in dihedral effect due to the surfaces without affecting winglet performance significantly.

6.4 Winglet Planform Area and Taper

In References 1, 27, and 28 it is observed that the effects of winglet taper ratio and planform area on the level of minimum induced drag and corresponding wing-root bending moment are small. In addition, the results listed in Chapter 2 of this report indicate that the effects of these two parameters on the lateral-directional stability and control derivatives are small, except for C_{y_β} and C_{ℓ_β}. The stability of these derivatives is slightly enhanced by an increase in winglet planform area and/or winglet aspect ratio.

For maximum induced drag efficiency, sectional normal force coefficients, c_n, on the outboard protion of the winglet become larger with decreasing taper ratio. Also, with decreasing winglet planform area, the level of c_n on the entire winglet rises. Both modifications can precipitate the onset of flow separation on the winglet. Conversely, increased taper ratio and planform area can delay flow separation. Therefore, these two parameters provide design freedom to maintain stall-free levels of sectional normal force coefficients for the desired span-load distribution.

6.5 Winglet Length

An increment in winglet length will produce a significant reduction in induced drag. However, this performance gain coincides with increases in wing and winglet bending moments, and dihedral effect for the wing-winglet configuration. The increase in wing and winglet root-bending moments will result in higher structural stresses, while

the increase in dihedral effect can produce changes in airplane stability and control which may not be certifiable. Therefore, the optimum length of the winglet must be a compromise between aerodynamic, structural, and stability and control considerations.

In addition, in References 1 and 28, it is observed that as the winglet becomes longer, the required normal force coefficients for the winglet increase to the point where flow separation will occur.

6.6 Winglet Incidence and Twist

The influence of winglet twist on lateral-directional stability and control is not discussed in this report. However, it is shown that winglet incidence causes only small changes in the stability of the various derivatives. Winglet incidence angle does have an important effect on the induced efficiency of the wing-winglet configuration. In addition, it provides design freedom to trade small reductions in induced efficiency for more significant reductions in root bending moment (Reference 27).

6.7 Winglet Cant Angle

This parameter has a powerful influence on induced drag, wing-root bending moment, and lateral-directional stability and control. Both root bending moment and dihedral effect increase continuously as the winglet is canted outward, while induced drag decreases with outward winglet cant. According to Reference 1, the optimum practical winglet configuration should have a small amount of outward cant

(approximately 10° to 20°). This angle is based on a trade-off study between induced drag reduction, skin friction, and wing bending moments.

However, it is possible to realize a significant reduction in induced drag at a very small penalty in wing-root bending moment if the winglet is canted inward. An additional advantage of inward cant is a smaller increment in dihedral effect due to the addition of winglets.

In summary, cant angle is a compromise between induced drag, structural stresses, airplane stability and control, and wing-winglet junction interference drag. Additional research is required to study the significance of interference drag in relation to induced drag reduction due to winglets as function of cant angle.

6.8 Additional Considerations

An issue which has not been discussed in the previous sections is the question of whether induced drag can be reduced more effectively by increasing the wingspan with a tip extension to increase wing aspect ratio than by using winglets. To answer that question, a comparison of the reduction in induced drag and the corresponding increment in structural weight between the tip extension and the nonplanar tip modification is required. For tip extensions and winglets, References 4 and 27 indicate that wing weight changes are approximately proportional to changes in wing-root bending moment:

$$\frac{(W_w)_{\text{modified}}}{(W_w)_{\text{basic}}} \simeq \frac{(M_r)_{\text{modified}}}{(M_r)_{\text{basic}}} \tag{6.1}$$

Consequently, wing weight will increase due to an increase in wing-root bending moment for a constant load factor. Results from several studies (References 4, 5, 27, 28, and 52) show that, at an identical level of root bending moment, a winglet provides a greater induced drag efficiency increment than does a tip extension. Alternatively, at an identical level of induced drag efficiency, a tip extension generates a greater wing-root bending moment increment than a winglet. This gain in induced efficiency for a winglet is the greatest for a wing which is highly loaded in the outboard region. However, these observations regarding the relative effectiveness of winglets and tip extensions to improve airplane performance are not conclusive. A detailed analysis must be conducted of the effects of these tip devices on (1) airplane stability and control, (2) flutter characteristics, (3) airplane performance, (4) wing-tip structure, and (5) airplane stalling and spinning characteristics.

The issue of airplane stalling characteristics has not yet been discussed. The stall characteristics of the winglet-equipped airplane of Reference 8 were slightly improved over the basic airplane. In the case of no sideslip stalls, the basic airplane displayed a tendency to roll off or drop a wing. The winglets appeared to prevent the wing tip from stalling early, thus reducing the tendency to roll off. This resistance to rolling off was also exhibited in stalls with moderate amount of sideslip. Additional research is required on the effects of winglets on stalling and also spinning characteristics.

CHAPTER 7

CONCLUSIONS AND RECOMMENDATIONS

7.1 Conclusions

A study has been conducted on the effects of nonplanar wing-tip-mounted surfaces (e.g., winglets) on the lateral-directional stability and control of light general aviation and agricultural type airplanes. The study consists of a theoretical and an experimental, in-flight investigation. It is shown that good correlations exist between the results of the various theoretical methods and experimental data. The results of this study are combined with data reported in the literature on the effects of these surfaces on airplane performance and wing-winglet structural stresses.

A lifting surface method has been used to perform a parametric study on the effects of various winglet parameters on lateral-directional stability derivatives of a general aviation type wing. The parametric study provides the following results, as summarized at the end of Chapter 2:

1. Of all lateral-directional stability derivatives the sideslip stability derivatives, C_{y_β}, C_{ℓ_β}, and C_{n_β}, are most significantly influenced by winglets. The roll-rate and yaw-rate derivatives are affected to a lesser degree.
2. The increment in dihedral effect due to winglets is significantly reduced as the winglet is moved aftward and/or swept backward. The directional stability increases due to these modifications.

3. Winglet cant angle affects C_{ℓ_β} and C_{ℓ_p} and has a strong effect on lift-induced drag and wing-root bending moment. Outward cant decreases induced drag, but it increases root-bending moment, dihedral effect, and roll damping.

4. The effect of winglet incidence angle on the stability derivatives appears to be small. Therefore, the incidence angle can be optimized for maximum wing-winglet performance without significantly affecting airplane stability and control

5. Wing sweep and wing twist produce changes in the contribution of the winglet to the yawing moment derivatives. Backward sweep and washout improve directional stability and cause C_{n_p} to become more positive. The other derivatives show only minor changes.

6. The effects of wing span and wing taper ratio on the winglet contribution to the stability derivatives are very small.

7. Winglet length has an important influence on dihedral effect, induced efficiency, and wing-root bending moment. Increased length produces an increase in induced efficiency, but it also causes an increment in wing-root bending moment and dihedral effect.

An in-flight investigation of winglets mounted on an agricultural research airplane has been conducted. Selected results are presented and indicate the following, as summarized in the final section of Chapter 5:

1. Static pressure and angle of attack position error become larger with increasing airplane angle of attack as a result of enhanced aerodynamic loading at the wing tips due to the winglets and proximity of the winglets to the flow measuring sensors.

2. Winglet aerodynamic loading is very much dependent on airplane angle of attack and angle of sideslip. The results obtained with several lifting surface methods show fair to good agreement with in-flight measured winglet loading.
3. Airplane stability and control derivatives are estimated from flight data using the equation error method. The data show that airplane sideslip stability derivatives are most significantly influenced by winglets. The other lateral-directional stability and control derivatives show much smaller changes due to winglets. A comparison of the estimated stability and control derivatives of the airplane without winglets with the derivatives of two other straight wing general aviation airplanes indicates similar trends and magnitudes.
4. Results obtained during a flight evaluation of the effects of winglets on airplane flying qualities show fair to good agreement with predicted results using the derivatives estimated from transient flight-test data.
5. For large sideslip angles, flow separation over the upwind wing tip and aileron appears to produce aileron stick force reversal. This separation is induced by the completely stalled upwind winglet.
6. Winglets produce an increment in Dutch roll roll-to-yaw ratio. Dutch roll damping and frequency are hardly affected.
7. Airplane roll mode time constant and (coordinated) roll performance display small changes due to winglets. Roll performance appears to be slightly more sluggish as a result of winglets.

8. Winglets cause a significant increment in the level of Dutch roll excitation following an aileron step input. This increment results in a high level of roll rate oscillations and large sideslip excursions.

In summary, results of both studies are largely in agreement and indicate that wing-tip-mounted nonplanar lifting surfaces can have a significant influence on airplane stability and control. Several potential solutions have been presented to reduce or eliminate the various stability and control problems. These solutions include (1) shifting or sweeping the surface aftward to reduce dihedral effect and improve directional stability; (2) reduction of dihedral effect by canting-in of the surface, or adding a wing-tip-mounted lifting surface with a negative dihedral angle; (3) reduction of adverse yaw due to aileron by adding an aileron-rudder interconnect to the airplane control system; (4) preventing nonlinearities in airplane lateral control by keeping sufficient distance between the wing-tip device and the lateral control surfaces.

7.2 Recommendations

The following pertinent research is proposed:

1. A study should be made of the influence of winglet cant angle on the level of interference drag in the wing-winglet junction.
2. The design of special NLF airfoils for winglets should be studied.
3. Effects of winglets on airplane stalling and spinning characteristics should be investigated in more detail.

4. Empirical correction factors for the degree of development of edge suction forces should be developed. At the moment, the theory of Reference 21 assumes fully developed leading-edge and tip suction forces. Experiments show that this assumption is not always valid.
5. A study should be made of the incremental effects of an additional wing-tip-mounted lifting surface with negative dihedral on the aerodynamic characteristics of a wing-winglet configuration.
6. A study should be conducted aimed at the design optimization of nonplanar wing-tip-mounted lifting surfaces.

REFERENCES

1. Whitcomb, R. T., "A Design Approach and Selected Wind-Tunnel Results at High Subsonic Speeds for Wing-Tip Mounted Winglets," NASA TN D-8260, July 1976.
2. Spillman, J. J., "The Use of Wing Tip Sails to Reduce Vortex Drag," Aeronautical Journal, September 1978, pp. 387-395.
3. Hackett, J. E., "Vortex Drag Reduction by Aft-Mounted Diffusing Vanes," ICAS paper 80-13.4, October 1980.
4. Flechner, S. G., and Jacobs, P. F., "Experimental Results of Winglets on First, Second, and Third Generation Jet Transports," NASA TM-72674, May 1978.
5. Loptien, G. W., "The Effect of Winglets on the KC-135A Aircraft," AFFDL-TR-78-124, November 1978.
6. Gilkey, R. D., "Design and Wind Tunnel Tests of Winglets on a DC-10 Wing," NASA CR-3119, April 1979.
7. Darel, I., Eliraz, Y., and Barnett, Y., "Winglet Development at Israel Aircraft Industries,"ICAS paper 80-12.5, October 1980.
8. Holmes, B. J., van Dam, C. P., Brown, P. W., and Deal, P. L., "Flight Evaluation of the Effect of Winglets on Performance and Handling Qualities of a Single-Engine General Aviation Airplane," NASA TM-81892, December 1980.
9. Spillman, J. J., Ratcliffe, H. Y., and McVitie, A., "Flight Experiments to Evaluate the Effect of Wing-Tip Sails on Fuel Consumption and Handling Characteristics," Aeronautical Journal, July 1979, pp. 279-281.
10. Hackett, J. E., "Vortex Drag Reduction by Diffusing Vanes: Design for the Thrush Agricultural Aircraft," SAE paper 810605, April 1981.

11. Reynolds, P. T., "The Learjet Longhorn Series: The First Jets with Winglets," SAE paper 79-0581, April 1979.

12. Rutan, B., "Development of a Small High-Aspect-Ratio Canard Aircraft," Society of Experimental Test Pilots, Technical Review, Vol. 13, No. 2, September 1976, pp. 93-101.

13. Jordan, F. L. Jr., "Development of Test Methods for Scale Model Simulation of Aerial Applications in NASA Langley Vortex Facility," NASA TM-81805, April 1980.

14. Parkin, C. S. and Spillman, J. J., "The Use of Wingtip Sails on a Spraying Aircraft to Reduce the Amount of Material Carried Off-Target by a Crosswind," Journal of Agricultural Engineering Research, Vol. 25, 1980, pp. 65-74.

15. Gifford, R. V., and van Dam, C. P., "The Design Integration of Wingtip Devices for Light General Aviation Aircraft", NASA TM-83252, August 1982.

16. Anon., "OMAC 1 Business Aircraft Makes Its Second Flight," Aviation Week and Space Technology, July 5, 1982, page 70.

17 Eliraz, Y., and Ilan, D., "Performance of the ARAVA Aircraft with Wing-Tip Winglets," Israel Journal of Technology, Vol. 15, 1977, pp. 35-43.

18. Johnson, J. L., Jr., McLemore, H. C., White, R., and Jordan, F. L., Jr., "Full Scale Wind-Tunnel Investigation of an Ayres S2R-800 Thrush Agricultural Airplane," SAE paper 79-0618, April 1979.

19 Ogburn, M. E., and Brown, P. W., "Exploratory Piloted Simulator Study of the Effects of Winglets on Handling Qualities of a Representative Agricultural Airplane," NASA TM-81817, April 1980.

20. Van Dam, C. P., "Effects of Wingtip Modifications on Handling Qualities of Agricultural Aircraft," SAE paper 810606, April 1981.

21. Lan, C. E., "Calculation of Lateral-Directional Stability Derivatives of Wings by a Nonplanar Quasi-Vortex-Lattice Method," NASA CR-165659, January 1981.

22. Goldhammer, M. I., "A Lifting Surface Theory for the Analysis of Nonplanar Lifting Systems," AIAA paper 76-16, January 1976.

23. Tulinius, J., "Unified Subsonic, Transonic, and Supersonic NAR Vortex Lattice," TFD-72-523, Los Angeles Div., North American Rockwell, April 1972.

24. Lan, C. E., "A Quasi-Vortex-Lattice Method in Thin Wing Theory," Journal of Aircraft, Vol. 11, No. 9, September 1974, pp. 518-527.

25. Toll, T. A., and Queijo, M. J., "Approximate Relations and Charts for Low-Speed Stability Derivatives of Swept Wings," NASA TN-1581, May 1948.

26. Queijo, M. J., "Theory for Computing Span Loads and Stability Derivatives due to Sideslip, Yawing, and Rolling for Wings in Subsonic Compressible Flow," NASA TN D-4229, December 1968.

27. Heyson, H. H., Riebe, G. D., and Fulton, C. L., "Theoretical Parametric Study of the Relative Advantages of Winglets and Wing-Tip Extensions," NASA TP-1020, September 1977.

28. Ishimitsu, K. K., VanDevender, N., Dodson, R., et al., "Design and Analysis of Winglets for Military Aircraft," AFFDL-TR-76-6, U.S. Air Force, February 1976.

29. Riley, D. R., "Wing-Tunnel Investigation and Analysis of the Effects of End Plates on the Aerodynamic Characteristics of an Unswept Wing," NASA TN-2440, August 1951.

30. Wolhart, W. D., and Thomas, D. F., Jr., "Static Longitudinal and Lateral Stability Characteristics at Low Speed of Unswept-Midwing Models Having Wings with an Aspect Ratio of 2, 4, or 6," NASA TN-3649, May 1956.

31. Fisher, L. R., and Michael, W. H., Jr., "An Investigation of the Effect of Vertical-Fin Location and Area on Low-Speed Lateral Stability Derivatives of a Semitailless Airplane Model," NACA RM L51A10, March 1951.

32. Bergey, K. H., "Leading Edge High Lift Devices for Agricultural Aircraft," SAE paper 810608, April 1981.

33. Fisher, B. D., Holmes, B. J., and Stough, H. P., "A Flight Evaluation of a Trailing Anemometer for Low-Speed Calibrations of Airspeed Systems on Research Aircraft," NASA TP-1135, February 1978.

34. Holmes, B. J., "Flight Evaluation of an Advanced Technology Light Twin-Engine Airplane (ATLIT)," NASA CR-2832, July 1977.

35. Klein, V., "Determination of Stability and Control Parameters of a Light Airplane from Flight Data Using Two Estimation Methods," NASA TP-1306, March 1979.

36. Suit, W. T., and Cannaday, R. L., "Comparison of Stability and Control Parameters for Light, Single-Engine, High-Winged Aircraft Using Different Flight Test and Parameter Estimation Techniques," NASA TM-80163, September 1979.

37. Cannaday, R. L., and Suit, W. T., "Effects of Control Inputs on the Estimation of Stability and Control Parameters of a Light Airplane," NASA TP-1043, December 1977.

38. Roskam, J., Airplane Flight Dynamics and Automatic Flight Controls, Part 1, Roskam Aviation and Engineering Corporation, Lawrence, Kansas.

39. Langdon, S. D., and Cross, W. V., "Fixed Wing Stability and Control, Theory and Flight Test Techniques," USNTPS-FTM-No. 103, U.S. Navy, August 1977.

40. Ellis, D. R., "Flying Qualities of Small General Aviation Airplanes; Part 2," FAA-RD-70-65, April 1970.

41. Ellis, D. R., "Flying Qualities of Small General Aviation Airplanes; Part 4," FAA-RD-71-118, December 1971.

42. Chalk, C. R., Neal, T. P., Harris, T. M., Pritchard, F. E., and Woodcock, R. J., "Background Information and User Guide for MIL-F-8785B(ASG), Military Specification - Flying Qualities of Piloted Airplanes," AFFDL-TR-69-72, U.S. Air Force, August 1969. (Available from DTIC as AD 860 856.)

43. Anon., "Military Specification: Flying Qualities of Piloted Airplanes," MIL-F-8785B(ASG), August 1969.

44. Conley, N. E., "Winglet Toe Out Angle Optimization for the Gates Learjet Longhorn Wing," Journal of Aircraft, Vol. 17, No.12, December 1980, pp. 851-855.

45. Crenshaw, K. R., "Stability and Control Characteristics of the Winglet Configured KC-135A," Masters Thesis, Air Force Institute of Technology, December 1976 (Rept. AD-A034940).

46. McGhee, R. J., Beasley, W. D., and Somers, D. M., "Low-Speed Aerodynamic Characteristics of a 13-Percent-Thick Airfoil Section Designed for General Aviation Applications," NASA TM X-72697, 1975.

47. McGhee, R. J., Beasley, W. D., and Whitcomb, R. T., "NASA Low-and Medium-Speed Airfoil Development," NASA TM-78709, 1979.

48. Somers, D. M., "Design and Experimental Results for a Natural-Laminar-Flow Airfoil for General Aviation Applications," NASA TP-1861, June 1981.

49. Somers, D. M., "Design and Experimental Results for a Flapped Natural-Laminar-Flow Airfoil for General Aviation Applications," NASA TP-1865, June 1981.

50. Montoya, L. C., Steers, L. L., Christopher, D., and Trujillo, B., "Natural Laminar Flow Glove Flight Results." Advanced Aerodynamics - Selected NASA Research. NASA CP-2208, 1981, pp. 11-20.

51. Holmes, B. J., and Obara, C. J., "Observations and Implications of Natural Laminar Flow on Practical Airplane Surfaces," ICAS paper 82-5.1.1, August 1982.

52. Dahlin, J. A., "Aerodynamic Evaluation of Winglets for Transport Aircraft," AIAA paper 81-1215, June 1981.

53. Morris, D. J., Croom, C. C., Holmes, B. J., and van Dam, C. P., "NASA Aerial Applications Wake Interaction Research," presented at 1982 Joint Technical Session of American Society of Agricultural Engineers and National Agricultural Aviation Association, paper AA-82-005, December 1982.

54. Van Dam, C. P., Holmes, B. J., and Pitts, C., "Effects of Winglets on Performance and Handling Qualities of General Aviation Aircraft," Journal of Aircraft, Vol. 18, No. 7, July 1981, pp. 587-591.

1. Report No.	2. Government Accession No.	3. Recipient's Catalog No.
NASA CR-3684		

4. Title and Subtitle	5. Report Date
ANALYSIS OF NONPLANAR WING-TIP-MOUNTED LIFTING SURFACES ON LOW-SPEED AIRPLANES	June 1983
	6. Performing Organization Code
7. Author(s) C. P. van Dam	8. Performing Organization Report No. KU-FRL-427-1
	10. Work Unit No.
9. Performing Organization Name and Address Flight Research Laboratory University of Kansas Center for Research, Inc. Lawrence, Kansas 66045	11. Contract or Grant No. NSG-1633
	13. Type of Report and Period Covered Contractor Report
12. Sponsoring Agency Name and Address National Aeronautics and Space Administration Washington, DC 20546	14. Sponsoring Agency Code

15. Supplementary Notes

University of Kansas Principal Investigator: Dr. Jan Roskam
Langley Technical Monitor: Dr. Bruce J. Holmes

16. Abstract

Nonplanar wing-tip-mounted lifting surfaces have shown to reduce lift-induced drag substantially. Winglets, which are small, nearly vertical, winglike surfaces, are an example of these devices. To achieve reduction in lift-induced drag, winglets produce significant side forces. Consequently, these surfaces can seriously affect airplane lateral-directional aerodynamic characteristics. Therefore, a study has been conducted on the effects of nonplanar wing-tip-mounted surfaces on the lateral-directional stability and control of low-speed general aviation airplanes.

The study consists of a theoretical and an experimental, in-flight investigation. The experimental investigation involves flight-tests of winglets on an agricultural airplane. Results of these tests demonstrate the significant influence of winglets on airplane lateral-directional aerodynamic characteristics. It is shown that good correlations exist between experimental data and theoretically predicted results. In addition, a lifting surface method has been used to perform a parametric study of the effects of various winglet parameters on lateral-directional stability derivatives of general aviation type wings.

17. Key Words (Suggested by Author(s))	18. Distribution Statement
Winglets Flight Tests Aerodynamic Characteristics Aerodynamic Loads Lateral-Directional Stability and Control General Aviation Aircraft	Unclassified - Unlimited Subject Category 02

19. Security Classif. (of this report)	20. Security Classif. (of this page)	21. No. of Pages	22. Price
Unclassified	Unclassified	178	A09

For sale by the National Technical Information Service, Springfield, Virginia 22161

NASA-Langley, 1983